Spring 2016

Stereographic Visualization of Bose-Einstein Condensate Clouds to Measure the Gravitational Constant

Ed Wesley Wells

STEREOGRAPHIC VISUALIZATION OF BOSE-EINSTEIN CONDENSATE CLOUDS TO MEASURE THE GRAVITATIONAL CONSTANT

by

ED WESLEY WELLS

(Under the Direction of Mark Edwards)

ABSTRACT

This thesis describes a set of tools that can be used for the rapid design of atom interferometer schemes suitable for measuring Newton's Universal Gravitation constant also known as "Big G". This tool set is especially applicable to Bose–Einstein–condensed systems present in NASA's Cold Atom Laboratory experiment to be deployed to the International Space Station in 2017. These tools include a method of approximating the solutions of the nonlinear Schrödinger or Gross–Pitaevskii equation (GPE) using the Lagrangian Variational Method. They also include a set of software tools for translating the approximate solutions of the GPE into images of the optical density into a format suitable for visualization with sterographic (3D) movies played back through a virtual–reality headset.

Key Words: Lagrangian Variational Method, Gravitational Constant, Bose-Einstein Condensate, Atom Interferometry, Visualization, Virtual Reality, Stereography

2009 *Mathematics Subject Classification*:

STEREOGRAPHIC VISUALIZATION OF BOSE-EINSTEIN CONDENSATE CLOUDS TO MEASURE THE GRAVITATIONAL CONSTANT

by

ED WESLEY WELLS

B.S., Georgia Southern University, 2002

A Thesis Submitted to the Graduate Faculty of Georgia Southern University in Partial

Fulfillment

of the Requirement for the Degree

MASTER OF SCIENCE

STATESBORO, GEORGIA

STEREOGRAPHIC VISUALIZATION OF BOSE-EINSTEIN CONDENSATE CLOUDS TO MEASURE THE GRAVITATIONAL CONSTANT

by

ED WESLEY WELLS

Major Professor:	Mark Edwards
	Yan Wu (Thesis Committee Chair)
Committee:	Goran Lesaja

Electronic Version Approved:

May 2016

DEDICATION

This thesis is dedicated to the next generation of my family: Victoria, Vivian, Lily-Ann, Emma-Lee, Isabella, and Aiden.

ACKNOWLEDGMENTS

This thesis is only possible thanks to the support and kindness of several people.

First, I must acknowledge my sincere gratitude to Mark Edwards for his impact on my academic and professional careers. Mark is the central adviser for this thesis and has provided the foundation on which it is built. In addition, as an undergraduate student Mark was my employer and helped fund the GSU Beowulf Cluster, which is the cornerstone on which I built my current career. His support was instrumental in my pursuit of graduate education.

Next, I wish to thank my committee chair Yan Wu and committee member Goran Lesaja. I've had the pleasure of attending courses with both professors over the course of a decade. The work was challenging and immensely rewarding. Their assistance as I returned for studies has made this thesis possible.

I wish to thank my sister Heather Parrish and her family: Andy, Lily, Emma, Johnny, and Debra. Without their love and support I could not have completed this work. They provided shelter, food, entertainment, and encouragement.

Finally, I wish to thank my long time partner Donna Boulineau. I love you.

TABLE OF CONTENTS

LIST OF TABLES

LIST OF FIGURES

Figure   Page

LIST OF SYMBOLS

A listing of a few common symbols. Additional symbols are explained as they are encountered in the text.

G	Gravitational Constant
g	Interaction coefficient in Gross-Pitaevskii Equation
N	Number of atoms in a Bose-Einstein Condensate
L_0	Scaled length unit
T_0	Scaled time unit
E_0	Scaled energy unit
ψ	Wave function
$\psi^\star$	Complex conjugate of the wave function
$|\psi|^2$	wave function times its complex conjugate, equivalent notation as $\psi^\star\psi$
ϕ	Trial or approximate wave function, distinct from an actual solution ψ
$\mathbf{r}$	Position vector: $x\hat{\mathbf{i}} + y\hat{\mathbf{j}} + z\hat{\mathbf{k}}$
α	Linear phase coefficient of the LVM trial wave function
β	Quadratic phase coefficient of the LVM trial wave function
$\mathbf{k}_j$	Initial momentum vector of of the jth condensate cloud when "kicked" by an optical lattice at $t = 0$
$\mathbf{w}_j$	Width vector for the jth condensate cloud
η	Substitute symbol for x, y, or z positions or labels in summations and products.
N_c	Number of condensate clouds
L	Lagrangian operator

A symbol utilizing a bar diacritic indicates that scaled units are being utilized, see section 4.1.2. For instance, x_j is the position of the jth condensate cloud along the $x-$axis. However, $\bar{x}_j$ is the coordinate for the same cloud in scaled units. Common symbols using scaled units include $\bar{\psi}$, $\bar{\eta}$, $\bar{\mathbf{w}}_j$, $\bar{\mathbf{k}}_j$, $\bar{\alpha}$, and $\bar{\beta}$.

The Gravitational Constant, G, is featured in Newton's Equation for the force of gravitational attraction between two point masses.

$$F = G\frac{m_1 m_2}{r^2}, \tag{1.1}$$

where, m_1 and m_2 are the masses of the two objects and r is the distance between two objects. "Big G" is the proportionality constant between the gravity force and the mass product over distance squared quantity and is one of the fundamental constants of nature. The current value of G recommended by the Committee on Data for Science and Technology, also known as CODATA, is [9]

$$G = 6.67408(\pm 0.00031) \times 10^{-11} \mathrm{m^3\,kg^{-1}\,s^{-2}}, \tag{1.2}$$

This value replaces the recommended values published in previous editions [8]. Also quoted is the (one standard deviation) uncertainty in G. Unfortunately, the uncertainty in the CODATA value has only been reduced by two orders–of–magnitude since G was first measured 200 years ago by Henry Cavendish [1].

The value of G has been notoriously difficult to measure [14]. Among all of the other recognized fundamental physical constants, it's value is known with the least precision. Table 1.1 presents a summary of measurements of Big G using the published Recommended Values from the CODATA organization. In addition, Cavendish measured the mean density of the Earth, from which Big G can be derived. Finally, the result of a recent terrestrial Atom Interferometry experiment is presented; notice this measurement is significantly different from the accepted measurements. For each value, the standard deviation in the error of the last two digits of G is presented. Notice, from 1969 through 2014 the uncertainty has moved only a single decimal place. Additionally, notice the swings of the uncertainty over time. Also, keep in mind

these are the recommended values from a detailed study covering many experimental measurements over a long period of time.

Year	G (scaled by 10^{11})	Std. Dev. (scaled by 10^{11})	Citation
1798	6.754		Cavendish (derived) [1]
1969	6.6732	0.00310	CODATA [2]
1973	6.6720	0.00410	CODATA [3]
1986	6.67259	0.00085	CODATA [4]
1998	6.673	0.00100	CODATA [5]
2002	6.6742	0.00100	CODATA [6]
2006	6.67428	0.00067	CODATA [7]
2010	6.67384	0.00080	CODATA [8]
2014	6.67408	0.00031	CODATA [9]
2014	6.67191	0.00099	Atom Interferometry [31]

Table 1.1: Summary of measurements of Big G (units of $m^3 kg^{-1} s^{-2}$) and one standard deviation in error u.

1.1 Importance of Big G

Improving the uncertainty in the value of G has relevancy to many fields of study and industry. In and of itself, increasing our collective knowledge of the universe is a goal of basic scientific inquiry. Because the quantity is known to such a low degree of certainty, establishing better certainty is an end unto itself.

Many celestial properties are dependent upon the precise value of G. Gravitational force is one of the four fundamental forces of nature, which include the Strong and Weak forces and the Electromagnetic force. Gravity is a comparatively weak force, but it acts at long ranges and is attractive between all masses. Additionally,

there is no known way to shield masses from gravitational attraction; in other words, there is not a repulsive gravitational force. Both the Strong and Weak force have ranges on the order of atomic nuclei and have attractive and repulsive effects. The Electromagnetic force only affects matter capable of carrying an electric charge. Additionally, the magnetic effects are attractive and repulsive and the electric effects can cancel themselves out with positive and negative charges.

Therefore, at cosmological scales in which large quantities of mass are present, the gravitational force is the dominant force affecting measurements of the movement and evolution of celestial bodies. For example, improving the uncertainty in G directly improves the accuracy of the measurements of the mass of the Earth and distance between the Sun and Earth. Since the Earth is not a perfect sphere, measurement of local gravity differences have important applications to mining, oceanography, and extraterrestrial navigation (e.g. satellite mapping and satellite guidance). As another example, a star's radius is determined by a balance of its internal radiation pressure pushing outward and the gravitation forces compressing its mass. The radius of a star affects its luminosity and thus the ability to observe it. The rate of expansion of the universe is dependent on G. Certainly, the recent LIGO [15] announcements detecting gravity waves [16] will present opportunities that either improve our understanding of G or are limited by the magnitude of it's uncertainty.

While we have discussed gravity on the cosmological scale, it is also an important contribution at the quantum scale. At small scales, the Planck units are useful to quantify common measurements. Quantum effects within this scale are modeled as continuous. However, below the Planck scale, quantum effects are indistinguishable from background fluctuations, so the Planck scale provides important limits to our reasoning about the quantum world. The Planck scale units for length, time, and mass depend upon G, the Planck constant, $\hbar$, and the speed of light in a vacuum, C.

$$\text{Planck length} = \frac{\hbar G^{1/2}}{c^3} \approx 1.6 \times 10^{-35} \text{m}$$

$$\text{Planck time} = \frac{\hbar G^{1/2}}{c^5} \approx 5.4 \times 10^{-44} \text{s}$$

$$\text{Planck mass} = \frac{\hbar c^{1/2}}{G} \approx 2.2 \times 10^{-8} \text{kg}.$$

Additionally, the Theory of General Relativity deals with gravity as a quantum effect. Improvements in the uncertainty of G should provide improvements in the study of General Relativity.

To conclude, G is an important quantity within the study of our physical world across all scales of investigation from the smallest quantum effects to overarching evolution of our universe. That G is so poorly defined affects our ability to distill knowledge across the entire breadth of scientific inquiry.

1.2   Crisis in Measuring Big G

Prior to the publications of Cavendish [1], measurements of G involved use of the Earth as a test mass. Gillies [14] notes many experiments involving the deflection of taught lines in the presence of mountains. However, Cavendish used a torsion balance to measure gravitational forces between test masses in a laboratory setting. His specific innovation was to measure gravitational effects orthogonal to the acceleration of gravity toward the earth. In doing so, he was able to remove the effects of the Earth's gravity and precisely measure the effects of gravitational attraction between relatively small test masses. Cavendish was attempting to ascertain the density of the Earth, but this afforded the estimation of G, upon which subsequent experiments have sought to improve in accuracy.

Since Cavendish published in 1798, the accuracy of the value of G has improved by only two orders of magnitude.

The gravitational force is one of the weaker forces of nature. The electromagnetic attraction between protons and neutrons is 10^40 greater than their gravitational attraction. This makes it difficult to separate the effects of gravitational force from the more dominant forces affecting small masses. Additionally, it is not possible to screen the gravitation effects from matter surrounding an experiment. Third, G is not dependent on any other physical constant, so it's value cannot be estimated from other observations. Finally, the experimental apparatus used to measure G is subjected to measurement errors from non-gravitational forces that must be properly mitigated.

1.3   Techniques to Measure Big G

The torsion balance utilized by Cavendish was constructed utilizing two small masses attached to a wooden rod and suspended from a thin rope. Much greater masses were held near the small masses using a separate suspension system. The force of gravitational attraction could be measured by the angle of deflection between the starting position of the small masses and their final position as they rotated toward the larger masses.

Gillies [14] and Quinn [30] describe multiple methods utilized to measure G subsequent to Cavendish. At the heart of each experimental apparatus is an attempt to influence a small mass using a larger mass. In general, either the deflection or rotation of some component is observed to measure the force of gravitational attraction. Gillies also discusses the physical limitations and sources of error within many such systems.

In more recent times, atom interferometry [33] has promised to measure Big G using unprecedented precision. In general, some property–like time of flight or deflection of the center of mass–of the motion of a gas of cold atoms is studied in the presence of a Test Mass. The cold atom gas can be manipulated and measured using

laser light. The atoms are manipulated in an isolated environment and their masses and energy states are known in advance. Unfortunately, the experiments to date have been disappointing. As recounted by Quinn, atom interferometry experiments to date have yielded far greater ranges of uncertainty than prior experiments. However, the Cold Atom Lab (CAL) [10] will be installed on the International Space Station (ISS) in the near future. Among other features, the CAL can create Bose-Einstein Condensates. With some modification, the CAL could be used as an atom interferometer and measure Big G within the microgravity environment of the ISS. The CAL is expected to maintain temperatures as low as one picoKelvin and run experiments for as long as 20 seconds.

This work documents a proposed atom interferometry experiment that could be feasible in the Cold Atom Laboratory environment to be installed in the International Space Station. However, this work is not a detailed experimental design. Rather the model being described is a tool set to evaluate the feasibility of creating atom interferometry experiments in the CAL for the measurement of Big G. These tools can help estimate the necessary mass and position of a Test Mass to create a measurable influence on clouds of Bose-Einstein Condensates.

Chapter 2 will introduce Bose-Einstein Condensates upon which an atom interferometry experiment is to be based. Chapter 3 will describe the basics of a novel atom interferometry experiment to measure Big G. Chapter 4 will develop the mathematical model for approximating and simulating this experiment. Chapter 5 will describe one technique to visualize one interesting property of the simulated experiment.

CHAPTER 2

BACKGROUND

2.1   Bose-Einstein Condensation

In the theory of quantum mechanics, the state of a system of N particles is described by a many–body wave function, $\Psi(\mathbf{r}_1\,\sigma_1,\ldots,\mathbf{r}_N\,\sigma_N,t)$. The many–body wave function depends, in general, on the space $(\mathbf{r})$ and spin (σ) coordinates of each particle and possibly the time, t. The "spin" of a particle is a characteristic that indicates that a particle possesses an intrinsic magnetic dipole moment. That is, the particle produces its own dipole magnetic field similar to that produced by a loop of current– bearing wire. Just as the magnetic moment of a loop of wire can be related to the orbital angular momentum of the charged particles circulating in the wire, the intrin- sic magnetic moment of elementary particles is viewed as originating from an intrinsic spin angular momentum of the particle.

In the quantum theory of angular momentum [17], the square of a particle's an- gular momentum can only take on the values $j(j+1)\hbar^2$ where the quantum number j can only have either non–negative integer or half–integer values. Elementary particles and aggregates of particles, such as atoms, can be classified into two types: fermions and bosons. Fermions are particles, or aggregates of particles, with half-integer spin while bosons have integer spin angular momentum. Systems of identical fermions behave very differently from systems of identical bosons.

The many–body wave function describing a system of identical fermions must obey the Pauli Exclusion Principle. This principle states that, if the coordinate labels (i.e., space and spin) of any two particles are interchanged, the many–body wave function must change its overall sign. The many–body wave function is anti– symmetric under particle exchange. If the many–body wave function of a system of N identical fermions can be written as the N–fold product of single–particle orbital

functions, then the Pauli Principle can be restated that no two identical fermions can occupy the same single–particle (which may include both space and spin variables) quantum state. One familiar example of the effect of this principle is the way atoms are denoted in the periodic table of the elements. The ground state of an atom in the periodic table is denoted by its *configuration*. For example, the ground–state configuration of carbon is written as $1s^2 2s^2 2p^2$. This notation means that the each of the six electrons in the carbon atom is placed in a single–particle orbital, such as $\psi_{1s}(\mathbf{r})$, with its spin–1/2 z projection either "spin–up" or "spin–down". No two carbon electrons occupy both the space orbital and spin state in the carbon ground state so that $1s^2$ refers to two carbon electrons occupying the $\psi_{1s}(\mathbf{r})$ orbital, one with spin–up and the other with spin–down.

The many–body wave function describing system of identical bosons must *not* change sign when the space and spin labels of any pair of particles is interchanged. The many–body wave function must be symmetric under particle exchange. In the single–particle view where the many–body wave function is the N–fold product of single–particle orbitals, there is no restriction on the number of bosonic particles that can occupy the same single–particle state. In fact, as will become clear later, bosonic particles in equilibrium prefer to occupy the same single–particle orbital since this is an effective way to lower the total energy of the system.

Atoms are systems of electrons, protons, and neutrons that can exhibit, in aggregate, either bosonic or fermionic character. Electrons, protons, and neutrons are, themselves, fermions. A neutral atom will be either a boson or a fermion depending on whether the total number of electrons, protons, and neutrons is even or odd. According the rules [17] for adding quantum angular momenta, the total angular momentum of a system of two half–integer angular momenta has integer character. Thus, if the total number of electrons, protons, and neutrons in an atom is even, the

atom is a boson. If the total number is odd, the atom is a fermion.

For example, the lithium atom has two isotopes with large relative abundances: ^{6}Li and ^{7}Li. Lithium has atomic number $Z = 3$ which counts the number of protons and the superscripted number is the nucleon number which counts the total number of protons and neutrons. Thus neutral ^{6}Li has three protons, three neutrons, and three electons making a total of nine particles. This makes ^{6}Li a fermionic atom. On the other hand ^{7}Li has one more neutron for a total of ten particles and so ^{7}Li is a boson.

A **Bose–Einstein condensate** or BEC is a system of N identical bosonic particles (either elementary or aggregate) where all of the particles occupy the same single–particle orbital. Bose–Einstein condensates form an essential part of the explanation of phenomena such as superfluidity (fluid flow without viscosity) and superconductivity (electric current flow without resistance) [26]. The case of superconductivity is an interesting example. When certain metals are cooled below a critical temperature, the process by which resistance–free flow of electric current arises is described microscopically by the so–called Bardeen–Cooper–Schrieffer (BCS) theory [23]. In the BCS theory, as the temperature falls, electrons form zero–momentum pairs called "Cooper pairs". This pair of electrons, viewed as a single particle acts like a boson. These bosonic Cooper pairs then undergo Bose–Einstein condensation and so all of the pairs behave identically and flow as a unit thus eliminating the electrical resistance. These examples show how BEC is a general phenomenon that occurs in many different types of systems.

Another system that can undergo Bose–Einstein condensation is a gas of identical bosonic atoms. If the gas is cold enough and dense enough, then condensation can occur. The general criterion for this to happen can be understood using the concept of "matter waves". The basic result of the theory of quantum mechanics is that

matter, just like light, can have wave–like properties. This concept was introduced in the 1924 PhD thesis of Louis Victor deBroglie. There deBroglie introduced the concept of matter waves and suggested that the matter or deBroglie wavelength of a "particle" could be written as $\lambda = 2\pi\hbar/p$ where $\hbar$ is Planck's constant and p is the magnitude of the particle's momentum (mass times velocity).

Using this concept, Satyendranath Bose [24] and then Albert Einstein [25] suggested in 1925 that particles in a gas could be cooled and confined to form a condensate. The cooling lowers the average speed and thus the momentum of the particles which in turn increases their matter wavelength. If these particles are simultaneously confined, then the volume per particle decreases. Eventually the matter waves of neighboring particles begin to overlap at which point the BEC phenomenon occurs and the system falls into the BEC state where the matter–wave shapes of all the particles is the same.

The first laboratory gaseous BEC of atoms was formed in 1995 by Eric Cornell and Carl Weiman at JILA. JILA, formerly known as the Joint Institute for Laboratory Astrophysics, is an institute run jointly by the University of Colorado at Boulder and the National Institute of Standards and Technology (NIST). A a gas of rubidium atoms (^{87}Rb) was first trapped and cooled using laser beams and then transferred to a magnetic trap. The gas was further cooled by a process known as evaporative cooling, similar to cooling soup by blowing on it. When the gas was cold enough ($T \approx 170$ nK) and dense enough ($\rho \approx 10^{14}$ atoms/cm^3), a BEC of about 2000 atoms was formed. The 2001 Nobel Prize in Physics was awarded for this work and to Wolfgang Ketterle at MIT for his demonstration of important properties of BECs.

BECs exhibit quantum properties on a macroscopic scale and are easy to control and probe making them useful for studying a wide range of quantum phenomena. This includes quantum interference between two condensates, which is a matter analogue

to interference of light due to the particle-wave duality. Studies of superfluidity, slowing of light pulses to very slow speeds, modeling black holes, and optical lattices of overlapping laser light fields have all been enabled or enhanced by BEC research [26]. Studies of optical coherence and interaction have direct analogs in BECs [28], allowing cross pollination of research between fields.

2.2 Mathematics of Quantum Mechanics

In the standard version of quantum mechanics, the state of a quantum system is described by a square–integrable wave function [17]. A measurable quantity, $\mathcal{A}$, is represented by an operator, $\hat{A}$, that acts on members of the space of valid quantum mechanical wave functions. These operators are required to be linear and hermitian and to possess a complete set of eigenvectors.

$$\hat{A}\psi_n = a_n\psi_n, \quad n = 1, 2, \ldots \tag{2.1}$$

The completeness property of the set of eigenvectors means that this set spans the space of wave functions capable of representing a state of the system. The theory predicts the outcomes of measurements by postulating that the only possible result of a measurement is one of the eigenvalues of the operator associated with the quantity measured. The hermiticity property of these operators guarantees that its eigenvalues will be real numbers. This is an important attribute of predicted measurement outcomes. If the wave function of the system at the time of measurement is known, the theory can also predict the probability of obtaining a particular eigenvalue, say a_m, when $\mathcal{A}$ is measured.

Another postulate of the theory is that, immediately after the measurement of the quantity $\mathcal{A}$ in which the outcome turns out to be eigenvalue a_m, the wave function of the system is the associated eigenvector, ψ_m. This postulate provides the

initial condition for the equation that governs the evolution of the system between measurements.

The equation postulated by quantum mechanics to govern the system evolution between measurements is the time–dependent Schrödinger equation (TDSE). For a system of N identical particles, this equation can be written as

$$i\hbar\frac{\partial}{\partial t}\Psi(\mathbf{r}_1,\ldots,\mathbf{r}_N,t) = \hat{H}_{MB}\Psi(\mathbf{r}_1,\ldots,\mathbf{r}_N,t),\qquad(2.2)$$

where $\hat{H}_{MB}$ is the operator that represents the total energy of the system and is called the Hamiltonian. The Hamiltonian for many–body systems of N identical particles that will be considered in this thesis takes the general form

$$\hat{H}_{MB} = \sum_{j=1}^{N}\left[-\frac{\hbar^2}{2M}\nabla_j^2 + V(\mathbf{r}_j,t)\right] + \sum_{j<k}V_{\text{int}}(\mathbf{r}_j,\mathbf{r}_k).\qquad(2.3)$$

The first term in the Hamiltonian is the sum over the kinetic energies of the individual particles; the second term is the sum over the potential energies of the particles; and the last term represents pairwise interactions and is a double sum over all pairs of particles with no self–interaction. In modeling interactions in Bose–Einstein–condensed systems, only binary scattering of particles will be considered here.

The wave function solution of the many–body TDSE must also satisfy the normalization condition:

$$\langle\Psi|\Psi\rangle \equiv \int d^3r_1\ldots\int d^3r_N\Psi^*(\mathbf{r}_1,\ldots,\mathbf{r}_N,t)\Psi(\mathbf{r}_1,\ldots,\mathbf{r}_N,t) = 1.\qquad(2.4)$$

Note that the above notation implies integration over all $3N$–dimensional space and that an asterisk superscript denotes complex conjugation in the physics literature. This condition ensures that the sum of the predicted probabilities of outcomes of a particular measurement will be unity.

2.3   Modeling Bose-Einstein Condensates

The many–body TDSE stated above is a completely intractable mathematical problem to solve. The only way to make progress in modeling a gas of N identical bosonic atoms is to resort to an approximation. One important method of approximating the solution of the TDSE is called the Variational Method [17]. In this method a specific form for the wave function solution of the many–body TDSE is assumed which contains parameters that can be varied. This "trial" wave function is inserted into the energy functional given by

$$E\left[\Psi\right] \equiv \frac{\langle\Psi|\left(i\hbar\frac{\partial}{\partial t} - \hat{H}_{MB}\right)|\Psi\rangle}{\langle\Psi|\Psi\rangle}. \tag{2.5}$$

The functional is minimized by demanding that the first variation vanish:

$$E[\Psi + \delta\Psi] - E[\Psi] = 0. \tag{2.6}$$

In order to carry out this procedure the scattering of pairs of atoms in the condensate must be modeled and a trial wave function devised.

The atoms in a Bose–Einstein condensate interact by pairwise collisions. The atoms participating in such a collision are both cold (i.e., slow–moving) and dilute (i.e., always far apart). Under these circumstances the scattering process that occurs can be described as a "contact interaction" in which the interaction potential is modeled as a Dirac delta function of the positions of the scattering atoms. The pairwise interaction potential appearing in $\hat{H}_{MB}$ thus takes the form [28]

$$V_{\text{int}}(\mathbf{r}_j, \mathbf{r}_k) = g\,\delta(\mathbf{r}_j - \mathbf{r}_k) \tag{2.7}$$

where

$$g = \frac{4\pi\hbar^2 a}{M}. \tag{2.8}$$

Here M is the mass of a condensate atom and a is the scattering length. The scattering length measures the strength of the atom–atom scattering in a cold, dilute gas of

identical bosonic atoms. If $a > 0$, the atoms repel each other on average and, if $a < 0$, atoms attract. More details on the binary scattering of atoms under these conditions can be found in Ref. [26]. The delta–function interaction potential is a pseudo–potential model that mimics the result that, for scattering of low–energy atoms that never get close together, the characteristics of the scattering are independent of the details of the true interaction.

With this form of the interaction potential, the many–body Hamiltonian reads as follows.

$$\hat{H}_{MB} = \sum_{j=1}^{N} \left[-\frac{\hbar^2}{2m} \nabla_j^2 + V(\mathbf{r}_j, t) \right] + g \sum_{j<k} \delta(\mathbf{r}_j - \mathbf{r}_k) \tag{2.9}$$

A BEC is a gas of identical bosonic atoms all of which are in the same single–particle state. If we denote the wave function for this single–particle state as $\phi(\mathbf{r}, t)$, then a natural trial wave function for the BEC is the N–fold product of this wave function evaluated at the location of each of the N atoms:

$$\Psi(\mathbf{r}_1, \mathbf{r}_2, \cdots, \mathbf{r}_N, t) = \prod_{i=1}^{N} \phi(\mathbf{r}_i, t). \tag{2.10}$$

Where, in the variational method, $\phi(\mathbf{r}, t)$ is allowed to vary arbitrarily except that the many–body wave function must remain normalized. This places the following condition on $\phi(\mathbf{r}, t)$:

$$
\begin{aligned}
\langle \Psi | \Psi \rangle &= \int d^3 r_1 \ldots \int d^3 r_N \Psi^*(\mathbf{r}_1, \ldots, \mathbf{r}_N, t) \Psi(\mathbf{r}_1, \ldots, \mathbf{r}_N, t) \\
&= \int d^3 r_1 \ldots \int d^3 r_N \left(\prod_{i=1}^{N} \phi(\mathbf{r}_i, t) \right)^* \left(\prod_{j=1}^{N} \phi(\mathbf{r}_j, t) \right) \\
&= \prod_{j=1}^{N} \left(\int d^3 r_j \phi^*(\mathbf{r}_j, t) \phi(\mathbf{r}_j, t) \right) \\
&= \left(\int d^3 r \, \phi^*(\mathbf{r}, t) \phi(\mathbf{r}, t) \right)^N = 1, \\
&\implies \int d^3 r \, \phi^*(\mathbf{r}, t) \phi(\mathbf{r}, t) = 1. \tag{2.11}
\end{aligned}
$$

Inserting this trial wave function into the energy functional, computing the first variation and setting it to zero yields the nonlinear Schrödinger equation:

$$i\hbar\frac{\partial}{\partial t}\phi(\mathbf{r},t) = -\frac{\hbar^2}{2m}\nabla^2\phi(\mathbf{r},t) + V_{\text{trap}}(\mathbf{r},t)\phi(\mathbf{r},t) + g(N-1)\left|\phi(\mathbf{r},t)\right|^2\phi(\mathbf{r},t). \quad (2.12)$$

The details of this can be found abundantly in the literature and in textbooks [26, 28] and so will not be reproduced here.

In most cases $N \gg 1$ so we approximate $N - 1 \approx N$. This yields the **Gross–Pitaevskii (GP) equation** :

$$\boxed{i\hbar\frac{\partial}{\partial t}\phi(\mathbf{r},t) = -\frac{\hbar^2}{2m}\nabla^2\phi(\mathbf{r},t) + V_{\text{trap}}(\mathbf{r},t)\phi(\mathbf{r},t) + gN\left|\phi(\mathbf{r},t)\right|^2\phi(\mathbf{r},t)} \quad (2.13)$$

This is the basic theoretical tool that is used to analyze and predict the behavior of gaseous Bose–Einstein condensates of atoms. It assumes that there are exactly N atoms in the gas and that its temperature is absolute zero. Even though reaching absolute zero is forbidden by the Third Law of Thermodynamics, most laboratory BECs can created at temperatures < 100 nK (nano–Kelvin) which is usually a good approximation.

2.4   Solving the Gross-Pitaevskii Equation

One method to numerically solve the Gross-Pitaevskii Equation (GPE) is to implement a split-step Crank-Nicolson method [11] and [19]. This is an example of a grid method, which discretizes time and space to solve the GPE. This scheme splits the Hamiltonian into derivative (Eq. 2.16) and non-derivative (Eq. 2.15) portions with known initial conditions.

$$H = H_1 + H_2 + H_3 + H_4 \quad (2.14)$$

$$H_1 = V_{\text{trap}}(\mathbf{r},t) + gN|\phi(\mathbf{r},t)|^2 \quad (2.15)$$

$$H_2 = -\frac{\hbar^2}{2m}\frac{\partial^2}{\partial x}$$

$$H_3 = -\frac{\hbar^2}{2m}\frac{\partial^2}{\partial y}$$

$$H_3 = -\frac{\hbar^2}{2m}\frac{\partial^2}{\partial z} \tag{2.16}$$

Using these split Hamiltonians we split the GPE into four equations.

$$i\hbar\frac{\partial}{\partial t}\phi(\mathbf{r},t) = H_1\phi(\mathbf{r},t) \tag{2.17}$$

$$i\hbar\frac{\partial}{\partial t}\phi(\mathbf{r},t) = H_2\phi(\mathbf{r},t) \tag{2.18}$$

$$i\hbar\frac{\partial}{\partial t}\phi(\mathbf{r},t) = H_3\phi(\mathbf{r},t) \tag{2.19}$$

$$i\hbar\frac{\partial}{\partial t}\phi(\mathbf{r},t) = H_4\phi(\mathbf{r},t) \tag{2.20}$$

We discretize our valuations over t using many steps of step size Δ. Thus, any time step may be known as $t_n = t_0 + n\Delta$, where t_0 is our initial time. We also must know the initial condition $\phi(x,y,z,0)$.

Given a time step n, we wish to solve for a new time step $n+1$. First, we find an intermediate solution to Eq. 2.17 we label $\phi^{n+\frac{1}{2}}$. We label the operator responsible for evolving the solution as X_{nd}, for "non-derivative".

$$\phi^{n+\frac{1}{2}} = X_{nd}(H_1)\phi^n \equiv e^{-i\Delta H_1}\phi^n \tag{2.21}$$

Next, we use the intermediate solution $\phi^{n+\frac{1}{2}}$ as an initial solution in a Crank-Nicolson step. We label the operator responsible for evolving the solution as X_{CN}, for "Crank-Nicolson".

$$\phi^{n+1} = X_{CN}(H_4)X_{CN}(H_3)X_{CN}(H_2)\phi^{n+\frac{1}{2}} \tag{2.22}$$

$$\equiv \left(\frac{1-i\Delta H_4/2}{1+i\Delta H_4/2}\right)\left(\frac{1-i\Delta H_3/2}{1+i\Delta H_3/2}\right)\left(\frac{1-i\Delta H_2/2}{1+i\Delta H_2/2}\right)\phi^{n+\frac{1}{2}} \tag{2.23}$$

Therefore, the final solution of the time propagation is the combination of Eqs. 2.21 and 2.23. This propagates the time from t_n to t_{n+1}.

$$\phi^{n+1} = X_{CN}(H_4)X_{CN}(H_3)X_{CN}(H_2)X_{nd}(H_1)\phi^n \tag{2.24}$$

By allowing Δ to remain very small, we preserve the normality of the wave function if propagating in real valued time. The errors in the terms are proportional to Δ^2 and may be ignored. Finally, the non-linear term $gN|\phi(\mathbf{r},t)|^2$ is not present in the Crank-Nicolson terms, which improves numeric stability and helps the solutions to converge.

Next, the scheme must be applied over space. The space is discretized into a grid along all space coordinates with step size h. The symmetry and dimensionality of the trap potential term in the GPE determines the shape of the grid. We will defer descriptions to the relevant literature [19] to discuss the different Crank-Nicolson schemes that can be employed to evaluate the discretized space. The schemes are typified by taking differences between the next time step and the intermediate time step, solving to find an equation for the next time step, and solving over all points in the discretized grid. The error of the full solution is second order in both the time step, Δ, and the space step, h. If these values are very small, the error terms are negligible.

2.5 Issues With Grid Methods

2.5.1 Require too much storage

We can demonstrate the computational requirements required to employ a grid method, like the split-step Crank-Nicolson scheme, using published examples [20] investigating Bose-Einstein Condensates. The computational requirements to evaluate the wave

function over a grid are typified by the following parameters.

1. A grid is established in three dimensions, with each grid position indexing a spacial coordinate, $\mathbf{r}_{ijk}$. The grid dimensions are N_x, N_y, N_z, representing the total length in each spacial dimension. Thus, the total number of grid points is $N_{total} = N_x N_y N_z$.

2. The wave function is evaluated at each (x, y, z) point, yielding a complex number. On commodity computer hardware a complex number requires 16 bytes, represented as a pair of 8 byte floating point values.

3. The wave function is evaluated over many small time steps T_{total}. In the example work, about 1% of the total time steps are actually stored for further processing.

The published examples are typified by grids with dimensions $N_x = 400$, $N_y = 400$, and $N_z = 200$ for $N_{total} = 32,000,000$ points. Each of these grids require $16\text{bytes} \times N_{total} = 512\,\text{MB}$ to store just the wave function values. Retaining 100 of the calculated time steps requires $\approx 50\,\text{GB}$ of wave function values to be stored. Additional storage is required for other values derived from the wave function, such as the density, velocity, or phase.

Current commodity storage hardware is easily capable of capturing several such runs. However, increasing the grid size or number of time steps requires a far greater increase in total storage. Finally, maintaining long term backups or archives of such information is a challenge on commodity hardware.

Therefore, a technique is desired to capture more granular data with far less storage demands.

2.5.2   Require too much time

Each time step is required to be very small since the error terms are the square of the step size. As described above, the resulting data from evaluating the spacial grid at each time step is impractical to store for all time steps. The complete evaluation requires on the order of days to complete, but only a small percentage of the total evaluations are retained for further processing. Additionally, the time to write to storage is a not-insignificant part of the total time for each evaluation.

Therefore, a technique is desired that requires less time to capture equivalent or better time-series. It is also desirable to avoid evaluating data that is not stored for further processing.

CHAPTER 3

ATOM INTERFEROMETRY

An interferometer is a device that uses the phenomenon of interference as a method of measurement. An example of this is the celebrated Michelson interferometer [18] used to measure the Earth's velocity relative to the ether. In this device, a light beam is split into two perpendicular pathways by a beam splitter and the two beams are re–joined at another beam splitter. This produces two final beams each of which is a superposition of beams that went via the two different pathways. Any difference between the environments of the two pathways causes a relative phase shift between the light beams. This gives rise to an interference pattern that can be used for measurement.

The basic message of quantum mechanics is that matter, like light, can have wave–like properties. Thus it is possible to make a matter–wave interferometer [33]. This is especially the case for systems of Bose–Einstein condensed atoms. Condensates can be split, rejoined, and split again [12] and the final clouds will consist of parts that traveled both pathways and can exhibit interference. In this chapter we describe an atom–interferometric scheme suitable for a precision measurement of Big G in the Cold Atom Laboratory aboard the International Space Station.

3.1 Proposed Atom Interferometer

Figure 3.1 displays the proposed sequence of events for a novel atom interferometer based on a Bose-Einstein Condensate. The scheme involves several events to measure Big G. For the sake of description, we'll assume only two clouds are split from the initial condensate. It is possible to create many clouds depending on the laser pulse used to split the initial condensate and our mathematical model will include this possibility.
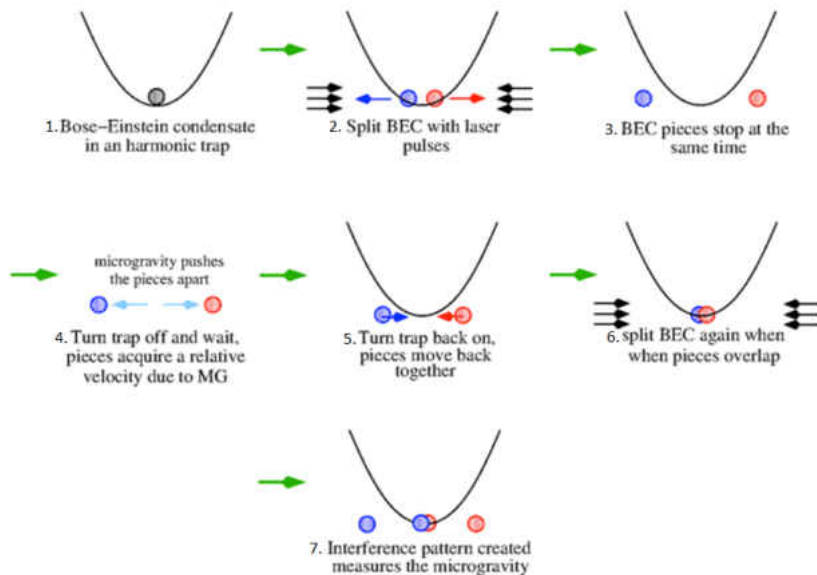
Figure 3.1: Sequence of events in proposed atom interferometer experiment. This sequence is repeated many times with a Test Mass (not shown) and without.

1. **Initial Condensate:** Condensate at rest within a harmonic potential. The number of atoms, N, is assumed to be known as is the quantum state of the condensate.

2. **Initial split:** The condensate is split using a laser pulse. Two or more condensate clouds move apart with velocity $+v$ and $-v$. We assume the clouds have the same number of atoms and do not interact.

3. **Separation:** The clouds are allowed to move further apart, being slowed by the harmonic potential, which acts as a restoring force, pulling the clouds back toward the center of the trap. The clouds should be allowed to separate until they are stationary.

4. **Evolution:** The harmonic potential is turned off. This allows the clouds to evolve independently for a period of time. The clouds are assumed to not interact at

this distance.

5. **Overlap:** The harmonic potential is restored, pulling the clouds back to the center of the trap where they encounter each other and overlap.

6. **Final Split:** The clouds are split again, which doubles the number of clouds from the initial split. Half of the clouds remain overlapped near the center of the trap. The other halves move apart as in the initial split.

7. **Interference:** Properties of the overlapped central clouds can be measured.

The sequence of events is repeated many times to average out the effects of random errors. The average of the effects provides a baseline measurement for the experiment. Next, we modify the experiment by adding a Test Mass. The range of motion of the clouds with respect to the initial condensate should be much smaller versus the distance to the Test Mass. The sequence of events is repeated again, many times, to obtain an average measurement of perturbations due to the Test Mass. The measurements with and without the Test Mass are compared to determine the influence attributed to the force of gravitational attraction to the Test Mass.

The Test Mass will have an attractive effect on all clouds in the system, pulling them towards the Test Mass. As gravitational force obeys an inverse square distance law, the clouds closer to the Test Mass will experience more attraction and be perturbed to a greater degree. It is expected this difference in perturbation is expressed in properties of the system during the overlap of the clouds in the Interference event. The overlap should appear different when comparing the properties with and without a Test mass. The position of the Test Mass can be chosen to enhance the non-symmetric effect.

3.2 Measuring Big G

Recall Newton's Equation for the Force of Gravity for this system,

$$F_G = G\frac{M_{TM}\,M}{|\mathbf{r}_{TM} - \mathbf{r}|^2} \tag{3.1}$$

where M_{TM} is the mass of the Test Mass and M is the mass of a condensate atom. The positions $\mathbf{r}_{TM}$ and $\mathbf{r}$ locate the center of mass of the Test Mass and an atom, respectively. It is assumed that $M_{TM} \gg m$ and $|\mathbf{r}_{TM}| \gg |\mathbf{r}|$. We also assume that point masses are sufficient to model the clouds and the Test Mass. We also assume that we can ignore the gravitational attraction between clouds. An F_G force term is required for each cloud created in the Initial Split and Final Split.

Big G should be derivable from measurements of properties of the of the overlapped clouds during the Interference event.

Center of Mass: When the clouds overlap, the center of mass for the overlapped clouds should be deflected relative to the center of mass from the initial condensate. This deflection should correspond to the force of gravitational attraction experienced by the two clouds in the direction of the Test Mass.

Interference: Much like the double-slit experiment [34] reveals the particle-wave duality of light, the overlapping clouds create matter wave interference patterns from the differences in relative velocities.

In an actual experiment, these properties are measured by imaging the clouds. Each image requires a new Bose-Einstein Condensate to be created and evolved through the events of the Atom Interferometry experiment. Each image captures the shadow from light being blocked by the condensate atoms; darker portions indicate higher density. The light destroys the quantum system so a new condensate must be created, evolved, and imaged for each time step being observed. It is expected

that variations in M_{TM} and $\mathbf{r}_{TM}$ should yield variations in the images that can be compared to measure the properties listed above. From these comparisons Big G can be derived.

As an order-of-magnitude approximation, we can derive Big G from an estimate of the Newtonian Equations of Motion. We assume the cloud centers move in one dimension, x. We also assume that we can measure the difference in the cloud centers during the Final Split with and without a Test Mass present. From Newton's Second Law, we know $F = ma \rightarrow a = \frac{F}{m}$. By rearranging Eq. 3.1, we can find the acceleration due to gravity. Additionally, we simplify the denominator by ignoring $\mathbf{r}$ as $|\mathbf{r}_{TM}| \gg |\mathbf{r}|$.

$$a_G = \frac{F_G}{M} = G\frac{M_{TM}}{|\mathbf{r}_{TM}|^2} \tag{3.2}$$

We assume the time spent in the Evolution phase–in which the trap is turned off–is much greater than the times spent with the trap turned on. The time spent in the Evolution phase is labeled T_D. During the Evolution phase the cloud centers move towards the Test Mass, which should change the acceleration. However, the change in acceleration due to this movement is small, so we assume the acceleration is constant. From Newton's Equations of Motion, we can determine the distance the cloud centers should be moved based on the acceleration due to gravity and the time spent in the Evolution phase. Specifically, we are estimating δx, the difference in the final position of the cloud centers along x with and without the Test Mass.

$$\delta x = \frac{1}{2}a_G T_D^2 \tag{3.3}$$

We can substitute Eq. 3.3 into Eq. 3.2 and solve for G.

$$G \approx \frac{2\delta x |\mathbf{r}_{TM}|^2}{M_{TM}T_D^2} \tag{3.4}$$

This should provide an order-of-magnitude estimate for Big G based on measuring the inputs and results of the Atom Interferometry simulation. This is not a precision measurement. Specifically, we will estimate Big G using a simulation in which Big G is an input parameter. Many assumptions are being made to simplify this analysis and must be accounted for in a proper analysis. Additionally, this analysis utilizes classical Newtonian physics while the system being simulated is quantum.

However, this analysis demonstrates that a visual inspection of the Final Split can provide the necessary information to estimate Big G. Additionally, we demonstrate the relationships that influence the design of a practical experiment: the Test Mass mass and position, the fidelity of measuring the position of the cloud centers, and the time span of the Evolution phase.

3.3   Parameter Estimation And Feasibility

In reality, we do not have a physical experiment with which to measure these effects. Further, as explained in section 2.5, simulating the Atom Interferometry experiment in great detail is expensive and time consuming. What is required is a means to estimate the magnitudes of M_{TM} and $\mathbf{r}_{TM}$ required to produce measurable effects. From Eq. 3.4 we see the magnitudes of these inputs determine the feasibility of the Atom Interferometer experiment to be conducted in the Cold Atom Laboratory on the International Space Station. If M_{TM} is too massive, it is prohibitively expensive to place the Test Mass in orbit as launch costs are on the order of \$10,000 per kilogram. Similarly, $|\mathbf{r}_{TM}|$ is limited by where the experiment can be installed on the ISS. Alternatively, we see that we can trade mass for time in the experiment. Thus, being able to quickly simulate this experiment with variations in M_{TM} and $\mathbf{r}_{TM}$ is a tool to study the feasibility of the experiment. More detailed simulations can provide better estimates based on the initial feasibility results.

The next chapter describes the mathematical model to rapidly simulate the Atom Interferometer with approximate solutions to the Gross-Pitaevskii Equation 2.13. The time-evolution of the model is derived using the Lagrangian Variational Method and a trial wave function based on Gaussian distributions extended with linear and nonlinear phase coefficients [22]. The phase coefficients are necessary to exhibit changes in position over time due to changes in the velocity. This also satisfies the preservation of probability current; probability cannot be created or destroyed over the course of the experiment.

The ISS is not a stationary object relative to observers on Earth. As such, an experiment aboard the station will exist in a rotational frame of reference. We extend the GPE to include terms for the rotational frame as well as effects of a Test Mass.

LVM EQUATIONS OF MOTION FOR THE GROSS–PITAEVSKII EQUATION IN THE ROTATING FRAME

4.1 Derivation of the 3D, N–Gaussian–cloud Lagrangian

4.1.1 The Lagrangian Variational Method

The Lagrangian Variational Method (LVM) can approximate the solutions of the time–dependent Gross–Pitaevskii equation [22] in the rotating frame. This equation has the form [26]:

$$i\hbar\frac{\partial}{\partial t}\Phi(\mathbf{r},t) = -\frac{\hbar^2}{2M}\nabla^2\Phi(\mathbf{r},t) + V_{\text{trap}}(\mathbf{r},t)\Phi(\mathbf{r},t) + gN\left|\Phi(\mathbf{r},t)\right|^2\Phi(\mathbf{r},t)$$
$$+ i\hbar\mathbf{\Omega}\cdot(\mathbf{r}\times\nabla)\,\Phi, \tag{4.1}$$

where $\mathbf{\Omega}$ is the angular velocity of the rotating frame.

The LVM is based on the fact that the GPE can be derived as the Euler–Lagrange equation of motion produced by the following Lagrangian density:

$$\mathcal{L}[\Phi^*,\Phi_x^*,\Phi_y^*,\Phi_z^*,\Phi_t^*] = \frac{i\hbar}{2}\left(\Phi\Phi_t^* - \Phi^*\Phi_t\right) + \frac{\hbar^2}{2M}\left(\Phi_x^*\Phi_x + \Phi_y^*\Phi_y + \Phi_z^*\Phi_z\right)$$
$$+ V(\mathbf{r},t)\Phi\Phi^* + \frac{1}{2}gN(\Phi)^2(\Phi^*)^2 + \Phi\left(\mathbf{\Omega}\cdot\hat{\mathbf{L}}\right)\Phi^*, \tag{4.2}$$

where $\hat{\mathbf{L}}$ is the angular momentum operator whose components are

$$\hat{L}_x = \frac{\hbar}{i}\left(y\frac{\partial}{\partial z} - z\frac{\partial}{\partial y}\right) \quad \hat{L}_y = \frac{\hbar}{i}\left(z\frac{\partial}{\partial x} - x\frac{\partial}{\partial z}\right) \quad \hat{L}_z = \frac{\hbar}{i}\left(x\frac{\partial}{\partial y} - y\frac{\partial}{\partial z}\right). \tag{4.3}$$

This Lagrangian density along with the following Euler–Lagrange equation of motion produces the GPE:

$$\frac{\partial}{\partial t}\left(\frac{\partial\mathcal{L}}{\partial\Phi_t^*}\right) + \frac{\partial}{\partial x}\left(\frac{\partial\mathcal{L}}{\partial\Phi_x^*}\right) + \frac{\partial}{\partial y}\left(\frac{\partial\mathcal{L}}{\partial\Phi_y^*}\right) + \frac{\partial}{\partial z}\left(\frac{\partial\mathcal{L}}{\partial\Phi_z^*}\right) - \frac{\partial\mathcal{L}}{\partial\Phi^*} = 0 \tag{4.4}$$

where

$$\Phi_t \equiv \frac{\partial \Phi}{\partial t}, \dots \text{ etc.} \tag{4.5}$$

The Lagrangian Variational Method consists of devising a *trial* wave function,

$$\Phi^{\text{trial}}(\mathbf{r}, t) = \Phi^{\text{trial}}(q_1(t), \dots, q_n(t); \mathbf{r}) \tag{4.6}$$

where the $\{q_i(t)\}$, $i = 1, \dots, n$ are *variational parameters* that only depend on the time, t. The equations of motion of these variational parameters are derived by computing the ordinary Lagrangian:

$$L(q_1(t), \dots, q_n(t)) = \int d^3r \, \mathcal{L}[(\Phi^{\text{trial}})^*, (\Phi^{\text{trial}})_x^*, (\Phi^{\text{trial}})_y^*, (\Phi^{\text{trial}})_z^*, (\Phi^{\text{trial}})_t^*] \tag{4.7}$$

and then using the ordinary Euler–Lagrange equation,

$$\frac{d}{dt}\left(\frac{\partial L}{\partial \dot{q}_k}\right) - \frac{\partial L}{\partial q_k} = 0, \quad k = 1, \dots, n \tag{4.8}$$

4.1.2   Scaled units

We can simplify the above method by introducing a set of units appropriate to the problem and a set of scaled variables (both independent and dependent). The scaled variables are defined by first establishing a *length unit*, L_0, and then defining energy and time units as follows:

$$E_0 \equiv \frac{\hbar^2}{2ML_0^2} \quad \text{and} \quad T_0 \equiv \frac{\hbar}{E_0} = \frac{2ML_0^2}{\hbar}. \tag{4.9}$$

We then introduce scaled variables which are generally denoted by barred quantities. These consist of scaled space and time coordinates:

$$\bar{x} \equiv \frac{x}{L_0} \quad \bar{y} \equiv \frac{y}{L_0} \quad \bar{z} \equiv \frac{z}{L_0} \quad \text{and} \quad \bar{t} \equiv \frac{t}{T_0}. \tag{4.10}$$

We also introduce the scaled condensate wave function for the solution of the GPE:

$$\Phi(\mathbf{r}, t) = L_0^{-3/2} \Psi(\bar{\mathbf{r}}, \bar{t}). \tag{4.11}$$

We can express the original GPE in terms of scaled quantities and this can be done for the Lagrangian density and its associated Euler–Lagrange equation as well.

In terms of scaled quantities, the GPE becomes:

$$i\frac{\partial \Psi}{\partial \bar{t}} = -\bar{\nabla}^2 \Psi + \bar{V}(\bar{\mathbf{r}}, \bar{t})\Psi + \bar{g}N \left|\Psi\right|^2 \Psi. \tag{4.12}$$

where $g \equiv \bar{g}E_0 L_0^3$ and $\bar{V}(\bar{\mathbf{r}}, \bar{t}) = V(\mathbf{r}, t)/E_0$. The scaled Lagrangian density becomes

$$\begin{aligned}
\bar{\mathcal{L}}\left[\Psi^*, \Psi_{\bar{x}}^*, \Psi_{\bar{y}}^*, \Psi_{\bar{z}}^*\right] &= \frac{i}{2}\left(\Psi\Psi_{\bar{t}}^* - \Psi^*\Psi_{\bar{t}}\right) + \bar{\nabla}\Psi^* \cdot \bar{\nabla}\Psi + \bar{V}(\bar{\mathbf{r}}, \bar{t})\Psi\Psi^* \\
&+ \frac{1}{2}\bar{g}N\left(\Psi^*\right)^2\left(\Psi\right)^2 + i\bar{\Omega}_z\left(\bar{y}\Psi\Psi_x^* - \bar{x}\Psi\Psi_y^*\right)
\end{aligned} \tag{4.13}$$

and the scaled Euler–Lagrange equation is given by

$$\frac{\partial}{\partial \bar{x}}\left(\frac{\partial \bar{\mathcal{L}}}{\partial \Psi_{\bar{x}}^*}\right) + \frac{\partial}{\partial \bar{y}}\left(\frac{\partial \bar{\mathcal{L}}}{\partial \Psi_{\bar{y}}^*}\right) + \frac{\partial}{\partial \bar{z}}\left(\frac{\partial \bar{\mathcal{L}}}{\partial \Psi_{\bar{z}}^*}\right) + \frac{\partial}{\partial \bar{t}}\left(\frac{\partial \bar{\mathcal{L}}}{\partial \Psi_{\bar{t}}^*}\right) - \frac{\partial \bar{\mathcal{L}}}{\partial \Psi^*} = 0. \tag{4.14}$$

Next we turn to the 3D, N_c–Gaussian–cloud trial wave function.

4.1.3 The 3D, N_c–Gaussian–cloud trial wave function

In the 3D, N_c–gaussian–cloud model we take the trial wave function to be a sum of N_c three–dimensional Gaussian clouds. The jth cloud has its own initial momentum, $\bar{\mathbf{k}}_j$ and set of variational parameters. These parameters consist of the cartesian coordinates of the cloud center: $\bar{x}_j$, $\bar{y}_j$, and $\bar{z}_j$; the widths along the x, y, and z directions: $\bar{w}_{jx}$, $\bar{w}_{jy}$, and $\bar{w}_{jz}$; the linear phase coefficients along the x, y, and z directions: $\bar{\alpha}_{jx}$, $\bar{\alpha}_{jy}$, and $\bar{\alpha}_{jz}$; and the quadratic phase coefficients along the x, y, and z directions: $\bar{\beta}_{jx}$, $\bar{\beta}_{jy}$, and $\bar{\beta}_{jz}$. The jth cloud also has its own normalization coefficient, A_j, which will be eliminated by fixing the number of atoms in each cloud.

The mathematical form (in scaled units) of the trial wave function is the following:

$$\Psi(\bar{\mathbf{r}}, \bar{t}) = \frac{1}{\sqrt{N_c}} \sum_{j=1}^{N_c} A_j(\bar{t}) e^{f_j(\bar{\mathbf{r}}, \bar{t}) + i\bar{\mathbf{k}}_j \cdot \bar{\mathbf{r}}} \tag{4.15}$$

where

$$
\begin{aligned}
f_j(\bar{\mathbf{r}}, \bar{t}) &= -\frac{(\bar{x} - \bar{x}_j)^2}{2\bar{w}_{jx}^2} - \frac{(\bar{y} - \bar{y}_j)^2}{2\bar{w}_{jy}^2} - \frac{(\bar{z} - \bar{z}_j)^2}{2\bar{w}_{jz}^2} \\
&+ i\bar{\alpha}_{jx}\bar{x} + i\bar{\alpha}_{jy}\bar{y} + i\bar{\alpha}_{jz}\bar{z} + i\bar{\beta}_{jx}\bar{x}^2 + i\bar{\beta}_{jy}\bar{y}^2 + i\bar{\beta}_{jz}\bar{z}^2 \\
&= \sum_{\eta=x,y,z} \left(-\frac{(\bar{\eta} - \bar{\eta}_j)^2}{2\bar{w}_{j\eta}^2} + i\bar{\alpha}_{j\eta}\bar{\eta} + i\bar{\beta}_{j\eta}\bar{\eta}^2 \right)
\end{aligned} \tag{4.16}
$$

We can write the trial wave function entirely in terms of coordinates as follows:

$$
\begin{aligned}
\Psi(\bar{\mathbf{r}}, \bar{t}) &= \frac{1}{\sqrt{N_c}} \sum_{j=1}^{N_c} A_j(\bar{t}) \exp\left\{ \sum_{\eta=x,y,z} \left(-\frac{(\bar{\eta} - \bar{\eta}_j)^2}{2\bar{w}_{j\eta}^2} + i\left(\bar{\alpha}_{j\eta} + \bar{k}_{j\eta}\right)\bar{\eta} + i\bar{\beta}_{j\eta}\bar{\eta}^2 \right) \right\} \\
&= \frac{1}{\sqrt{N_c}} \sum_{j=1}^{N_c} A_j(\bar{t}) \prod_{\eta=x,y,z} \exp\left\{ -\frac{(\bar{\eta} - \bar{\eta}_j)^2}{2\bar{w}_{j\eta}^2} + i\left(\bar{\alpha}_{j\eta} + \bar{k}_{j\eta}\right)\bar{\eta} + i\bar{\beta}_{j\eta}\bar{\eta}^2 \right\} \\
&\equiv \frac{1}{\sqrt{N_c}} \sum_{j=1}^{N_c} A_j(\bar{t}) \prod_{\eta=x,y,z} e^{f_{j\eta}(\bar{\eta},\bar{t}) + i\bar{k}_{j\eta}\bar{\eta}} \\
&= \frac{1}{\sqrt{N_c}} \sum_{j=1}^{N_c} A_j(\bar{t}) \exp\left\{ \sum_{\eta=x,y,z} \left(f_{j\eta}(\bar{\eta},\bar{t}) + i\bar{k}_{j\eta}\bar{\eta} \right) \right\}
\end{aligned}
$$

$$\tag{4.17}$$

where

$$
f_{j\eta}(\bar{\eta}, \bar{t}) \equiv -\frac{(\bar{\eta} - \bar{\eta}_j)^2}{2\bar{w}_{j\eta}^2} + i\bar{\alpha}_{j\eta}\bar{\eta} + i\bar{\beta}_{j\eta}\bar{\eta}^2. \tag{4.18}
$$

We can calculate the Lagrangian associated with this trial wave function by integrating $\bar{\mathcal{L}}$ over all space:

$$
\bar{L}\left(\left\{ \bar{\mathbf{r}}_{\mathbf{j}}, \bar{\mathbf{w}}_{\mathbf{j}}, \bar{\alpha}_{\mathbf{j}}, \bar{\beta}_{\mathbf{j}} \right\}_{j=1}^{N_c} \right) = \int_{-\infty}^{\infty} d\bar{x} \int_{-\infty}^{\infty} d\bar{y} \int_{-\infty}^{\infty} d\bar{z} \, \bar{\mathcal{L}}\left[\Psi^*, \Psi_{\bar{x}}^*, \Psi_{\bar{y}}^*, \Psi_{\bar{z}}^* \right]. \tag{4.19}
$$

The equation of motion for a given variational parameter, $q_j(\bar{t})$, is then given by the ordinary Euler–Lagrange equation:

$$
\frac{\partial}{\partial \bar{t}} \left(\frac{\partial \bar{L}}{\partial \dot{q}_j} \right) - \frac{\partial \bar{L}}{\partial q_j} = 0, \quad j = 1, \ldots, N_c. \tag{4.20}
$$

With these tools in hand we can now compute the Lagrangian.

The rotating–frame Lagrangian has five terms and can be written as follows.

$$\bar{L} = \bar{L}_1 + \bar{L}_2 + \bar{L}_3 + \bar{L}_4 + \bar{L}_5 \tag{4.21}$$

where

$$
\begin{aligned}
\bar{L}_1 &\equiv \frac{i}{2} \int_{-\infty}^{\infty} d\bar{x} \int_{-\infty}^{\infty} d\bar{y} \int_{-\infty}^{\infty} d\bar{z} \left(\Psi \Psi_{\bar{t}}^* - \Psi^* \Psi_{\bar{t}} \right) \\
\bar{L}_2 &\equiv \int_{-\infty}^{\infty} d\bar{x} \int_{-\infty}^{\infty} d\bar{y} \int_{-\infty}^{\infty} d\bar{z} \, \bar{\nabla} \Psi^* \cdot \bar{\nabla} \Psi \\
\bar{L}_3 &\equiv \int_{-\infty}^{\infty} d\bar{x} \int_{-\infty}^{\infty} d\bar{y} \int_{-\infty}^{\infty} d\bar{z} \, \bar{V}(\bar{\mathbf{r}}, \bar{t}) \Psi \Psi^* \\
\bar{L}_4 &\equiv \frac{1}{2} \bar{g} N \int_{-\infty}^{\infty} d\bar{x} \int_{-\infty}^{\infty} d\bar{y} \int_{-\infty}^{\infty} d\bar{z} \left(\Psi^* \right)^2 \left(\Psi \right)^2 \\
\bar{L}_5 &\equiv i \bar{\Omega}_z \int_{-\infty}^{\infty} d\bar{x} \int_{-\infty}^{\infty} d\bar{y} \int_{-\infty}^{\infty} d\bar{z} \, \Psi \left(\bar{y} \Psi_x^* - \bar{x} \Psi_y^* \right)
\end{aligned}
\tag{4.22}
$$

Next we derive, in turn, the value of each of these terms and then put together the full Lagrangian.

4.1.4 Constraints on the trial wave function

Here we make several assumptions about the physical system which have material effects on the values of the variational parameters. These are as follows:

1. We assume that each of the N_c clouds are moving at sufficiently different velocities such that any integral of a quantity containing a factor like $e^{i\left(\bar{k}_{j\eta} - \bar{k}_{j'\eta}\right)\bar{\eta}}$ where $j \neq j'$ can be neglected. If the clouds move with sufficiently different velocities, these factors will be rapidly oscillating and their integrals can be neglected.

2. The $A_j(\bar{t})$ are real for all j. This derives from the assumption that the system is a single condensate and has an overall constant phase.

3. The number of atoms in each cloud is fixed. Clouds do not exchange atoms. This plus the normalization condition, fixes a relationship (derived below) between A_j and the widths $\bar{w}_{j\eta}$ where $\eta = x, y, z$.

We can use these assumptions plus the normalization condition on the trial wave function to derive conditions that constrain the values of the A_j.

To find these conditions we require that the full trial wave function be normalized to unity:

$$
\begin{aligned}
1 &= \int d^3\bar{r} \, |\Psi(\bar{\mathbf{r}}, \bar{t})|^2 \\
&= \int d^3\bar{r} \left(\frac{1}{\sqrt{N_c}} \sum_{j=1}^{N_c} A_j(\bar{t}) \exp\left\{ \sum_{\eta=x,y,z} \left(f_{j\eta}(\bar{\eta}, \bar{t}) + i\bar{k}_{j\eta}\bar{\eta} \right) \right\} \right)^* \\
&\quad \times \left(\frac{1}{\sqrt{N_c}} \sum_{j'=1}^{N_c} A_{j'}(\bar{t}) \exp\left\{ \sum_{\eta=x,y,z} \left(f_{j'\eta}(\bar{\eta}, \bar{t}) + i\bar{k}_{j'\eta}\bar{\eta} \right) \right\} \right) \quad (4.23)
\end{aligned}
$$

We can simplify the above integral by dropping all of the terms in the product $\Psi^*\Psi$ that contain rapidly oscillating exponentials such as $e^{i(\bar{k}_{j\eta} - \bar{k}_{j'\eta})\bar{\eta}}$ where $j \neq j'$. In this case our normalization condition simplifies to

$$
\begin{aligned}
1 &= \frac{1}{N_c} \int d^3\bar{r} \left(\sum_{j=1}^{N_c} A_j^2(\bar{t}) \exp\left\{ \sum_{\eta=x,y,z} \left(f_{j\eta}(\bar{\eta}, \bar{t}) + f_{j\eta}^*(\bar{\eta}, \bar{t}) \right) \right\} \right) \\
&= \frac{1}{N_c} \sum_{j=1}^{N_c} A_j^2(\bar{t}) \int d^3\bar{r} \exp\left\{ \sum_{\eta=x,y,z} \left(f_{j\eta}(\bar{\eta}, \bar{t}) + f_{j\eta}^*(\bar{\eta}, \bar{t}) \right) \right\} \\
&= \frac{1}{N_c} \sum_{j=1}^{N_c} A_j^2(\bar{t}) \int d^3\bar{r} \exp\left\{ \sum_{\eta=x,y,z} \left(-\frac{(\bar{\eta} - \bar{\eta}_j)^2}{\bar{w}_{j\eta}^2} \right) \right\} \\
&= \frac{1}{N_c} \sum_{j=1}^{N_c} A_j^2(\bar{t}) \prod_{\eta=x,y,z} \int_{-\infty}^{\infty} d\bar{\eta} \exp\left\{ -\frac{(\bar{\eta} - \bar{\eta}_j)^2}{\bar{w}_{j\eta}^2} \right\} \\
&= \frac{1}{N_c} \sum_{j=1}^{N_c} A_j^2(\bar{t}) \prod_{\eta=x,y,z} \left(\pi^{1/2} \bar{w}_{j\eta} \right) \\
1 &= \frac{1}{N_c} \sum_{j=1}^{N_c} A_j^2(\bar{t}) \left(\pi^{3/2} \bar{w}_{jx}(\bar{t}) \bar{w}_{jy}(\bar{t}) \bar{w}_{jz}(\bar{t}) \right) \quad (4.24)
\end{aligned}
$$

where the value of the integral above is derived in Appendix A Eq. (A.8).

This last expression is the condition for the trial wave function to be normalized. However, our assumption that the number of atoms in each cloud is fixed adds a further restriction to the above expression. That is that each cloud is individually normalized. This gives, finally,

$$A_j^2(\bar{t})\pi^{3/2}\bar{w}_{jx}(\bar{t})\bar{w}_{jy}(\bar{t})\bar{w}_{jz}(\bar{t}) = 1, \quad j = 1, \ldots, N_c. \tag{4.25}$$

These constraints together automatically satisfy Eq. (4.24) and enable the elimination of all of the A_j in the final Lagrangian.

4.1.5 Derivation of $\bar{L}_1$

The $\bar{L}_1$ term of the Lagrangian has the form

$$\bar{L}_1 = \int d^3\bar{r}\bar{\mathcal{L}}_1 = \frac{i}{2}\int d^3\bar{r}\left(\Psi(\bar{\mathbf{r}},\bar{t})\Psi_{\bar{t}}^*(\bar{\mathbf{r}},\bar{t}) - \Psi^*(\bar{\mathbf{r}},\bar{t})\Psi_{\bar{t}}(\bar{\mathbf{r}},\bar{t})\right) \tag{4.26}$$

In order to compute this integral is convenient to rewrite the integrand as follows:

$$\bar{\mathcal{L}}_1 = \frac{i}{2}\left(\Psi(\bar{\mathbf{r}},\bar{t})\Psi_{\bar{t}}^*(\bar{\mathbf{r}},\bar{t}) - \Psi^*(\bar{\mathbf{r}},\bar{t})\Psi_{\bar{t}}(\bar{\mathbf{r}},\bar{t})\right) = \operatorname{Im}\left\{\Psi^*(\bar{\mathbf{r}},\bar{t})\Psi_{\bar{t}}(\bar{\mathbf{r}},\bar{t})\right\} \tag{4.27}$$

where $\operatorname{Im}(z)$ denotes the imaginary part of the complex number z. Thus we can now write $\bar{L}_1$ as follows.

$$\bar{L}_1 = \operatorname{Im}\left\{\int d^3\bar{r}\Psi^*(\bar{\mathbf{r}},\bar{t})\Psi_{\bar{t}}(\bar{\mathbf{r}},\bar{t})\right\} = \int d^3\bar{r}\operatorname{Im}\left\{\Psi^*(\bar{\mathbf{r}},\bar{t})\Psi_{\bar{t}}(\bar{\mathbf{r}},\bar{t})\right\} \tag{4.28}$$

This form is more convenient for calculation.

To proceed, we next insert the trial wave function into $\Psi^*\Psi_{\bar{t}}$. It will be efficient first to calculate $\Psi_{\bar{t}}$ using the following form of the trial wave function,

$$\Psi(\bar{\mathbf{r}},\bar{t}) = \frac{1}{\sqrt{N_c}}\sum_{j=1}^{N_c}A_j(\bar{t})e^{f_j(\bar{\mathbf{r}},\bar{t})+\bar{\mathbf{k}}_j\cdot\bar{\mathbf{r}}}. \tag{4.29}$$

It is easy to see that the partial time derivative of this is

$$\Psi_{\bar{t}}(\bar{\mathbf{r}}, \bar{t}) = \frac{1}{\sqrt{N_c}} \sum_{j=1}^{N_c} \left(\dot{A}_j(\bar{t}) + A_j(\bar{t}) \dot{f}_j(\bar{\mathbf{r}}, \bar{t}) \right) e^{f_j(\bar{\mathbf{r}}, \bar{t}) + \bar{\mathbf{k}}_j \cdot \bar{\mathbf{r}}}, \tag{4.30}$$

where the dot denotes partial differentiation with respect to $\bar{t}$.

Next we multiply the above by Ψ^* to get

$$
\begin{aligned}
\Psi^* \Psi_{\bar{t}} &= \left(\frac{1}{\sqrt{N_c}} \sum_{j=1}^{N_c} A_j(\bar{t}) e^{f_j(\bar{\mathbf{r}}, \bar{t}) + \bar{\mathbf{k}}_j \cdot \bar{\mathbf{r}}} \right)^* \\
&\times \left(\frac{1}{\sqrt{N_c}} \sum_{j'=1}^{N_c} \left(\dot{A}_{j'}(\bar{t}) + A_{j'}(\bar{t}) \dot{f}_{j'}(\bar{\mathbf{r}}, \bar{t}) \right) e^{f_{j'}(\bar{\mathbf{r}}, \bar{t}) + \bar{\mathbf{k}}_{j'} \cdot \bar{\mathbf{r}}} \right) \\
&\approx \frac{1}{N_c} \sum_{j=1}^{N_c} \left(A_j(\bar{t}) \dot{A}_j(\bar{t}) + A_j^2(\bar{t}) \dot{f}_j(\bar{\mathbf{r}}, \bar{t}) \right) e^{f_j(\bar{\mathbf{r}}, \bar{t}) + f_j^*(\bar{\mathbf{r}}, \bar{t})} \tag{4.31}
\end{aligned}
$$

where in the second equality we have dropped terms that contained rapidly oscillating exponentials (i.e., any terms where $j \neq j'$) as they would be negligible after integration. We have also used the assumption that the A_j are real.

We next take the imaginary part of this last expression. In doing so it is important to note that $f_j + f_j^*$ is real so that the exponential of this will also be real. Thus we can see that, since the term in the above containing the factor $A_j \dot{A}_j$ is real, it will not contribute to the imaginary part. In fact the only factor in the above with an imaginary part is $\dot{f}_j$. Thus, taking the imaginary part of Eq. (4.31) becomes

$$
\begin{aligned}
\text{Im} \left\{ \Psi^* \Psi_{\bar{t}} \right\} &\approx \frac{1}{N_c} \sum_{j=1}^{N_c} A_j^2(\bar{t}) \text{Im} \left\{ \dot{f}_j(\bar{\mathbf{r}}, \bar{t}) \right\} e^{f_j(\bar{\mathbf{r}}, \bar{t}) + f_j^*(\bar{\mathbf{r}}, \bar{t})} \\
&= \frac{1}{N_c} \sum_{j=1}^{N_c} A_j^2(\bar{t}) \left[\sum_{\eta=x,y,z} \left(\dot{\bar{\alpha}}_{j\eta} \bar{\eta} + \dot{\bar{\beta}}_{j\eta} \bar{\eta}^2 \right) \right] \exp \left\{ \sum_{\eta'=x,y,z} \left(-\frac{\left(\bar{\eta}' - \bar{\eta}'_j \right)^2}{\bar{w}_{j\eta'}^2} \right) \right\} \\
&= \frac{1}{N_c} \sum_{j=1}^{N_c} A_j^2(\bar{t}) \left[\sum_{\eta=x,y,z} \left(\dot{\bar{\alpha}}_{j\eta} \bar{\eta} + \dot{\bar{\beta}}_{j\eta} \bar{\eta}^2 \right) \right] \prod_{\eta'=x,y,z} \exp \left\{ -\frac{\left(\bar{\eta}' - \bar{\eta}'_j \right)^2}{\bar{w}_{j\eta'}^2} \right\} \tag{4.32}
\end{aligned}
$$

We now insert this expression into the integral for $\bar{L}_1$.

Inserting Eq. (4.32) into Eq. (4.28) we have

$$\bar{L}_1 = \frac{1}{N_c} \sum_{j=1}^{N_c} A_j^2(\bar{t}) \sum_{\eta=x,y,z} \int d^3\bar{r} \left(\dot{\bar{\alpha}}_{j\eta} \bar{\eta} + \dot{\bar{\beta}}_{j\eta} \bar{\eta}^2 \right) \prod_{\eta'=x,y,z} \exp \left\{ -\frac{\left(\bar{\eta}' - \bar{\eta}'_j \right)^2}{\bar{w}_{j\eta'}^2} \right\}$$

$$= \frac{1}{N_c} \sum_{j=1}^{N_c} \sum_{\eta=x,y,z} \left(\frac{1}{\pi^{1/2} \bar{w}_{j\eta}} \right) \int d^3\bar{r} \left(\dot{\bar{\alpha}}_{j\eta} \bar{\eta} + \dot{\bar{\beta}}_{j\eta} \bar{\eta}^2 \right) \exp \left\{ -\frac{(\bar{\eta} - \bar{\eta}_j)^2}{\bar{w}_{j\eta}^2} \right\}.$$

$$(4.33)$$

Note that each of the 3D integrals appearing in the sum over x, y, and z consists of two dimensions (the one that is not η) whose single–variable integral is that same as that found in the normalization integral while the integral over the "η" dimension contains the factor $(\dot{\bar{\alpha}}_{j\eta}\eta + \dot{\bar{\beta}}_{j\eta}\eta^2)$. We have used the constraint $A_j^2 (\pi^{1/2} \bar{w}_{jx})(\pi^{1/2} \bar{w}_{jy})(\pi^{1/2} \bar{w}_{jz}) = 1$ to rewrite the results of integration over the "non–η" dimensions times the A_j^2 factor in terms of $\bar{w}_{j\eta}$.

The remaining integrals over η are evaluated in Appendix A and are given in Eqs. (A.9) and (A.10). This gives us our final expression for $\bar{L}_1$:

$$\boxed{\bar{L}_1 = \frac{1}{N_c} \sum_{j=1}^{N_c} \sum_{\eta=x,y,z} \left(\dot{\bar{\alpha}}_{j\eta} \bar{\eta}_j + \dot{\bar{\beta}}_{j\eta} \left(\bar{\eta}_j^2 + \frac{1}{2} \bar{w}_{j\eta}^2 \right) \right)}$$

$$(4.34)$$

Next we turn to the derivation of $\bar{L}_2$.

4.1.6 Derivation of $\bar{L}_2$

The expression for $\bar{L}_2$ is given by

$$\bar{L}_2 \equiv \int d^3\bar{r} \sum_{\eta=x,y,z} \Psi_{\bar{\eta}}^* \Psi_{\bar{\eta}} = \sum_{\eta=x,y,z} \int d^3\bar{r} \Psi_{\bar{\eta}}^* \Psi_{\bar{\eta}}$$

$$(4.35)$$

To proceed we must calculate the space derivative of the trial wave function. It will be most convenient to do this using the form

$$\Psi(\bar{\mathbf{r}}, \bar{t}) = \frac{1}{\sqrt{N_c}} \sum_{j=1}^{N_c} A_j(\bar{t}) \exp \left\{ \sum_{\eta'=x,y,z} \left(f_{j\eta'}(\bar{\eta}', \bar{t}) + i \bar{k}_{j\eta'} \bar{\eta}' \right) \right\}$$

$$(4.36)$$

where

$$f_{j\eta}(\bar{\eta}, \bar{t}) = -\frac{(\bar{\eta} - \bar{\eta}_j)^2}{2 \bar{w}_{j\eta}^2} + i \left(\bar{\alpha}_{j\eta} \bar{\eta} + \bar{\beta}_{j\eta} \bar{\eta}^2 \right) \equiv f_{j\eta}^{(r)}(\bar{\eta}, \bar{t}) + i f_{j\eta}^{(i)}(\bar{\eta}, \bar{t}).$$

$$(4.37)$$

36

In the above we have introduced the real and imaginary parts of $f_{j\eta}$ for later convenience.

It is straightforward to compute the derivative of Ψ in this form, we obtain

$$
\begin{aligned}
\Psi_{\bar{\eta}}(\bar{\mathbf{r}}, \bar{t}) &= \frac{1}{\sqrt{N_c}} \sum_{j=1}^{N_c} A_j(\bar{t}) \exp\left\{ \sum_{\eta'=x,y,z} \left(f_{j\eta'}(\bar{\eta}', \bar{t}) + i\bar{k}_{j\eta'}\bar{\eta}' \right) \right\} \\
&\times \left(\frac{\partial f_{j\eta}^{(r)}}{\partial\bar{\eta}} + i\left(\frac{\partial f_{j\eta}^{(i)}}{\partial\bar{\eta}} + \bar{k}_{j\eta} \right) \right)
\end{aligned}
\tag{4.38}
$$

If we multiply the above by its complex conjugate and neglect the rapidly oscillating terms we get

$$
\begin{aligned}
\Psi_{\bar{\eta}}^* \Psi_{\bar{\eta}} &= \frac{1}{N_c} \sum_{j=1}^{N_c} A_j^2(\bar{t}) \exp\left\{ \sum_{\eta'=x,y,z} \left(f_{j\eta'}^* + f_{j\eta'} \right) \right\} \\
&\times \left(\left(\frac{\partial f_{j\eta}^{(r)}}{\partial\bar{\eta}} \right)^2 + \left(\frac{\partial f_{j\eta}^{(i)}}{\partial\bar{\eta}} + \bar{k}_{j\eta} \right)^2 \right) \\
&= \frac{1}{N_c} \sum_{j=1}^{N_c} A_j^2(\bar{t}) \exp\left\{ -\sum_{\eta'=x,y,z} \frac{\left(\eta' - \eta_j'\right)^2}{\bar{w}_{j\eta'}^2} \right\} \\
&\times \left(\frac{\left(\eta - \eta_j\right)^2}{\bar{w}_{j\eta}^4} + \left(\bar{\alpha}_{j\eta} + \bar{k}_{j\eta} + 2\bar{\beta}_{j\eta}\eta \right)^2 \right)
\end{aligned}
\tag{4.39}
$$

We now insert this form into Eq. (4.35):

$$
\begin{aligned}
\bar{L}_2 &= \frac{1}{N_c} \sum_{j=1}^{N_c} A_j^2(\bar{t}) \sum_{\eta=x,y,z} \int d^3\bar{r} \exp\left\{ -\sum_{\eta'=x,y,z} \frac{\left(\eta' - \eta_j'\right)^2}{\bar{w}_{j\eta'}^2} \right\} \\
&\times \left(\frac{\left(\eta - \eta_j\right)^2}{\bar{w}_{j\eta}^4} + \left(\bar{\alpha}_{j\eta} + \bar{k}_{j\eta} + 2\bar{\beta}_{j\eta}\eta \right)^2 \right)
\end{aligned}
\tag{4.40}
$$

Each term in the sum over η above contains a 3D integral. For each 3D integral, two of the integrations are over coordinates that are not equal to η. These have the form of integral J_1 found in Appendix A and have the value of $\pi^{1/2} \times \bar{w}$. The remaining integral is over the coordinate that is equal to the current value of η in the sum and this integral has the extra factor shown above. We can use the constraint equations

derived in Eqs. (4.25) to eliminate the product of A_j^2 with the value of the two non–η integrals. Performing this elimination yields the following form for $\bar{L}_2$:

$$
\bar{L}_2 = \frac{1}{N_c} \sum_{j=1}^{N_c} \sum_{\eta=x,y,z} \left(\frac{1}{\pi^{1/2}\bar{w}_{j\eta}} \right) \int_{-\infty}^{\infty} d\eta \exp\left\{ -\frac{(\eta-\eta_j)^2}{\bar{w}_{j\eta}^2} \right\}
$$
$$
\times \quad \left(\frac{(\eta-\eta_j)^2}{\bar{w}_{j\eta}^4} + \left(\bar{\alpha}_{j\eta} + \bar{k}_{j\eta} + 2\bar{\beta}_{j\eta}\eta \right)^2 \right) \tag{4.41}
$$

While it is possible to use the integrals derived in Appendix A, here it is a little easier to perform the integration directly. To do this we let $x = (\eta - \eta_j)/\bar{w}_{j\eta}$ and change the integration variable to x in the integral below:

$$
I \equiv \int_{-\infty}^{\infty} d\eta \exp\left\{ -\frac{(\eta-\eta_j)^2}{\bar{w}_{j\eta}^2} \right\} \left(\frac{(\eta-\eta_j)^2}{\bar{w}_{j\eta}^4} + \left(\bar{\alpha}_{j\eta} + \bar{k}_{j\eta} + 2\bar{\beta}_{j\eta}\eta \right)^2 \right)
$$
$$
= \int_{-\infty}^{\infty} \bar{w}_{j\eta}\, dx\, e^{-x^2} \left(\frac{x^2}{\bar{w}_{j\eta}^2} + \left(\bar{\alpha}_{j\eta} + \bar{k}_{j\eta} + 2\bar{\beta}_{j\eta}\left(\bar{\eta}_j + \bar{w}_{j\eta}x \right) \right)^2 \right)
$$
$$
= \int_{-\infty}^{\infty} \bar{w}_{j\eta}\, dx\, e^{-x^2} \left(\left(\frac{1}{\bar{w}_{j\eta}^2} + 4\bar{\beta}_{j\eta}^2\bar{w}_{j\eta}^2 \right) x^2 \right.
$$
$$
+ \quad 4\bar{\beta}_{j\eta}\bar{w}_{j\eta}\left(\bar{\alpha}_{j\eta} + \bar{k}_{j\eta} + 2\bar{\beta}_{j\eta}\bar{\eta}_j \right)x + \left(\bar{\alpha}_{j\eta} + \bar{k}_{j\eta} + 2\bar{\beta}_{j\eta}\bar{\eta}_j \right)^2 \bigg)
$$
$$
= \left(\pi^{1/2}\bar{w}_{j\eta} \right) \left(\frac{1}{2}\left(\frac{1}{\bar{w}_{j\eta}^2} + 4\bar{\beta}_{j\eta}^2\bar{w}_{j\eta}^2 \right) + \left(\bar{\alpha}_{j\eta} + \bar{k}_{j\eta} + 2\bar{\beta}_{j\eta}\bar{\eta}_j \right)^2 \right) \tag{4.42}
$$

Inserting this last expression in place of the integral in $\bar{L}_2$ we have the final expression for $\bar{L}_2$:

$$
\boxed{\bar{L}_2 = \frac{1}{N_c} \sum_{j=1}^{N_c} \sum_{\eta=x,y,z} \left(\frac{1}{2\bar{w}_{j\eta}^2} + 2\bar{\beta}_{j\eta}^2\bar{w}_{j\eta}^2 + \left(\bar{\alpha}_{j\eta} + \bar{k}_{j\eta} + 2\bar{\beta}_{j\eta}\bar{\eta}_j \right)^2 \right).} \tag{4.43}
$$

Next we turn to the derivation of $\bar{L}_3$.

4.1.7 Derivation of $\bar{L}_3$

The expression for $\bar{L}_3$ is

$$
\bar{L}_3 \equiv \int d^3\bar{r}\, \bar{V}_{\text{trap}}(\bar{\mathbf{r}}, \bar{t}) \Psi^*(\bar{\mathbf{r}}, \bar{t}) \Psi(\bar{\mathbf{r}}, \bar{t}) \tag{4.44}
$$
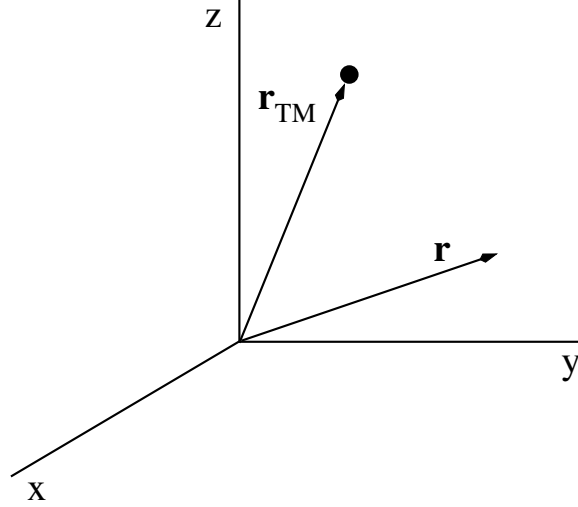
Figure 4.1: A test mass is located $\mathbf{r}_{TM}$ and $\mathbf{r}$ denotes the point at which the gravitational field of the test mass is evaluated.

The potential must be specified in order to compute this term.

Here we will take the potential to be the sum of the trap potential (assumed here to be a 3D harmonic oscillator) plus the gravitational potential energy of point test mass:

$$V_{\text{trap}}(\mathbf{r}) = \sum_{\eta=x,y,z} \frac{1}{2}M\omega_{T,\eta}^2\eta^2 + V_{gravity}(\mathbf{r}). \tag{4.45}$$

The gravitational potential energy between a mass M at point $\mathbf{r}$ due to a test mass, M_{TM}, and located at $\mathbf{r}_{TM}$, as shown in Fig. 4.1, is given by

$$V_{gravity}(\mathbf{r}) = -\frac{GM_{TM}M}{|\mathbf{r} - \mathbf{r}_{TM}|} \tag{4.46}$$

where G is the Newtonian Universal Gravitational Constant also known as "Big G" and M is the mass of a condensate atom. We shall assume here that the test mass is far away from the origin of coordinates compared to the location of the condensate. That is, we assume that $|\mathbf{r}_{TM}| \gg |\mathbf{r}|$ and we can make a Taylor expansion of $V_{gravity}(\mathbf{r})$

to second order around the origin:

$$V_{gravity}(\mathbf{r}) \approx -\frac{GM_{TM}M}{|\mathbf{r}_{TM}|} - \frac{GM_{TM}M}{2|\mathbf{r}_{TM}|^3}\left(|\mathbf{r}|^2 + 2|\mathbf{r}_{TM}|\hat{\mathbf{u}}_{TM}\cdot\mathbf{r}\right), \qquad (4.47)$$

where

$$\hat{\mathbf{u}}_{TM} \equiv \frac{\mathbf{r}_{TM}}{|\mathbf{r}_{TM}|}. \qquad (4.48)$$

The first term in $V_{gravity}$ is a constant everywhere in space. Since only energy differences have physical meaning, we can adjust the origin of our energy scale so that this term can be ignored. Thus we can write this approximate potential as

$$\begin{aligned} V_{gravity}(\mathbf{r}) &= -\frac{1}{2}M\omega_{TM}^2\left(x^2 + y^2 + z^2\right) \\ &+ \frac{1}{2}M\omega_{TM}^2(2|\mathbf{r}_{TM}|)\left(u_{TM,x}x + u_{TM,y}y + u_{TM,z}z\right) \end{aligned} \qquad (4.49)$$

where

$$\omega_{TM} \equiv \left(\frac{GM_{TM}}{|\mathbf{r}_{TM}^3|}\right)^{1/2}. \qquad (4.50)$$

Thus the full potential is

$$V_{\text{trap}}(\mathbf{r}, t) = \sum_{\eta=x,y,z}\frac{1}{2}M\omega_{T,\eta}^2\eta^2 - \sum_{\eta=x,y,z}\frac{1}{2}M\omega_{TM}^2\left(\eta^2 + 2|\mathbf{r}_{TM}|u_{TM,\eta}\eta\right), \qquad (4.51)$$

where $\omega_{T,\eta}$, $\eta = x, y, z$ are the frequencies of the harmonic trap potential. The frequency ω_{TM} is the coefficient of the second–order approximation to the gravitational potential energy produced by the test mass and the $u_{TM,\eta}$ are the components of the unit vector that points from the origin towards the test mass location.

In scaled units this potential has the form

$$\bar{V}(\bar{\mathbf{r}}, \bar{t}) = \sum_{\eta=x,y,z}\left[\frac{1}{4}\left(\bar{\omega}_{T,\eta}^2 - \bar{\omega}_{TM}^2\right)\bar{\eta}^2 - \frac{1}{2}\bar{\omega}_{TM}^2|\bar{\mathbf{r}}_{TM}|u_{TM,\eta}\bar{\eta}\right]. \qquad (4.52)$$

If we multiply Ψ by its complex conjugate and neglect the rapidly oscillating terms (which will integrate to approximately zero anyway) we obtain

$$\Psi^*\Psi \approx \frac{1}{N_c}\sum_{j=1}^{N_c}A_j^2(\bar{t})\exp\left\{\sum_{\eta=x,y,z}\left(f_{j\eta}(\bar{\eta}, \bar{t}) + f_{j\eta}^*(\bar{\eta}, \bar{t})\right)\right\}$$

$$= \frac{1}{N_c} \sum_{j=1}^{N_c} A_j^2(\bar{t}) \exp\left\{ -\sum_{\eta=x,y,z} \left(\frac{(\bar{\eta} - \bar{\eta}_j)^2}{\bar{w}_{j\eta}^2} \right) \right\} \tag{4.53}$$

With these expressions we can now calculate $\bar{L}_3$.

Inserting Eqs. (4.52) and (4.53) into Eq. (4.44) we have

$$
\begin{aligned}
\bar{L}_3 &= \int d^3\bar{r} \left(\frac{1}{N_c} \sum_{j=1}^{N_c} A_j^2(\bar{t}) \exp\left\{ -\sum_{\eta'=x,y,z} \left(\frac{(\bar{\eta}' - \bar{\eta}'_j)^2}{\bar{w}_{j\eta'}^2} \right) \right\} \right) \\
&\quad \times \left(\sum_{\eta=x,y,z} \left[\frac{1}{4} \left(\bar{\omega}_{T,\eta}^2 - \bar{\omega}_{TM}^2 \right) \bar{\eta}^2 - \frac{1}{2} \bar{\omega}_{TM}^2 |\bar{\mathbf{r}}_{TM}| \bar{\eta} \right] \right) \\
&= \frac{1}{N_c} \sum_{j=1}^{N_c} A_j^2(\bar{t}) \sum_{\eta=x,y,z} \frac{1}{4} \left(\bar{\omega}_{T,\eta}^2 - \bar{\omega}_{TM}^2 \right) \\
&\quad \times \int d^3\bar{r}\, \bar{\eta}^2 \exp\left\{ -\sum_{\eta'=x,y,z} \left(\frac{(\bar{\eta}' - \bar{\eta}'_j)^2}{\bar{w}_{j\eta'}^2} \right) \right\} \\
&\quad - \frac{1}{2N_c} \sum_{j=1}^{N_c} A_j^2(\bar{t}) \sum_{\eta=x,y,z} \frac{1}{2} \bar{\omega}_{TM}^2 |\bar{\mathbf{r}}_{TM}| u_{TM,\eta} \\
&\quad \times \int d^3\bar{r}\, \bar{\eta} \exp\left\{ -\sum_{\eta'=x,y,z} \left(\frac{(\bar{\eta}' - \bar{\eta}'_j)^2}{\bar{w}_{j\eta'}^2} \right) \right\}
\end{aligned}
\tag{4.54}
$$

Now we can perform the integration over the two dimensions not equal to η in the sum and use the constraint equations to eliminate A_j^2. Doing this yields the final expression for $\bar{L}_3$ is

$$\boxed{ \bar{L}_3 = \frac{1}{N_c} \sum_{j=1}^{N_c} \sum_{\eta=x,y,z} \left\{ \frac{1}{4} \left(\bar{\omega}_{T,\eta}^2 - \bar{\omega}_{TM}^2 \right) \left(\bar{\eta}_j^2 + \frac{1}{2} \bar{w}_{j\eta}^2 \right) - \frac{1}{2} \bar{\omega}_{TM}^2 |\bar{\mathbf{r}}_{TM}| u_{TM,\eta} \bar{\eta}_j \right\} } \tag{4.55}$$

Finally, we turn to $\bar{L}_4$.

4.1.8 Derivation of $\bar{L}_4$

The expression for $\bar{L}_4$ is

$$\bar{L}_4 \equiv \frac{1}{2} \bar{g} N \int d^3\bar{r}\, |\Psi|^4 \tag{4.56}$$

In order to perform this integral we must first calculate $|\Psi|^4$. We can write this quantity as follows:

$$
\begin{aligned}
|\Psi|^4 &= \left[\left(\frac{1}{\sqrt{N_c}}\sum_{j_1=1}^{N_c} A_{j_1}(\bar{t})\exp\left\{\sum_{\eta_1=x,y,z}\left(f_{j_1\eta_1}(\bar{\eta}_1,\bar{t})+i\bar{k}_{j_1\eta_1}\bar{\eta}_1\right)\right\}\right)^{*}\right.\\
&\quad\left.\times\left(\frac{1}{\sqrt{N_c}}\sum_{j_2=1}^{N_c} A_{j_2}(\bar{t})\exp\left\{\sum_{\eta_2=x,y,z}\left(f_{j_2\eta_2}(\bar{\eta}_2,\bar{t})+i\bar{k}_{j_2\eta_2}\bar{\eta}_2\right)\right\}\right)\right]^2\\
&= \frac{1}{N_c^2}\left[\sum_{j_1,j_2=1}^{N_c} A_{j_1}A_{j_2}\exp\left\{\sum_{\eta=x,y,z}\left(f^{*}_{j_1\eta}+f_{j_2\eta}+i\left(\bar{k}_{j_2\eta}-\bar{k}_{j_1\eta}\right)\bar{\eta}\right)\right\}\right]^2
\end{aligned}
$$

$$(4.57)$$

where we have dropped the display of the functional dependence of the A_j and $f_{j\eta}$ in the last line to save space.

We can write the double sum inside the square brackets as a single sum where $j_1 = j_2$ and the original double sum with the provision that $j_1 \neq j_2$ and write out the square:

$$
\begin{aligned}
|\Psi|^4 &= \frac{1}{N_c^2}\left[\sum_{j_1=1}^{N_c} A_{j_1}^2\exp\left\{\sum_{\eta=x,y,z}\left(f^{*}_{j_1\eta}+f_{j_1\eta}\right)\right\}\right.\\
&\quad\left.+\sum_{\substack{j_1,j_2=1\\j_1\neq j_2}}^{N_c} A_{j_1}A_{j_2}\exp\left\{\sum_{\eta=x,y,z}\left(f^{*}_{j_1\eta}+f_{j_2\eta}+i\left(\bar{k}_{j_2\eta}-\bar{k}_{j_1\eta}\right)\bar{\eta}\right)\right\}\right]^2\\
&= \frac{1}{N_c^2}\left[\sum_{j_1=1}^{N_c} A_{j_1}^2\exp\left\{\sum_{\eta=x,y,z}\left(f^{*}_{j_1\eta}+f_{j_1\eta}\right)\right\}\right.\\
&\quad\left.+\sum_{\substack{j_1,j_2=1\\j_1\neq j_2}}^{N_c} A_{j_1}A_{j_2}\exp\left\{\sum_{\eta=x,y,z}\left(f^{*}_{j_1\eta}+f_{j_2\eta}+i\left(\bar{k}_{j_2\eta}-\bar{k}_{j_1\eta}\right)\bar{\eta}\right)\right\}\right]\\
&\quad\times\left[\sum_{j_1'=1}^{N_c} A_{j_1'}^2\exp\left\{\sum_{\eta'=x,y,z}\left(f^{*}_{j_1'\eta'}+f_{j_1'\eta'}\right)\right\}\right.\\
&\quad\left.+\sum_{\substack{j_1',j_2'=1\\j_1'\neq j_2'}}^{N_c} A_{j_1'}A_{j_2'}\exp\left\{\sum_{\eta'=x,y,z}\left(f^{*}_{j_1'\eta'}+f_{j_2'\eta'}+i\left(\bar{k}_{j_2'\eta'}-\bar{k}_{j_1'\eta'}\right)\bar{\eta}'\right)\right\}\right]
\end{aligned}
$$

$$\approx \frac{1}{N_c^2} \left[\left(\sum_{j_1=1}^{N_c} A_{j_1}^2 \exp \left\{ \sum_{\eta=x,y,z} \left(f_{j_1\eta}^* + f_{j_1\eta} \right) \right\} \right) \right.$$

$$\times \left(\sum_{j_1'=1}^{N_c} A_{j_1'}^2 \exp \left\{ \sum_{\eta'=x,y,z} \left(f_{j_1'\eta'}^* + f_{j_1'\eta'} \right) \right\} \right)$$

$$+ \left(\sum_{\substack{j_1,j_2=1 \\ j_1 \neq j_2}}^{N_c} A_{j_1} A_{j_2} \exp \left\{ \sum_{\eta=x,y,z} \left(f_{j_1\eta}^* + f_{j_2\eta} + i \left(\bar{k}_{j_2\eta} - \bar{k}_{j_1\eta} \right) \bar{\eta} \right) \right\} \right)$$

$$\left. \times \left(\sum_{\substack{j_1',j_2'=1 \\ j_1' \neq j_2'}}^{N_c} A_{j_1'} A_{j_2'} \exp \left\{ \sum_{\eta'=x,y,z} \left(f_{j_1'\eta'}^* + f_{j_2'\eta'} + i \left(\bar{k}_{j_2'\eta'} - \bar{k}_{j_1'\eta'} \right) \bar{\eta}' \right) \right\} \right) \right]$$

$$(4.58)$$

When multiplying out the square we want to neglect terms that contain rapidly oscillating exponentials. We cannot do this all in one step. The single sums definitely do not contain exponentials but the double sums definitely do. Thus, a single–sum times a double–sum will definitely have exponentials while a single–sum times a single–sum definitely will not. Finally, the double–sum times the double–sum will have some terms with exponentials and some not. Hence, in the above when we multiplied out the square we kept the single–sum times the single–sum and the double–sum times the double–sum and dropped the cross terms.

Now we can rewrite the above expression as follows:

$$|\Psi|^4 \approx \frac{1}{N_c^2} \left[\sum_{j_1,j_2=1}^{N_c} A_{j_1}^2 A_{j_2}^2 \exp \left\{ \sum_{\eta=x,y,z} \left(f_{j_1\eta}^* + f_{j_1\eta} + f_{j_2\eta}^* + f_{j_2\eta} \right) \right\} \right.$$

$$+ \sum_{\substack{j_1,j_2=1 \\ j_1 \neq j_2}}^{N_c} \sum_{\substack{j_1',j_2'=1 \\ j_1' \neq j_2'}}^{N_c} A_{j_1} A_{j_2} A_{j_1'} A_{j_2'}$$

$$\left. \times \exp \left\{ \sum_{\eta=x,y,z} \left(f_{j_1\eta}^* + f_{j_2\eta} + f_{j_1'\eta}^* + f_{j_2'\eta} + i \left(\bar{k}_{j_2\eta} - \bar{k}_{j_1\eta} + \bar{k}_{j_2'\eta} - \bar{k}_{j_1'\eta} \right) \bar{\eta} \right) \right\} \right]$$

$$(4.59)$$

The second term above still has oscillating terms. We only want to keep the non–

oscillating terms. The terms that don't oscillate are those where $j_1' = j_2$ and $j_2' = j_1$ (since $j_1 = j_2$ and $j_1' = j_2'$ are excluded already). Thus we can evaluate the primed sums keeping only those terms where $j_1' = j_2$ and $j_2' = j_1$:

$$
\begin{aligned}
|\Psi|^4 \ \approx \ & \frac{1}{N_c^2} \Bigg[\sum_{j_1,j_2=1}^{N_c} A_{j_1}^2 A_{j_2}^2 \exp \Bigg\{ \sum_{\eta=x,y,z} \Big(f_{j_1\eta}^* + f_{j_1\eta} + f_{j_2\eta}^* + f_{j_2\eta} \Big) \Bigg\} \\
& + \sum_{\substack{j_1,j_2=1 \\ j_1 \neq j_2}} A_{j_1}^2 A_{j_2}^2 \exp \Bigg\{ \sum_{\eta=x,y,z} \Big(f_{j_1\eta}^* + f_{j_2\eta} + f_{j_2\eta}^* + f_{j_1\eta} \Big) \Bigg\} \Bigg]
\end{aligned}
$$

$$(4.60)$$

The two double sums appearing in the expression above are the same with one exception: the second double sum requires $j_1 \neq j_2$ while the first double sum has no such restriction. We can write the first sum as two terms: a single sum where $j_1 = j_2$ and a double sum where $j_1 \neq j_2$. This second term will then be identical to the second term in the original expression. Carrying out this procedure gives.

$$
\begin{aligned}
|\Psi|^4 \ \approx \ & \frac{1}{N_c^2} \Bigg[\sum_{j_1=1}^{N_c} A_{j_1}^4 \exp \Bigg\{ \sum_{\eta=x,y,z} \Big(2f_{j_1\eta}^* + 2f_{j_1\eta} \Big) \Bigg\} \\
& + 2 \sum_{\substack{j_1,j_2=1 \\ j_1 \neq j_2}} A_{j_1}^2 A_{j_2}^2 \exp \Bigg\{ \sum_{\eta=x,y,z} \Big(f_{j_1\eta}^* + f_{j_1\eta} + f_{j_2\eta}^* + f_{j_2\eta} \Big) \Bigg\} \Bigg]
\end{aligned}
$$

$$(4.61)$$

We are now in a position to write $|\Psi|^4$ in terms of coordinates. The result is

$$
\begin{aligned}
|\Psi|^4 \ \approx \ & \frac{1}{N_c^2} \Bigg[\sum_{j_1=1}^{N_c} A_{j_1}^4 \exp \Bigg\{ - \sum_{\eta=x,y,z} \Bigg(\frac{2\left(\bar{\eta} - \bar{\eta}_{j_1}\right)^2}{\bar{w}_{j_1\eta}^2} \Bigg) \Bigg\} \\
& + 2 \sum_{\substack{j_1,j_2=1 \\ j_1 \neq j_2}} A_{j_1}^2 A_{j_2}^2 \exp \Bigg\{ - \sum_{\eta=x,y,z} \Bigg(\frac{\left(\bar{\eta} - \bar{\eta}_{j_1}\right)^2}{\bar{w}_{j_1\eta}^2} + \frac{\left(\bar{\eta} - \bar{\eta}_{j_2}\right)^2}{\bar{w}_{j_2\eta}^2} \Bigg) \Bigg\} \Bigg]
\end{aligned}
$$

$$(4.62)$$

We now consider the exponent of the exponential appearing in the second term above.

Consider the quantity

$$S\left(\bar{\eta}_{j_1}, \bar{w}_{j_1\eta}, \bar{\eta}_{j_2}, \bar{w}_{j_2\eta}; \bar{\eta}\right) \equiv \frac{\left(\bar{\eta} - \bar{\eta}_{j_1}\right)^2}{\bar{w}_{j_1\eta}^2} + \frac{\left(\bar{\eta} - \bar{\eta}_{j_2}\right)^2}{\bar{w}_{j_2\eta}^2}. \tag{4.63}$$

We can rewrite this as

$$S\left(\bar{\eta}_{j_1}, \bar{w}_{j_1\eta}, \bar{\eta}_{j_2}, \bar{w}_{j_2\eta}; \bar{\eta}\right) = \frac{\left(\bar{\eta} - \bar{\eta}_{j_1j_2}\right)^2}{\bar{w}_{j_1j_2\eta}^2} + \frac{\left(\bar{\eta}_{j_1} - \bar{\eta}_{j_2}\right)^2}{\bar{w}_{j_1\eta}^2 + \bar{w}_{j_2\eta}^2} \tag{4.64}$$

where

$$\bar{\eta}_{j_1j_2} \equiv \frac{\bar{w}_{j_1\eta}^2 \bar{\eta}_{j_2} + \bar{w}_{j_2\eta}^2 \bar{\eta}_{j_1}}{\bar{w}_{j_1\eta}^2 + \bar{w}_{j_2\eta}^2} \quad \text{and} \quad \bar{w}_{j_1j_2\eta} \equiv \frac{\bar{w}_{j_1\eta} \bar{w}_{j_2\eta}}{\left(\bar{w}_{j_1\eta}^2 + \bar{w}_{j_2\eta}^2\right)^{1/2}} \tag{4.65}$$

We can show this by multiplying out the squares in the definition of S and completing the square:

$$\begin{aligned}
S\left(\bar{\eta}\right) &= \frac{\left(\bar{\eta} - \bar{\eta}_{j_1}\right)^2}{\bar{w}_{j_1\eta}^2} + \frac{\left(\bar{\eta} - \bar{\eta}_{j_2}\right)^2}{\bar{w}_{j_2\eta}^2} \\
&= \frac{\bar{\eta}^2 - 2\bar{\eta}_{j_1}\bar{\eta} + \bar{\eta}_{j_1}^2}{\bar{w}_{j_1\eta}^2} + \frac{\bar{\eta}^2 - 2\bar{\eta}_{j_2}\bar{\eta} + \bar{\eta}_{j_2}^2}{\bar{w}_{j_2\eta}^2} \\
&= \left(\frac{1}{\bar{w}_{j_1\eta}^2} + \frac{1}{\bar{w}_{j_2\eta}^2}\right)\bar{\eta}^2 - 2\left(\frac{\bar{\eta}_{j_1}}{\bar{w}_{j_1\eta}^2} + \frac{\bar{\eta}_{j_2}}{\bar{w}_{j_2\eta}^2}\right)\bar{\eta} + \left(\frac{\bar{\eta}_{j_1}^2}{\bar{w}_{j_1\eta}^2} + \frac{\bar{\eta}_{j_2}^2}{\bar{w}_{j_2\eta}^2}\right) \\
&= \left(\frac{\bar{w}_{j_1\eta}^2 + \bar{w}_{j_2\eta}^2}{\bar{w}_{j_1\eta}^2 \bar{w}_{j_2\eta}^2}\right)\bar{\eta}^2 - 2\left(\frac{\bar{w}_{j_1\eta}^2 \bar{\eta}_{j_2} + \bar{w}_{j_2\eta}^2 \bar{\eta}_{j_1}}{\bar{w}_{j_1\eta}^2 \bar{w}_{j_2\eta}^2}\right)\bar{\eta} + \left(\frac{\bar{w}_{j_1\eta}^2 \bar{\eta}_{j_2}^2 + \bar{w}_{j_2\eta}^2 \bar{\eta}_{j_1}^2}{\bar{w}_{j_1\eta}^2 \bar{w}_{j_2\eta}^2}\right) \\
&\equiv a\bar{\eta}^2 - 2b\bar{\eta} + c = a\left(\bar{\eta} - \frac{b}{a}\right)^2 + c - \frac{b^2}{a}
\end{aligned} \tag{4.66}$$

where we defined a, b, and c as

$$a \equiv \frac{\bar{w}_{j_1\eta}^2 + \bar{w}_{j_2\eta}^2}{\bar{w}_{j_1\eta}^2 \bar{w}_{j_2\eta}^2}, \quad b \equiv \frac{\bar{w}_{j_1\eta}^2 \bar{\eta}_{j_2} + \bar{w}_{j_2\eta}^2 \bar{\eta}_{j_1}}{\bar{w}_{j_1\eta}^2 \bar{w}_{j_2\eta}^2} \quad c \equiv \frac{\bar{w}_{j_1\eta}^2 \bar{\eta}_{j_2}^2 + \bar{w}_{j_2\eta}^2 \bar{\eta}_{j_1}^2}{\bar{w}_{j_1\eta}^2 \bar{w}_{j_2\eta}^2}. \tag{4.67}$$

It is important to note that

$$\frac{b}{a} = \frac{\bar{w}_{j_1\eta}^2 \bar{\eta}_{j_2} + \bar{w}_{j_2\eta}^2 \bar{\eta}_{j_1}}{\bar{w}_{j_1\eta}^2 + \bar{w}_{j_2\eta}^2} = \bar{\eta}_{j_1j_2} \quad \text{and} \quad a = \frac{1}{\bar{w}_{j_1j_2\eta}^2}. \tag{4.68}$$

These will be immediately useful.

With these definitions it is easy to see how the square is completed. Now we can rewrite S by replacing the a, b, and c with their definitions:

$$S(\eta) = a\left(\bar{\eta} - \frac{b}{a}\right)^2 + c - \frac{b^2}{a}$$

$$= \frac{(\bar\eta - \bar\eta_{j_1 j_2})^2}{\bar w_{j_1 j_2 \eta}^2} + \frac{\bar w_{j_1 \eta}^2 \bar\eta_{j_2}^2 + \bar w_{j_2 \eta}^2 \bar\eta_{j_1}^2}{\bar w_{j_1 \eta}^2 \bar w_{j_2 \eta}^2} - \left(\frac{\bar w_{j_1 \eta}^2 \bar\eta_{j_2} + \bar w_{j_2 \eta}^2 \bar\eta_{j_1}}{\bar w_{j_1 \eta}^2 \bar w_{j_2 \eta}^2} \right)^2$$

$$\times \quad \left(\frac{\bar w_{j_1 \eta}^2 \bar w_{j_2 \eta}^2}{\bar w_{j_1 \eta}^2 + \bar w_{j_2 \eta}^2} \right)$$

$$= \frac{(\bar\eta - \bar\eta_{j_1 j_2})^2}{\bar w_{j_1 j_2 \eta}^2} + \frac{\left(\bar w_{j_1 \eta}^2 \bar\eta_{j_2}^2 + \bar w_{j_2 \eta}^2 \bar\eta_{j_1}^2 \right)}{\bar w_{j_1 \eta}^2 \bar w_{j_2 \eta}^2} - \frac{\left(\bar w_{j_1 \eta}^2 \bar\eta_{j_2} + \bar w_{j_2 \eta}^2 \bar\eta_{j_1} \right)^2}{\bar w_{j_1 \eta}^2 \bar w_{j_2 \eta}^2 \left(\bar w_{j_1 \eta}^2 + \bar w_{j_2 \eta}^2 \right)}$$

$$= \frac{(\bar\eta - \bar\eta_{j_1 j_2})^2}{\bar w_{j_1 j_2 \eta}^2} + \frac{\left(\bar w_{j_1 \eta}^2 \bar\eta_{j_2}^2 + \bar w_{j_2 \eta}^2 \bar\eta_{j_1}^2 \right) \left(\bar w_{j_1 \eta}^2 + \bar w_{j_2 \eta}^2 \right) - \left(\bar w_{j_1 \eta}^2 \bar\eta_{j_2} + \bar w_{j_2 \eta}^2 \bar\eta_{j_1} \right)^2}{\bar w_{j_1 \eta}^2 \bar w_{j_2 \eta}^2 \left(\bar w_{j_1 \eta}^2 + \bar w_{j_2 \eta}^2 \right)}$$

$$= \frac{(\bar\eta - \bar\eta_{j_1 j_2})^2}{\bar w_{j_1 j_2 \eta}^2}$$

$$+ \quad \frac{\bar w_{j_1 \eta}^4 \bar\eta_{j_2}^2 + \bar w_{j_1 \eta}^2 \bar w_{j_2 \eta}^2 \bar\eta_{j_2}^2 + \bar w_{j_1 \eta}^2 \bar w_{j_2 \eta}^2 \bar\eta_{j_1}^2 + \bar w_{j_2 \eta}^4 \bar\eta_{j_1}^2 - \bar w_{j_1 \eta}^4 \bar\eta_{j_2}^2 - 2\bar w_{j_1 \eta}^2 \bar w_{j_2 \eta}^2 \bar\eta_{j_1} \bar\eta_{j_2} - \bar w_{j_2 \eta}^4 \bar\eta_{j_1}^2}{\bar w_{j_1 \eta}^2 \bar w_{j_2 \eta}^2 \left(\bar w_{j_1 \eta}^2 + \bar w_{j_2 \eta}^2 \right)}$$

$$= \frac{(\bar\eta - \bar\eta_{j_1 j_2})^2}{\bar w_{j_1 j_2 \eta}^2} + \frac{\bar w_{j_1 \eta}^2 \bar w_{j_2 \eta}^2 \bar\eta_{j_2}^2 + \bar w_{j_1 \eta}^2 \bar w_{j_2 \eta}^2 \bar\eta_{j_1}^2 - 2\bar w_{j_1 \eta}^2 \bar w_{j_2 \eta}^2 \bar\eta_{j_1} \bar\eta_{j_2}}{\bar w_{j_1 \eta}^2 \bar w_{j_2 \eta}^2 \left(\bar w_{j_1 \eta}^2 + \bar w_{j_2 \eta}^2 \right)}$$

$$= \frac{(\bar\eta - \bar\eta_{j_1 j_2})^2}{\bar w_{j_1 j_2 \eta}^2} + \frac{\bar w_{j_1 \eta}^2 \bar w_{j_2 \eta}^2 \left(\bar\eta_{j_2}^2 + \bar\eta_{j_1}^2 - 2\bar\eta_{j_1} \bar\eta_{j_2} \right)}{\bar w_{j_1 \eta}^2 \bar w_{j_2 \eta}^2 \left(\bar w_{j_1 \eta}^2 + \bar w_{j_2 \eta}^2 \right)}$$

$$= \frac{(\bar\eta - \bar\eta_{j_1 j_2})^2}{\bar w_{j_1 j_2 \eta}^2} + \frac{\left(\bar\eta_{j_1}^2 - 2\bar\eta_{j_1} \bar\eta_{j_2} + \bar\eta_{j_2}^2 \right)}{\bar w_{j_1 \eta}^2 + \bar w_{j_2 \eta}^2}$$

$$S(\bar\eta) = \frac{(\bar\eta - \bar\eta_{j_1 j_2})^2}{\bar w_{j_1 j_2 \eta}^2} + \frac{(\bar\eta_{j_1} - \bar\eta_{j_2})^2}{\bar w_{j_1 \eta}^2 + \bar w_{j_2 \eta}^2} \tag{4.69}$$

Thus Eq. (4.69) is identical to Eq. (4.64). It's like magic!

Using this magic formula we can rewrite $|\Psi|^4$ so that the integrals will be easy.

We have

$$|\Psi|^4 \approx \frac{1}{N_c^2} \left[\sum_{j_1=1}^{N_c} A_{j_1}^4 \exp\left\{ - \sum_{\eta=x,y,z} \left(\frac{2(\bar\eta - \bar\eta_{j_1})^2}{\bar w_{j_1 \eta}^2} \right) \right\} \right.$$

$$+ \quad 2 \sum_{\substack{j_1, j_2 = 1 \\ j_1 \neq j_2}} A_{j_1}^2 A_{j_2}^2 \exp\left\{ - \sum_{\eta=x,y,z} \left(\frac{(\bar\eta - \bar\eta_{j_1})^2}{\bar w_{j_1 \eta}^2} + \frac{(\bar\eta - \bar\eta_{j_2})^2}{\bar w_{j_2 \eta}^2} \right) \right\} \right]$$

$$= \frac{1}{N_c^2} \left[\sum_{j_1=1}^{N_c} A_{j_1}^4 \exp\left\{ - \sum_{\eta=x,y,z} \left(\frac{(\bar\eta - \bar\eta_{j_1})^2}{(\bar w_{j_1 \eta}/\sqrt{2})^2} \right) \right\} \right.$$

$$+ \quad 2 \sum_{\substack{j_1, j_2 = 1 \\ j_1 \neq j_2}} A_{j_1}^2 A_{j_2}^2 \exp\left\{ - \sum_{\eta=x,y,z} \left(\frac{(\bar\eta - \bar\eta_{j_1 j_2})^2}{\bar w_{j_1 j_2 \eta}^2} + \frac{(\bar\eta_{j_1} - \bar\eta_{j_2})^2}{\bar w_{j_1 \eta}^2 + \bar w_{j_2 \eta}^2} \right) \right\} \right]$$

(4.70)

Now we are finally ready to calculate $\bar{L}_4$!

Inserting this form (Eq. (4.70)) into $\bar{L}_4$ we have

$$
\begin{aligned}
\bar{L}_4 &= \frac{\left(\frac{1}{2}\bar{g}N\right)}{N_c^2}\left[\sum_{j_1=1}^{N_c} A_{j_1}^4 \int d^3\bar{r}\, \exp\left\{-\sum_{\eta=x,y,z}\left(\frac{(\bar{\eta}-\bar{\eta}_{j_1})^2}{(\bar{w}_{j_1\eta}/\sqrt{2})^2}\right)\right\}\right.\\
&+ 2\sum_{\substack{j_1,j_2=1\\j_1\neq j_2}} A_{j_1}^2 A_{j_2}^2 \int d^3\bar{r}\, \exp\left\{-\sum_{\eta=x,y,z}\left(\frac{(\bar{\eta}-\bar{\eta}_{j_1j_2})^2}{\bar{w}_{j_1j_2\eta}^2}+\frac{(\bar{\eta}_{j_1}-\bar{\eta}_{j_2})^2}{\bar{w}_{j_1\eta}^2+\bar{w}_{j_2\eta}^2}\right)\right\}\right]\\
&= \frac{\left(\frac{1}{2}\bar{g}N\right)}{N_c^2}\left[\sum_{j_1=1}^{N_c} A_{j_1}^4 \int d^3\bar{r}\, \exp\left\{-\sum_{\eta=x,y,z}\left(\frac{(\bar{\eta}-\bar{\eta}_{j_1})^2}{(\bar{w}_{j_1\eta}/\sqrt{2})^2}\right)\right\}\right.\\
&+ 2\sum_{\substack{j_1,j_2=1\\j_1\neq j_2}} A_{j_1}^2 A_{j_2}^2 \exp\left\{-\sum_{\eta=x,y,z}\left(\frac{(\bar{\eta}_{j_1}-\bar{\eta}_{j_2})^2}{\bar{w}_{j_1\eta}^2+\bar{w}_{j_2\eta}^2}\right)\right\}\\
&\times \left.\int d^3\bar{r}\, \exp\left\{-\sum_{\eta=x,y,z}\left(\frac{(\bar{\eta}-\bar{\eta}_{j_1j_2})^2}{\bar{w}_{j_1j_2\eta}^2}\right)\right\}\right]\\
&= \frac{\left(\frac{1}{2}\bar{g}N\right)}{N_c^2}\left[\sum_{j_1=1}^{N_c} \left(\frac{1}{\pi^{3/2}\bar{w}_{j_1x}\bar{w}_{j_1y}\bar{w}_{j_1z}}\right)^2 \int d^3\bar{r}\, \exp\left\{-\sum_{\eta=x,y,z}\left(\frac{(\bar{\eta}-\bar{\eta}_{j_1})^2}{(\bar{w}_{j_1\eta}/\sqrt{2})^2}\right)\right\}\right.\\
&+ 2\sum_{\substack{j_1,j_2=1\\j_1\neq j_2}} \left(\frac{1}{\pi^{3/2}\bar{w}_{j_1x}\bar{w}_{j_1y}\bar{w}_{j_1z}}\right)\left(\frac{1}{\pi^{3/2}\bar{w}_{j_2x}\bar{w}_{j_2y}\bar{w}_{j_2z}}\right)\exp\left\{-\sum_{\eta=x,y,z}\left(\frac{(\bar{\eta}_{j_1}-\bar{\eta}_{j_2})^2}{\bar{w}_{j_1\eta}^2+\bar{w}_{j_2\eta}^2}\right)\right\}\\
&\times \left.\int d^3\bar{r}\, \exp\left\{-\sum_{\eta=x,y,z}\left(\frac{(\bar{\eta}-\bar{\eta}_{j_1j_2})^2}{\bar{w}_{j_1j_2\eta}^2}\right)\right\}\right]
\end{aligned}
$$

(4.71)

In the last step we used the constraint equations again. All that is left now is to perform the integrations!

Finally we take the current form of $\bar{L}_4$ and do the integrals (very easy now since we already did the hard work!):

$$
\bar{L}_4 = \frac{\left(\frac{1}{2}\bar{g}N\right)}{N_c^2}\left[\sum_{j_1=1}^{N_c} \left(\frac{1}{\pi^{3/2}\bar{w}_{j_1x}\bar{w}_{j_1y}\bar{w}_{j_1z}}\right)^2 \int d^3\bar{r}\, \exp\left\{-\sum_{\eta=x,y,z}\left(\frac{(\bar{\eta}-\bar{\eta}_{j_1})^2}{(\bar{w}_{j_1\eta}/\sqrt{2})^2}\right)\right\}\right.
$$

$$
+\ 2 \sum_{\substack{j_1,j_2=1\\ j_1\neq j_2}} \left(\frac{1}{\pi^{3/2}\bar{w}_{j_1x}\bar{w}_{j_1y}\bar{w}_{j_1z}}\right)\left(\frac{1}{\pi^{3/2}\bar{w}_{j_2x}\bar{w}_{j_2y}\bar{w}_{j_2z}}\right)\exp\left\{-\sum_{\eta=x,y,z}\left(\frac{(\bar{\eta}_{j_1}-\bar{\eta}_{j_2})^2}{\bar{w}_{j_1\eta}^2+\bar{w}_{j_2\eta}^2}\right)\right\}
$$

$$
\times\ \int d^3\bar{r}\,\exp\left\{-\sum_{\eta=x,y,z}\left(\frac{(\bar{\eta}-\bar{\eta}_{j_1j_2})^2}{\bar{w}_{j_1j_2\eta}^2}\right)\right\}\Bigg]
$$

$$
=\ \frac{\left(\frac{1}{2}\bar{g}N\right)}{N_c^2}\Bigg[\sum_{j_1=1}^{N_c}\left(\frac{1}{\pi^{3/2}\bar{w}_{j_1x}\bar{w}_{j_1y}\bar{w}_{j_1z}}\right)^2\left(\left(\frac{\pi^{1/2}}{2^{1/2}}\bar{w}_{j_1x}\right)\left(\frac{\pi^{1/2}}{2^{1/2}}\bar{w}_{j_1y}\right)\left(\frac{\pi^{1/2}}{2^{1/2}}\bar{w}_{j_1z}\right)\right)
$$

$$
+\ 2\sum_{\substack{j_1,j_2=1\\ j_1\neq j_2}}\left(\frac{1}{\pi^{3/2}\bar{w}_{j_1x}\bar{w}_{j_1y}\bar{w}_{j_1z}}\right)\left(\frac{1}{\pi^{3/2}\bar{w}_{j_2x}\bar{w}_{j_2y}\bar{w}_{j_2z}}\right)\exp\left\{-\sum_{\eta=x,y,z}\left(\frac{(\bar{\eta}_{j_1}-\bar{\eta}_{j_2})^2}{\bar{w}_{j_1\eta}^2+\bar{w}_{j_2\eta}^2}\right)\right\}
$$

$$
\times\ \left(\pi^{1/2}\bar{w}_{j_1j_2x}\right)\left(\pi^{1/2}\bar{w}_{j_1j_2y}\right)\left(\pi^{1/2}\bar{w}_{j_1j_2y}\right)\Bigg]
$$

$$
=\ \frac{\left(\frac{1}{2}\bar{g}N\right)}{N_c^2}\Bigg[\sum_{j_1=1}^{N_c}\left(\frac{1}{(2\pi)^{3/2}\bar{w}_{j_1x}\bar{w}_{j_1y}\bar{w}_{j_1z}}\right)
$$

$$
+\ 2\sum_{\substack{j_1,j_2=1\\ j_1\neq j_2}}\left(\frac{\bar{w}_{j_1j_2x}}{\pi^{1/2}\bar{w}_{j_1x}\bar{w}_{j_2x}}\right)\left(\frac{\bar{w}_{j_1j_2y}}{\pi^{1/2}\bar{w}_{j_1y}\bar{w}_{j_2y}}\right)\left(\frac{\bar{w}_{j_1j_2z}}{\pi^{1/2}\bar{w}_{j_1z}\bar{w}_{j_2z}}\right)
$$

$$
\times\ \exp\left\{-\sum_{\eta=x,y,z}\left(\frac{(\bar{\eta}_{j_1}-\bar{\eta}_{j_2})^2}{\bar{w}_{j_1\eta}^2+\bar{w}_{j_2\eta}^2}\right)\right\}\Bigg]
$$

$$
=\ \frac{\left(\frac{1}{2}\bar{g}N\right)}{(2\pi)^{3/2}N_c^2}\Bigg[\sum_{j_1=1}^{N_c}\left(\frac{1}{\bar{w}_{j_1x}\bar{w}_{j_1y}\bar{w}_{j_1z}}\right)
$$

$$
+\ 2\times2^{3/2}\sum_{\substack{j_1,j_2=1\\ j_1\neq j_2}}\frac{\exp\left\{-\frac{(\bar{x}_{j_1}-\bar{x}_{j_2})^2}{\bar{w}_{j_1x}^2+\bar{w}_{j_2x}^2}\right\}}{\left(\bar{w}_{j_1x}^2+\bar{w}_{j_2x}^2\right)^{1/2}}\frac{\exp\left\{-\frac{(\bar{y}_{j_1}-\bar{y}_{j_2})^2}{\bar{w}_{j_1y}^2+\bar{w}_{j_2y}^2}\right\}}{\left(\bar{w}_{j_1y}^2+\bar{w}_{j_2y}^2\right)^{1/2}}\frac{\exp\left\{-\frac{(\bar{z}_{j_1}-\bar{z}_{j_2})^2}{\bar{w}_{j_1z}^2+\bar{w}_{j_2z}^2}\right\}}{\left(\bar{w}_{j_1z}^2+\bar{w}_{j_2z}^2\right)^{1/2}}\Bigg]
$$

$$
\tag{4.72}
$$

Thus our final expression for $\bar{L}_4$ becomes

$$
\bar{L}_4=\frac{\left(\frac{1}{2}\bar{g}N\right)}{(2\pi)^{3/2}N_c^2}\Bigg[\sum_{j_1=1}^{N_c}\left(\frac{1}{\bar{w}_{j_1x}\bar{w}_{j_1y}\bar{w}_{j_1z}}\right)+2^{5/2}\sum_{\substack{j_1,j_2=1\\ j_1\neq j_2}}^{N_c}\prod_{\eta=x,y,z}\left(\frac{\exp\left\{-\frac{(\bar{\eta}_{j_1}-\bar{\eta}_{j_2})^2}{\bar{w}_{j_1\eta}^2+\bar{w}_{j_2\eta}^2}\right\}}{\left(\bar{w}_{j_1\eta}^2+\bar{w}_{j_2\eta}^2\right)^{1/2}}\right)\Bigg]
$$

4.1.9 Derivation of $\bar{L}_5$

The term $\bar{L}_5$ accounts for the possibility that the system is in a rotating frame. We will assume here that the system only rotates around the $\bar{z}$ axis. The $\bar{L}_5$ term of the Lagrangian thus has the form

$$\bar{L}_5 = i\bar{\Omega}_z \int d^3\bar{r} \, \Psi \left(\bar{y}\Psi_x^* - \bar{x}\Psi_y^* \right) \equiv i\bar{\Omega}_z \left(\bar{L}_{5y} - \bar{L}_{5x} \right) \tag{4.73}$$

It will be easy to evaluate this term if we note that $\bar{L}_{5y}$ defined by

$$\bar{L}_{5y} = \int d\bar{r}^3 \, \Psi \bar{y}\Psi_x^* \tag{4.74}$$

can be turned $\bar{L}_{5x}$ by interchanging $\bar{x}$ and $\bar{y}$. Thus we need only evaluate $\bar{L}_{5y}$.

The integral can be done straightforwardly by first evaluating the first space derivative of $\bar{\Psi}$. This is most easily done by rewriting $\bar{\Psi}$ as follows:

$$\bar{\Psi}(\bar{\mathbf{r}}, \bar{t}) = \frac{1}{\sqrt{N_c}} \sum_{j=1}^{N_c} A_j \exp \left\{ \sum_{\eta'=x',y',z'} \left(f_{j\eta'} + i\bar{k}_{j\eta'}\bar{\eta}' \right) \right\} \tag{4.75}$$

where

$$f_{j\eta'} = -\frac{(\bar{\eta} - \bar{\eta}_j)^2}{2\bar{w}_{j\eta}^2} + i\left(\bar{\alpha}_{j\eta}\bar{\eta} + \bar{\beta}_{j\eta}\bar{\eta}^2 \right) \equiv f_{j\eta}^{(r)} + if_{j\eta}^{(i)}. \tag{4.76}$$

With this form, we can express the derivative of Ψ as

$$\bar{\Psi}_\eta = \frac{1}{\sqrt{N_c}} \sum_{j=1}^{N_c} A_j \exp \left\{ \sum_{\eta'=x',y',z'} \left(f_{j\eta'} + i\bar{k}_{j\eta'}\bar{\eta}' \right) \right\} \left(-\frac{(\bar{\eta} - \bar{\eta}_j)}{\bar{w}_{j\eta}^2} + i\left(\bar{\alpha}_{j\eta} + 2\bar{\beta}_{j\eta}\bar{\eta} + \bar{k}_{j\eta} \right) \right) \tag{4.77}$$

Inserting this into Eq. 4.1.9 for the derivative of $\bar{\Psi}$ and neglecting rapidly oscillating terms, we finally obtain

$$i\bar{\Omega}_z \bar{L}_{5y} = \frac{1}{N_c} \sum_{j=1}^{N_c} \bar{\Omega}_z \bar{y}_j \left(\bar{\alpha}_{jx} + \bar{k}_{jx} + 2\bar{\beta}_{jx}\bar{x}_j \right) \tag{4.78}$$

and so the final expression for $\bar{L}_5$ is

$$\boxed{\bar{L}_5 = \frac{1}{N_c} \sum_{j=1}^{N_c} \bar{\Omega}_z \left[\bar{y}_j \left(\bar{\alpha}_{jx} + \bar{k}_{jx} + 2\bar{\beta}_{jx}\bar{x}_j \right) - \bar{x}_j \left(\bar{\alpha}_{jy} + \bar{k}_{jy} + 2\bar{\beta}_{jy}\bar{y}_j \right) \right]} \tag{4.79}$$

4.1.10 The final Lagrangian

Now that we have derived all five pieces of $\bar{L}$ it is time to put it all together. We have

$$
\begin{aligned}
\bar{L} &= \frac{1}{N_c} \sum_{j=1}^{N_c} \sum_{\eta=x,y,z} \left(\dot{\bar{\alpha}}_{j\eta} \bar{\eta}_j + \dot{\bar{\beta}}_{j\eta} \left(\bar{\eta}_j^2 + \frac{1}{2} \bar{w}_{j\eta}^2 \right) \right) \\
&+ \frac{1}{N_c} \sum_{j=1}^{N_c} \sum_{\eta=x,y,z} \left(\frac{1}{2\bar{w}_{j\eta}^2} + 2\bar{\beta}_{j\eta}^2 \bar{w}_{j\eta}^2 + \left(\bar{\alpha}_{j\eta} + \bar{k}_{j\eta} + 2\bar{\beta}_{j\eta}\bar{\eta}_j \right)^2 \right) \\
&+ \frac{1}{N_c} \sum_{j=1}^{N_c} \sum_{\eta=x,y,z} \left\{ \frac{1}{4} \left(\bar{\omega}_{T,\eta}^2 - \bar{\omega}_{TM}^2 \right) \left(\bar{\eta}_j^2 + \frac{1}{2} \bar{w}_{j\eta}^2 \right) - \frac{1}{2} \bar{\omega}_{TM}^2 |\bar{\mathbf{r}}_{TM}| u_{TM,\eta} \bar{\eta}_j \right\} \\
&+ \frac{\left(\frac{1}{2} \bar{g} N \right)}{(2\pi)^{3/2} N_c^2} \left[\sum_{j_1=1}^{N_c} \left(\frac{1}{\bar{w}_{j_1x} \bar{w}_{j_1y} \bar{w}_{j_1z}} \right) + 2^{5/2} \sum_{\substack{j_1,j_2=1 \\ j_1 \neq j_2}}^{N_c} \prod_{\eta=x,y,z} \left(\frac{\exp\left\{ -\frac{(\bar{\eta}_{j_1} - \bar{\eta}_{j_2})^2}{\bar{w}_{j_1\eta}^2 + \bar{w}_{j_2\eta}^2} \right\}}{\left(\bar{w}_{j_1\eta}^2 + \bar{w}_{j_2\eta}^2 \right)^{1/2}} \right) \right] \\
&+ \frac{1}{N_c} \sum_{j=1}^{N_c} \bar{\Omega}_z \left[\bar{y}_j \left(\bar{\alpha}_{jx} + \bar{k}_{jx} + 2\bar{\beta}_{jx} \bar{x}_j \right) - \bar{x}_j \left(\bar{\alpha}_{jy} + \bar{k}_{jy} + 2\bar{\beta}_{jy} \bar{y}_j \right) \right]
\end{aligned}
\tag{4.80}
$$

We can combine the first three sums into a single sum as follows:

$$
\begin{aligned}
\bar{L} &= \frac{1}{N_c} \sum_{j=1}^{N_c} \sum_{\eta=x,y,z} \left(\dot{\bar{\alpha}}_{j\eta} \bar{\eta}_j + \dot{\bar{\beta}}_{j\eta} \left(\bar{\eta}_j^2 + \frac{1}{2} \bar{w}_{j\eta}^2 \right) + \frac{1}{2\bar{w}_{j\eta}^2} + 2\bar{\beta}_{j\eta}^2 \bar{w}_{j\eta}^2 \right. \\
&\quad \left. + \left(\bar{\alpha}_{j\eta} + \bar{k}_{j\eta} + 2\bar{\beta}_{j\eta} \bar{\eta}_j \right)^2 + \frac{1}{4} \left(\bar{\omega}_{T,\eta}^2 - \bar{\omega}_{TM}^2 \right) \left(\bar{\eta}_j^2 + \frac{1}{2} \bar{w}_{j\eta}^2 \right) - \frac{1}{2} \bar{\omega}_{TM}^2 |\bar{\mathbf{r}}_{TM}| u_{TM,\eta} \bar{\eta}_j \right) \\
&+ \frac{\left(\frac{1}{2} \bar{g} N \right)}{(2\pi)^{3/2} N_c^2} \left[\sum_{j_1=1}^{N_c} \left(\frac{1}{\bar{w}_{j_1x} \bar{w}_{j_1y} \bar{w}_{j_1z}} \right) + 2^{5/2} \sum_{\substack{j_1,j_2=1 \\ j_1 \neq j_2}}^{N_c} \prod_{\eta=x,y,z} \left(\frac{\exp\left\{ -\frac{(\bar{\eta}_{j_1} - \bar{\eta}_{j_2})^2}{\bar{w}_{j_1\eta}^2 + \bar{w}_{j_2\eta}^2} \right\}}{\left(\bar{w}_{j_1\eta}^2 + \bar{w}_{j_2\eta}^2 \right)^{1/2}} \right) \right] \\
&+ \frac{1}{N_c} \sum_{j=1}^{N_c} \bar{\Omega}_z \left[\bar{y}_j \left(\bar{\alpha}_{jx} + \bar{k}_{jx} + 2\bar{\beta}_{jx} \bar{x}_j \right) - \bar{x}_j \left(\bar{\alpha}_{jy} + \bar{k}_{jy} + 2\bar{\beta}_{jy} \bar{y}_j \right) \right]
\end{aligned}
\tag{4.81}
$$

For purposes of deriving the equations of motion for the parameters we will write our Lagrangian in the following form:

$$
\begin{aligned}
\bar{L} &= \frac{1}{N_c} \sum_{j'=1}^{N_c} \sum_{\eta'=x,y,z} \left(\dot{\bar{\alpha}}_{j'\eta'} \bar{\eta}'_{j'} + \dot{\bar{\beta}}_{j'\eta'} \left(\bar{\eta}'^2_{j'} + \frac{1}{2} \bar{w}_{j'\eta'}^2 \right) + \frac{1}{2\bar{w}_{j'\eta'}^2} + 2\bar{\beta}_{j'\eta'}^2 \bar{w}_{j'\eta'}^2 \right. \\
&\quad \left. + \left(\bar{\alpha}_{j'\eta'} + \bar{k}_{j'\eta'} + 2\bar{\beta}_{j'\eta'} \bar{\eta}'_{j'} \right)^2 + \frac{1}{4} \left(\bar{\omega}_{T,\eta'}^2 - \bar{\omega}_{TM}^2 \right) \left(\bar{\eta}'^2_j + \frac{1}{2} \bar{w}_{j\eta'}^2 \right) \right.
\end{aligned}
$$

$$- \frac{1}{2}\bar{\omega}_{TM}^2 |\bar{\mathbf{r}}_{TM}| u_{TM,\eta'} \bar{\eta}'_j \bigg) + \bar{L}_4(\bar{\eta}, \bar{\mathbf{w}})$$

$$+ \frac{1}{N_c} \sum_{j=1}^{N_c} \bar{\Omega}_z \left[\bar{y}_j \left(\bar{\alpha}_{jx} + \bar{k}_{jx} + 2\bar{\beta}_{jx}\bar{x}_j \right) - \bar{x}_j \left(\bar{\alpha}_{jy} + \bar{k}_{jy} + 2\bar{\beta}_{jy}\bar{y}_j \right) \right] \qquad (4.82)$$

where

$$\bar{L}_4(\bar{\eta}, \bar{\mathbf{w}}) = \frac{\left(\frac{1}{2}\bar{g}N\right)}{(2\pi)^{3/2}N_c^2} \left[\sum_{j_1=1}^{N_c} \left(\frac{1}{\bar{w}_{j_1x}\bar{w}_{j_1y}\bar{w}_{j_1z}} \right) + 2^{5/2} \sum_{\substack{j_1,j_2=1 \\ j_1 \neq j_2}}^{N_c} \prod_{\eta'=x,y,z} \left(\frac{\exp\left\{ -\frac{\left(\bar{\eta}'_{j_1} - \bar{\eta}'_{j_2}\right)^2}{\bar{w}_{j_1\eta'}^2 + \bar{w}_{j_2\eta'}^2} \right\}}{\left(\bar{w}_{j_1\eta'}^2 + \bar{w}_{j_2\eta'}^2 \right)^{1/2}} \right) \right] .$$

$$(4.83)$$

It will turn out that the final equations of motion can be cast in terms of derivatives of $\bar{L}_4$. We now turn to this derivation.

4.2   Derivation of the 3D, N–gaussian–cloud equations of motion

The final set of equations of motion for the parameters of the N_c–cloud, Gaussian trial wave function divides naturallly into two parts: (1) an equation of motion for the coordinates of the center of each cloud, and (2) an equation of motion for the x,y, and z widths of each cloud. As we shall see, while each variational parameter, q_j, obeys an equation of motion set by the ordinary Euler–Lagrange equation:

$$\frac{d}{d\bar{t}} \left(\frac{\partial \bar{L}}{\partial \dot{q}_j} \right) - \frac{\partial \bar{L}}{\partial q_j} = 0, \qquad (4.84)$$

it will be possible to derive second–order differential equations for both the centers and widths reminiscent of Newton's Laws of Motion. In the full set of equations of motion, only the centers and widths and their time derivatives need to be solved for. All other parameters can be written in terms of these.

    We begin with the derivation of the equations for the center coordinates of the Gaussian clouds.

4.2.1 Equations of motion for the cloud centers

To obtain the equations of motion (EOMs) for the cloud–center coordinates we need the EOMs for the $\bar{\alpha}_{j\eta}$ and the $\bar{\eta}_j$. We begin with the EOMs for the $\bar{\alpha}_{j\eta}$. The Euler–Lagrange equation for these are

$$\frac{d}{d\bar{t}}\left(\frac{\partial \bar{L}}{\partial \dot{\bar{\alpha}}_{j\eta}}\right) - \frac{\partial \bar{L}}{\partial \bar{\alpha}_{j\eta}} = 0, \quad j = 1,\ldots,N_c, \ \eta = x,y,z. \tag{4.85}$$

We can compute the derivatives of $\bar{L}$ using Eq. (4.82). The derivative of $\bar{L}$ with respect to $\dot{\bar{\alpha}}_{j\eta}$ is

$$\frac{\partial \bar{L}}{\partial \dot{\bar{\alpha}}_{j\eta}} = \frac{1}{N_c}\eta_j, \quad j = 1,\ldots,N_c \ \eta = x,y,z. \tag{4.86}$$

The derivatives of $\bar{L}$ with respect to $\bar{\alpha}_{j\eta}$ are

$$\begin{aligned}
\frac{\partial \bar{L}}{\partial \bar{\alpha}_{jx}} &= \frac{1}{N_c}\left[2\bar{\alpha}_{jx} + 2\bar{k}_{jx} + 4\bar{\beta}_{jx}\bar{x}_j + \bar{\Omega}_z\bar{y}_j\right] \\
\frac{\partial \bar{L}}{\partial \bar{\alpha}_{jy}} &= \frac{1}{N_c}\left[2\bar{\alpha}_{jy} + 2\bar{k}_{jy} + 4\bar{\beta}_{jy}\bar{y}_j - \bar{\Omega}_z\bar{x}_j\right] \\
\frac{\partial \bar{L}}{\partial \bar{\alpha}_{jz}} &= \frac{1}{N_c}\left[2\bar{\alpha}_{jz} + 2\bar{k}_{jz} + 4\bar{\beta}_{jz}\bar{z}_j\right]
\end{aligned} \tag{4.87}$$

Thus the EOMs for the $\bar{\alpha}_{j\eta}$ are

$$\begin{aligned}
\dot{x}_j &= 2\bar{\alpha}_{jx} + 2\bar{k}_{jx} + 4\bar{\beta}_{jx}\bar{x}_j + \bar{\Omega}_z\bar{y}_j \\
\dot{y}_j &= 2\bar{\alpha}_{jy} + 2\bar{k}_{jy} + 4\bar{\beta}_{jy}\bar{y}_j - \bar{\Omega}_z\bar{x}_j \\
\dot{z}_j &= 2\bar{\alpha}_{jz} + 2\bar{k}_{jz} + 4\bar{\beta}_{jz}\bar{z}_j
\end{aligned} \tag{4.88}$$

To complete the derivation we need the EOMs associated with the $\bar{\eta}_j$.

The $\bar{\eta}_j$ Euler–Lagrange EOMs read

$$\frac{d}{d\bar{t}}\left(\frac{\partial \bar{L}}{\partial \dot{\bar{\eta}}_j}\right) - \frac{\partial \bar{L}}{\partial \bar{\eta}_j} = 0, \quad j = 1,\ldots,N_c, \ \eta = x,y,z. \tag{4.89}$$

We can easily calculate the derivatives appearing above

$$\frac{\partial \bar{L}}{\partial \dot{\bar{\eta}}_j} = 0, \quad j = 1,\ldots,N_c \ \eta = x,y,z \tag{4.90}$$

and

$$
\begin{aligned}
\frac{\partial \bar{L}}{\partial \bar{x}_j} &= \frac{1}{N_c}\Big[\dot{\bar{\alpha}}_{jx} + 2\dot{\bar{\beta}}_{jx}\bar{x}_j + 2\left(\bar{\alpha}_{jx} + \bar{k}_{jx} + 2\bar{\beta}_{jx}\bar{x}_j\right)\left(2\bar{\beta}_{jx}\right) \\
&\quad + \frac{1}{2}\left(\bar{\omega}_{T,x}^2 - \bar{\omega}_{TM}^2\right)\bar{x}_j - \frac{1}{2}\bar{\omega}_{TM}^2|\mathbf{r}_{TM}|u_{TM,x} + N_c\frac{\partial \bar{L}_4}{\partial \bar{x}_j} + 2\bar{\Omega}_z(\bar{\beta}_{jx} - \bar{\beta}_{jy})\bar{y}_j\Big] \\
\frac{\partial \bar{L}}{\partial \bar{y}_j} &= \frac{1}{N_c}\Big[\dot{\bar{\alpha}}_{jy} + 2\dot{\bar{\beta}}_{jy}\bar{y}_j + 2\left(\bar{\alpha}_{jy} + \bar{k}_{jy} + 2\bar{\beta}_{jy}\bar{y}_j\right)\left(2\bar{\beta}_{jy}\right) \\
&\quad + \frac{1}{2}\left(\bar{\omega}_{T,y}^2 - \bar{\omega}_{TM}^2\right)\bar{y}_j - \frac{1}{2}\bar{\omega}_{TM}^2|\mathbf{r}_{TM}|u_{TM,y} + N_c\frac{\partial \bar{L}_4}{\partial \bar{y}_j} + 2\bar{\Omega}_z(\bar{\beta}_{jx} - \bar{\beta}_{jy})\bar{x}_j\Big] \\
\frac{\partial \bar{L}}{\partial \bar{z}_j} &= \frac{1}{N_c}\Big[\dot{\bar{\alpha}}_{jz} + 2\dot{\bar{\beta}}_{jz}\bar{z}_j + 2\left(\bar{\alpha}_{jz} + \bar{k}_{jz} + 2\bar{\beta}_{jz}\bar{z}_j\right)\left(2\bar{\beta}_{jz}\right) \\
&\quad + \frac{1}{2}\left(\bar{\omega}_{T,z}^2 - \bar{\omega}_{TM}^2\right)\bar{z}_j - \frac{1}{2}\bar{\omega}_{TM}^2|\mathbf{r}_{TM}|u_{TM,z} + N_c\frac{\partial \bar{L}_4}{\partial \bar{z}_j}\Big]
\end{aligned}
\tag{4.91}
$$

Thus the EOMs associated with the $\bar{\eta}_j$ are

$$
\begin{aligned}
0 &= \dot{\bar{\alpha}}_{jx} + 2\dot{\bar{\beta}}_{jx}\bar{x}_j + 2\left(\bar{\alpha}_{jx} + \bar{k}_{jx} + 2\bar{\beta}_{jx}\bar{x}_j\right)\left(2\bar{\beta}_{jx}\right) \\
&\quad + \frac{1}{2}\left(\bar{\omega}_{T,x}^2 - \bar{\omega}_{TM}^2\right)\bar{x}_j - \frac{1}{2}\bar{\omega}_{TM}^2|\mathbf{r}_{TM}|u_{TM,x} + N_c\frac{\partial \bar{L}_4}{\partial \bar{x}_j} + 2\bar{\Omega}_z(\bar{\beta}_{jx} - \bar{\beta}_{jy})\bar{y}_j \\
0 &= \dot{\bar{\alpha}}_{jy} + 2\dot{\bar{\beta}}_{jy}\bar{y}_j + 2\left(\bar{\alpha}_{jy} + \bar{k}_{jy} + 2\bar{\beta}_{jy}\bar{y}_j\right)\left(2\bar{\beta}_{jy}\right) \\
&\quad + \frac{1}{2}\left(\bar{\omega}_{T,y}^2 - \bar{\omega}_{TM}^2\right)\bar{y}_j - \frac{1}{2}\bar{\omega}_{TM}^2|\mathbf{r}_{TM}|u_{TM,y} + N_c\frac{\partial \bar{L}_4}{\partial \bar{y}_j} + 2\bar{\Omega}_z(\bar{\beta}_{jx} - \bar{\beta}_{jy})\bar{x}_j \\
0 &= \dot{\bar{\alpha}}_{jz} + 2\dot{\bar{\beta}}_{jz}\bar{z}_j + 2\left(\bar{\alpha}_{jz} + \bar{k}_{jz} + 2\bar{\beta}_{jz}\bar{z}_j\right)\left(2\bar{\beta}_{jz}\right) \\
&\quad + \frac{1}{2}\left(\bar{\omega}_{T,z}^2 - \bar{\omega}_{TM}^2\right)\bar{z}_j - \frac{1}{2}\bar{\omega}_{TM}^2|\mathbf{r}_{TM}|u_{TM,z} + N_c\frac{\partial \bar{L}_4}{\partial \bar{z}_j}
\end{aligned}
\tag{4.92}
$$

We can simplify these equations by using Eqs. 4.88:

$$2\dot{\alpha}_{jx} + 4\dot{\bar{\beta}}_{jx}\bar{x}_j + 4\bar{\beta}_{jx}\dot{\bar{x}}_j = -\left(\bar{\omega}_{T,x}^2 - \bar{\omega}_{TM}^2\right)\bar{x}_j + \bar{\omega}_{TM}^2|\mathbf{r}_{TM}|u_{TM,x} - 2N_c\frac{\partial \bar{L}_4}{\partial \bar{x}_j} + 4\bar{\Omega}_z\bar{\beta}_{jy}\bar{y}_j$$

$$2\dot{\alpha}_{jy} + 4\dot{\bar{\beta}}_{jy}\bar{y}_j + 4\bar{\beta}_{jy}\dot{\bar{y}}_j = -\left(\bar{\omega}_{T,y}^2 - \bar{\omega}_{TM}^2\right)\bar{y}_j + \bar{\omega}_{TM}^2|\mathbf{r}_{TM}|u_{TM,y} - 2N_c\frac{\partial \bar{L}_4}{\partial \bar{y}_j} - 4\bar{\Omega}_z\bar{\beta}_{jx}\bar{x}_j$$

$$2\dot{\alpha}_{jz} + 4\dot{\bar{\beta}}_{jz}\bar{z}_j + 4\bar{\beta}_{jz}\dot{\bar{z}}_j = -\left(\bar{\omega}_{T,z}^2 - \bar{\omega}_{TM}^2\right)\bar{z}_j + \bar{\omega}_{TM}^2|\mathbf{r}_{TM}|u_{TM,z} - 2N_c\frac{\partial \bar{L}_4}{\partial \bar{z}_j}$$

$$(4.93)$$

To find the EOMs for the $\bar{\eta}_j$ alone, we differentiate both sides of Eqs. (4.88):

$$\ddot{\bar{x}}_j = 2\dot{\alpha}_{jx} + 4\dot{\bar{\beta}}_{jx}\bar{x}_j + 4\bar{\beta}_{jx}\dot{\bar{x}}_j + \bar{\Omega}_z\dot{\bar{y}}_j$$

$$\ddot{\bar{y}}_j = 2\dot{\alpha}_{jy} + 4\dot{\bar{\beta}}_{jy}\bar{y}_j + 4\bar{\beta}_{jy}\dot{\bar{y}}_j - \bar{\Omega}_z\dot{\bar{x}}_j$$

$$\ddot{\bar{z}}_j = 2\dot{\alpha}_{jz} + 4\dot{\bar{\beta}}_{jz}\bar{z}_j + 4\bar{\beta}_{jz}\dot{\bar{z}}_j$$

$$(4.94)$$

Combining the above equations with Eqs. 4.93 yields the equations of motion for the center coordinates and their derivatives.

$$\ddot{\bar{x}}_j - \bar{\Omega}_z\dot{\bar{y}}_j = -\left(\bar{\omega}_{T,x}^2 - \bar{\omega}_{TM}^2\right)\bar{x}_j + \bar{\omega}_{TM}^2|\mathbf{r}_{TM}|u_{TM,x} - 2N_c\frac{\partial \bar{L}_4}{\partial \bar{x}_j} + 4\bar{\Omega}_z\bar{\beta}_{jy}\bar{y}_j$$

$$\ddot{\bar{y}}_j + \bar{\Omega}_z\dot{\bar{x}}_j = -\left(\bar{\omega}_{T,y}^2 - \bar{\omega}_{TM}^2\right)\bar{y}_j + \bar{\omega}_{TM}^2|\mathbf{r}_{TM}|u_{TM,y} - 2N_c\frac{\partial \bar{L}_4}{\partial \bar{y}_j} - 4\bar{\Omega}_z\bar{\beta}_{jx}\bar{x}_j$$

$$\ddot{\bar{z}}_j = -\left(\bar{\omega}_{T,z}^2 - \bar{\omega}_{TM}^2\right)\bar{z}_j + \bar{\omega}_{TM}^2|\mathbf{r}_{TM}|u_{TM,z} - 2N_c\frac{\partial \bar{L}_4}{\partial \bar{z}_j}$$

$$(4.95)$$

These equations may be written in a form reminiscent of Newton's 2nd Law of motion.

$$\ddot{\bar{x}}_j + \left(\bar{\omega}_{T,x}^2 - \bar{\omega}_{TM}^2\right)\bar{x}_j = 4\bar{\Omega}_z\bar{\beta}_{jy}\bar{y}_j + \bar{\Omega}_z\dot{\bar{y}}_j + \bar{\omega}_{TM}^2|\mathbf{r}_{TM}|u_{TM,x} - 2N_c\frac{\partial \bar{L}_4}{\partial \bar{x}_j}$$

$$\ddot{\bar{y}}_j + \left(\bar{\omega}_{T,y}^2 - \bar{\omega}_{TM}^2\right)\bar{y}_j = -4\bar{\Omega}_z\bar{\beta}_{jx}\bar{x}_j - \bar{\Omega}_z\dot{\bar{x}}_j + \bar{\omega}_{TM}^2|\mathbf{r}_{TM}|u_{TM,y} - 2N_c\frac{\partial \bar{L}_4}{\partial \bar{y}_j}$$

$$\ddot{\bar{z}}_j + \left(\bar{\omega}_{T,z}^2 - \bar{\omega}_{TM}^2\right)\bar{z}_j = \bar{\omega}_{TM}^2|\mathbf{r}_{TM}|u_{TM,z} - 2N_c\frac{\partial \bar{L}_4}{\partial \bar{z}_j}$$

$$(4.96)$$

These are the final equations of motion for positions and velocities of the centers of the Gaussian clouds. The derivative of $\bar{L}_4$ will be given in Appendix B. Note that

these equations do not form a closed set since the $\bar{L}_4$ derivative also contains the widths.

4.2.2   Equations of motion for the cloud widths

Next we turn to the EOMs for the cloud widths. We can also derive a second–order EOM for the widths similar to that for the centers. To derive this equation we first consider the EOMs associated with the $\bar{\beta}_{j\eta}$. The Euler–Lagrange equation for these quanties is

$$\frac{d}{d\bar{t}}\left(\frac{\partial \bar{L}}{\partial \dot{\bar{\beta}}_{j\eta}}\right) - \frac{\partial \bar{L}}{\partial \bar{\beta}_{j\eta}} = 0, \quad j = 1,\ldots,N_c,\ \eta = x,y,z. \tag{4.97}$$

The derivatives of $\bar{L}$ appearing above are as follows. First we have the derivative with respect to the $\dot{\bar{\beta}}_{j\eta}$:

$$\frac{\partial \bar{L}}{\partial \dot{\bar{\beta}}_{j\eta}} = \frac{1}{N_c}\left[\bar{\eta}_{j\eta}^2 + \frac{1}{2}\bar{w}_{j\eta}^2\right], \tag{4.98}$$

and the derivative with respect to the $\bar{\beta}_{j\eta}$ is

$$\frac{\partial \bar{L}}{\partial \bar{\beta}_{j\eta}} = \frac{1}{N_c}\left[4\bar{\beta}_{j\eta}\bar{w}_{j\eta}^2 + 2\left(\bar{\alpha}_{j\eta} + \bar{k}_{j\eta} + 2\bar{\beta}_{j\eta}\bar{\eta}_j\right)(2\bar{\eta}_j)\right]. \tag{4.99}$$

With these derivatives, the EOM associated with the $\bar{\beta}_{j\eta}$ is

$$2\bar{\eta}_j\dot{\bar{\eta}}_j + \bar{w}_{j\eta}\dot{\bar{w}}_{j\eta} = 4\bar{\beta}_{j\eta}\bar{w}_{j\eta}^2 + (4\bar{\eta}_j)\left(\bar{\alpha}_{j\eta} + \bar{k}_{j\eta} + 2\bar{\beta}_{j\eta}\bar{\eta}_j\right) + 2\left(\delta_{\eta,x} - \delta_{\eta,y}\right)\bar{\Omega}_z\bar{x}_j\bar{y}_j \tag{4.100}$$

where these equations hold for $j = 1,\ldots,N_c$ and $\eta = x,y,z$ and $\delta_{x,\eta}$ is the Kronecker delta.

We can simplify Eq. (4.100) by substituting the expression for $\dot{\bar{\eta}}_j$ from Eq. (4.88):

$$2\bar{\eta}_j\left(2\bar{\alpha}_{j\eta} + 2\bar{k}_{j\eta} + 4\bar{\beta}_{j\eta}\bar{\eta}_j\right) + \bar{w}_{j\eta}\dot{\bar{w}}_{j\eta} = 4\bar{\beta}_{j\eta}\bar{w}_{j\eta}^2 + (4\bar{\eta}_j)\left(\bar{\alpha}_{j\eta} + \bar{k}_{j\eta} + 2\bar{\beta}_{j\eta}\bar{\eta}_j\right) \tag{4.101}$$

Note that the first term on the left–hand–side (LHS) cancels the second term on the right–hand–side (RHS). This leaves us with a particularly simple relationship between $\bar{\beta}_{j\eta}$ and $\bar{w}_{j\eta}$ and $\dot{\bar{w}}_{j\eta}$ which can be expressed this way

$$\dot{\bar{w}}_{j\eta} = 4\bar{\beta}_{j\eta}\bar{w}_{j\eta} \quad j = 1,\ldots,N_c\ \eta = x,y,z \tag{4.102}$$

This equation will be key in deriving the equation for the widths. Note also that, if the widths and their derivatives are solved for, then the values of the $\bar{\beta}_{j\eta}$ can be immediately calculated.

Next we need the EOM associated with the $\bar{w}_{j\eta}$. The Euler–Lagrange equation is

$$\frac{d}{d\bar{t}}\left(\frac{\partial \bar{L}}{\partial \dot{\bar{w}}_{j\eta}}\right) - \frac{\partial \bar{L}}{\partial \bar{w}_{j\eta}} = 0, \quad j = 1,\ldots,N_c,\ \eta = x,y,z. \tag{4.103}$$

The derivatives appearing here can be calculated as follows. The derivative with respect to the $\dot{\bar{w}}_{j\eta}$ is

$$\frac{\partial \bar{L}}{\partial \dot{\bar{w}}_{j\eta}} = 0. \tag{4.104}$$

The derivative with respect to the $\bar{w}_{j\eta}$ is

$$\frac{\partial \bar{L}}{\partial \bar{w}_{j\eta}} = \frac{1}{N_c}\left[\dot{\bar{\beta}}_{j\eta}\bar{w}_{j\eta} - \frac{1}{\bar{w}_{j\eta}^3} + 4\bar{\beta}_{j\eta}^2\bar{w}_{j\eta} + \frac{1}{4}\left(\bar{\omega}_{T,\eta}^2 - \bar{\omega}_{TM}^2+\right)\bar{w}_{j\eta} + N_c\frac{\partial \bar{L}_4}{\partial \bar{w}_{j\eta}}\right]. \tag{4.105}$$

Inserting these derivatives into the Euler–Lagrange equation can be written in this form

$$\dot{\bar{\beta}}_{j\eta}\bar{w}_{j\eta} + 4\bar{\beta}_{j\eta}^2\bar{w}_{j\eta} + \frac{1}{4}\left(\bar{\omega}_{T,\eta}^2 - \bar{\omega}_{TM}^2\right)\bar{w}_{j\eta} = \frac{1}{\bar{w}_{j\eta}^3} - N_c\frac{\partial \bar{L}_4}{\partial \bar{w}_{j\eta}} \tag{4.106}$$

The first two terms of this equation can be related to the second derivative of the $\bar{w}_{j\eta}$.

If we differentiate both sides of Eq. (4.102) we obtain

$$\ddot{\bar{w}}_{j\eta} = 4\dot{\bar{\beta}}_{j\eta}\bar{w}_{j\eta} + 4\bar{\beta}_{j\eta}\dot{\bar{w}}_{j\eta} = 4\dot{\bar{\beta}}_{j\eta}\bar{w}_{j\eta} + 16\bar{\beta}_{j\eta}^2\bar{w}_{j\eta}$$

$$\frac{1}{4}\ddot{\bar{w}}_{j\eta} = \dot{\bar{\beta}}_{j\eta}\bar{w}_{j\eta} + 4\bar{\beta}_{j\eta}^2\bar{w}_{j\eta} \tag{4.107}$$

where in the second equality on the first line we used the Eq. (4.102) to replace $\dot{\bar{w}}_{j\eta}$. Note now that the RHS of the above equation is identical to the first two terms in Eq. (4.106) and so these terms can be replaced with $(1/4)\ddot{\bar{w}}_{j\eta}$. This yields the final evolution equation for the widths:

$$\ddot{\bar{w}}_{j\eta} + \left(\bar{\omega}_{T,\eta}^2 - \bar{\omega}_{TM}^2\right)\bar{w}_{j\eta} = \frac{4}{\bar{w}_{j\eta}^3} - 4N_c\frac{\partial \bar{L}_4}{\partial \bar{w}_{j\eta}} \tag{4.108}$$

where $j = 1, \ldots, N_c$ and $\eta = x, y, z$ and the derivative of $\bar{L}_4$ will be given in Appendix B. The equations of motion for the cloud widths are unaffected by the rotating–frame terms. This is especially satisfying physically.

4.2.3   Full set of equations of motion

Now we are finally able to set out the full equations of motion for all of the variational parameters. They consist of a pair of second–order ordinary differential equation for the cloud centers and widths as well as expressions for the $\bar{\beta}_{j\eta}$ and the $\bar{\alpha}_{j\eta}$ in terms of the centers, width and their first derivatives:

$$\ddot{\bar{x}}_j + \left(\bar{\omega}_{T,x}^2 - \bar{\omega}_{TM}^2\right)\bar{x}_j = 4\bar{\Omega}_z\bar{\beta}_{jy}\bar{y}_j + \bar{\Omega}_z\dot{\bar{y}}_j + \bar{\omega}_{TM}^2|\mathbf{r}_{TM}|u_{TM,x} - 2N_c\frac{\partial\bar{L}_4}{\partial\bar{x}_j}$$

$$\ddot{\bar{y}}_j + \left(\bar{\omega}_{T,y}^2 - \bar{\omega}_{TM}^2\right)\bar{y}_j = -4\bar{\Omega}_z\bar{\beta}_{jx}\bar{x}_j - \bar{\Omega}_z\dot{\bar{x}}_j + \bar{\omega}_{TM}^2|\mathbf{r}_{TM}|u_{TM,y} - 2N_c\frac{\partial\bar{L}_4}{\partial\bar{y}_j}$$

$$\ddot{\bar{z}}_j + \left(\bar{\omega}_{T,z}^2 - \bar{\omega}_{TM}^2\right)\bar{z}_j = \bar{\omega}_{TM}^2|\mathbf{r}_{TM}|u_{TM,z} - 2N_c\frac{\partial\bar{L}_4}{\partial\bar{z}_j}$$

$$\ddot{\bar{w}}_{j\eta} + \left(\bar{\omega}_{T,\eta}^2 - \bar{\omega}_{TM}^2\right)\bar{w}_{j\eta} = \frac{4}{\bar{w}_{j\eta}^3} - 4N_c\frac{\partial\bar{L}_4}{\partial\bar{w}_{j\eta}}$$

$$\dot{\bar{w}}_{j\eta} = 4\bar{\beta}_{j\eta}\bar{w}_{j\eta}$$

$$\bar{\alpha}_{j\eta} = \frac{1}{2}\dot{\bar{\eta}}_j - \bar{k}_{j\eta} - 2\bar{\beta}_{j\eta}\bar{\eta}_j$$

$$j = 1, \ldots, N_c$$

$$\eta = x, y, z.$$

Recall that the $\bar{k}_{j\eta}$ are assumed known and correspond to the components of the initial velocities of the N_c clouds in the system. These equation can't be solved with specifying the initial conditions. We assume that these equations describe approximately the evolution of the condensate for the case where a condensate is formed and then split into N_c *equal–size* clouds with known wave vectors. In this case the initial positions of the cloud center are all the same and correspond to the location of the original condensate. The initial velocities of the cloud centers are determined from

the given wave vectors which are already explicitly included in the trial wave function so that (in scaled units) we must have

$$\dot{\bar{\eta}}_j(0) = 2\bar{k}_{j\eta}. \tag{4.109}$$

Now, since, from the above EOM for $\bar{\alpha}_{j\eta}$ we see that

$$\dot{\bar{\eta}}_j(0) = 2\bar{\alpha}_{j\eta}(0) + 2\bar{k}_{j\eta} + 4\bar{\beta}_{j\eta}(0)\bar{\eta}_{j\eta}(0). \tag{4.110}$$

Now we have

$$\bar{\beta}_{j\eta}(0) = \frac{\dot{\bar{w}}_{j\eta}(0)}{\bar{w}_{j\eta}(0)} = 0 \tag{4.111}$$

since we assume that, for a initially stationary condensate we will have $\dot{\bar{w}}(0) = 0$. Thus we must also have $\bar{\alpha}_{j\eta}(0) = 0$. The guiding principle is that the initial conditions for the variational parameter, at the time the condensate is initially formed, are such that the variational equations will be stationary (i.e. none of the parameter will varying in time unless conditions changes). Thus, if we assume that the initial widths are denoted by $\bar{w}_{j\eta}(0) = \bar{w}_{j\eta}^{(0)}$, then the initial conditions for the variational parameters at the time a condensate is newly formed are the following:

$$\bar{\eta}_j(0) = \bar{\eta}_j^{(0)} \quad \dot{\bar{\eta}}_j(0) = 2\bar{k}_{j\eta} \quad \bar{w}_{j\eta}(0) = \bar{w}_{j\eta}^{(0)} \quad \dot{\bar{w}}_{j\eta}(0) = 0 \tag{4.112}$$

These initial conditions determine all of the others.

One final note regarding the initial widths. Since the variational widths should remain stationary for an initially formed condensate, the initial widths, $\bar{w}_{j\eta}^{(0)}$ must satisfy the width EOM with the time derivative term set to zero. That is

$$\left(\bar{\omega}_{T,\eta}^2 - \bar{\omega}_{TM}^2\right)\bar{w}_{j\eta}^{(0)} = \frac{4}{\left(\bar{w}_{j\eta}^{(0)}\right)^3} - 4N_c\frac{\partial\bar{L}_4}{\partial\bar{w}_{j\eta}}(\bar{w}_{j\eta}^{(0)}) \tag{4.113}$$

for all j and η. It is usual to drop the term containing $\bar{\omega}_{TM}$ since it is small and usually unknown.

CHAPTER 5

VISUALIZATION

5.1 Virtual Reality and Stereography

Visualizations of the simulation results summarize the properties and relationships we wish to study in the raw data. In general, visualizations are projections of multi-dimensional data onto a two dimensional plane. A specific summarization technique must be defined to compose a useful visual result. In our case, the result we wish to visualize is the optical density, which is described in detail below.

However, we are also able to choose the medium in which the visualization is composed. For this work, we choose to display the optical density as a stereographic projection viewed in a virtual reality headset. Stereographic projections of a common subject are pairs of images rendered from slightly different vantage points. The variation in vantage points simulates the human perspective such that some details in the subject occlude other details. Occlusion provides a sense of depth, enabling the interpretation of how details of the subject are arranged in three dimension. In the context of rendering optical density, it is hoped that adding depth enables features such as fringes, holes, discontinuities, and boundaries to be more readily visible.

Virtual reality headsets, like the Oculus Rift [21] (see figure 5.1), are now generally available in consumer markets. The Oculus Rift headset includes a high definition screen, similar to a commodity cell phone or tablet screen. High index spherical lenses aid in focusing the viewer's vision and alleviating eye strain. Infrared LED lights surrounding the headset enables tracking of the placement and orientation of the headset relative to a camera placed in front of the user. The Oculus is not a stand-alone system and requires a computer to render the visuals it will display.

The Oculus enables an individual to experience stereographic visualizations for relatively low cost. The Oculus is also more portable than a 3D capable television

Figure 5.1: Oculus Rift: a virtual reality headset.

or projection system. The headset tracking data can be used to pan and rotate the viewpoint to locate interesting features of the visualized data. The work below describes a near real time system to display stereographic movies that can be viewed on a virtual reality headset. These efforts can be extended into a true real time visualization capability that can take advantage of head tracking data. We describe projections of optical density, but visualizations of phase and velocity fields are also feasible.

5.2 Composing Scenes for Virtual Reality

In this chapter, we discuss how to create visualizations of the time-evolving Bose-Einstein Condensate wave functions based on the LVM trial wave function and Equations of Motion from section 4.2.3. We consider how to calculate the optical density in subsections 5.2.1 and 5.2.2, which is one property of interest. To do so, we must consider how to determine which points to within the bounding volume are to be used for each calculation. This is accomplished using a method known as ray casting, described in subsections 5.2.4 and 5.2.5. Section 5.2.6 describe how to pick the rays

being used to query the BEC volume. Next, we describe pairs of projection planes used to create stereographic projections in subsection 5.2.6.

5.2.1 Calculating Optical Density

In chapter 4, we created a model of the time-evolution of Bose-Einstein Condensate clouds in a harmonic potential. The wave function describes the state of the system. One value of interest is the optical density, which is the portion of the probability density, $\int_{-\infty}^{\infty} d^3r \, |\Psi(\mathbf{r}, t)|^2$, integrated along a vector passing through the condensate. In a physical experiment, we can photograph a BEC; doing so destroys the condensate so each photograph of a time-evolved system requires a separate condensate to be formed and evolved. The light passing through the condensate forms a shadow, which is captured with a camera. The value at each pixel of the camera sensor is the optical density; see [20] for examples.

The Equations of Motion (EoM) are used to evolve the condensate clouds in time. At each time step, the EoM are evaluated to generate the parameters for each cloud position, width, and phase terms. From these terms, we can calculate the value of the wave function all any position of interest within the bounding volume defined for the condensate.

Contrast this with our discussion of the split-step Crank-Nicolson (CN) method in section 2.4. In the CN method, we were required to store the evaluation of the wave function on a 3-D grid and over time. There are generally tens or hundreds of millions of grid points at each time step. We were also required to calculate very fine-grained time steps just to store and process many fewer. However, the results of the EoM mean we only store about a dozen values–per BEC cloud–at each time step. Additionally, since the wave function can be evaluated in near real-time, it does not have to be evaluated and stored. Additionally, since we can calculate the

time-evolution to any desired time-step without intermediary calculations, we do not have to sample fine-grained time steps as a matter of necessity.

5.2.2   Equation for Optical Density

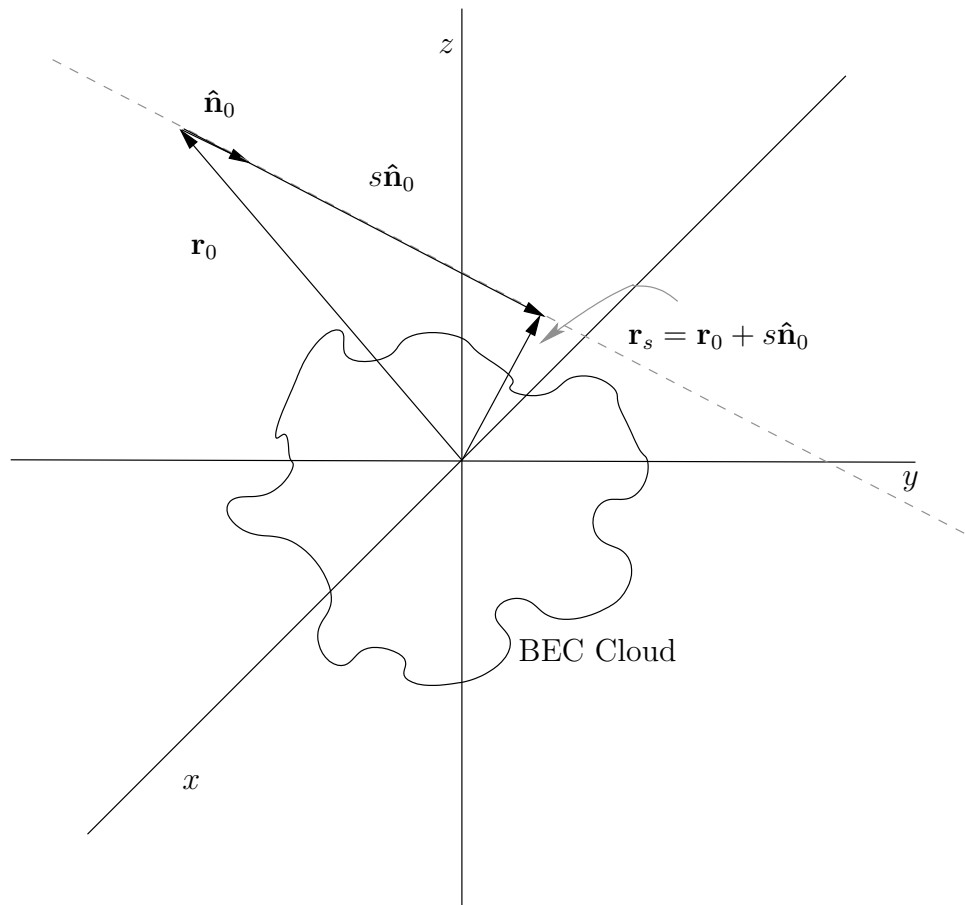Figure 5.2: Defining a single ray cast through the cloud calculating each position $\mathbf{r}_s$ along the ray.

For the moment, we will assume that we may define a vector $\mathbf{r}$ which intersects some portion of the condensate volume. We will define how to calculate useful $\mathbf{r}$'s in the subsections below.

In Figure 5.2, we show a condensate anchored in a Cartesian coordinate system

with unit vectors $\hat{\mathbf{i}}, \hat{\mathbf{j}}$, and $\hat{\mathbf{k}}$ in the x, y, and z axes. The vector $\mathbf{r}_0 = x_0\hat{\mathbf{i}} + y_0\hat{\mathbf{j}} + z_0\hat{\mathbf{k}}$, rooted at the origin, defines a point in space from which we will observe the optical density. From this point, the unit vector $\hat{\mathbf{n}}_0$ defines rays that intersect the volume containing the clouds. We are interested in equal spaced slices s along $\hat{\mathbf{n}}_0$. Therefore, any point along $\hat{\mathbf{n}}_0$ can be defined as such.

$$\mathbf{r}(s) = \mathbf{r}_0 + \hat{\mathbf{n}}_0 s \tag{5.1}$$

$$= (x_0 + n_{0_x}s)\hat{\mathbf{i}} + (y_0 + n_{0_y}s)\hat{\mathbf{j}} + (z_0 + n_{0_z}s)\hat{\mathbf{k}} \tag{5.2}$$

$$= \mathbf{x}(s) + \mathbf{y}(s) + \mathbf{z}(s) \tag{5.3}$$

It is the vector $\mathbf{r}(s)$, over all s within the bounding volume, that defines the limits of the integration for our optical density. The optical density, calculated along this vector, is defined as

$$\rho_{\mathrm{OD}} = \int\limits_{-\infty}^{\infty} \mathrm{d}s \, |\Psi(\mathbf{r}(s), t)|^2 \tag{5.4}$$

5.2.3 Scaled Units

As in Section 4.1.2, we scale the units to the small scale of a Bose-Einstein Condensate. We must use the same value for the length scaling factor L_0 to correctly interpret the results of our LVM calculations.

For reference, a common scaling factor is $L_0 = 10^{-5}m$.

$$s \equiv L_0 \, \bar{s} \tag{5.5}$$

$$\mathbf{r}_0 \equiv L_0 \, \bar{\mathbf{r}}_0 \tag{5.6}$$

$$r(s) \equiv L_0 \, \bar{\mathbf{r}}(s) \equiv L_0 \left(\bar{\mathbf{x}}(\bar{s}) + \bar{\mathbf{y}}(\bar{s}) + \bar{\mathbf{z}}(\bar{s}) \right) \tag{5.7}$$

$$t \equiv T_0 \bar{t} \tag{5.8}$$

$$\Psi(\mathbf{r}, t) \equiv L_0^{-3/2} \, \bar{\Psi}(\bar{\mathbf{r}}, \bar{t}) \tag{5.9}$$

$$\rho_{OD}(\mathbf{r}(s), t) \equiv L_0^{-2} \, \bar{\rho}_O(\bar{\mathbf{r}}, \bar{t}) \tag{5.10}$$

$$\equiv \int_{-\infty}^{\infty} \mathrm{d}\bar{s} \, |\bar{\Psi}(\bar{\mathbf{r}}_0(\bar{s}), \bar{t})|^2 \tag{5.11}$$

5.2.4   Integrating Optical Density

Referring to Figure 5.2, we must calculate the optical density by projecting a vector through our condensate bounding volume and integrating the wave function. Our wave function is the same trial wave function utilized for the LVM method (in scaled units).

$$\Psi(\bar{\mathbf{r}}(\bar{s}), \bar{t}) = \frac{1}{\sqrt{N_c}} \sum_{j=1}^{N_c} e^{f_j(\bar{\mathbf{r}}(\bar{s}), \bar{t}) + i\bar{\mathbf{k}}_j \cdot \bar{\mathbf{r}}(\bar{s})} \tag{5.12}$$

where

$$f_j(\bar{\mathbf{r}}(\bar{s}), \bar{t}) = \sum_{\eta=x,y,z} \left(-\frac{(\bar{\eta} - \bar{\eta}_j)^2}{2\bar{w}_{j\eta}^2} + i\bar{\alpha}_{j\eta}\bar{\eta} + i\bar{\beta}_{j\eta}\bar{\eta}^2 \right) \tag{5.13}$$

Recall, there may be j condensate clouds, $\bar{\eta}_j$ is the position of a cloud center, $\bar{w}_{j\eta}$ is the width of a cloud, $\bar{\alpha}_{j\eta}$ is the linear phase coefficient and $\bar{\beta}_{j\eta}$ is the quadratic phase coefficient, where $\eta = x, y, z$. All terms are in scaled units and are the results of the LVM evaluation method. Each term is relevant to the current time step.

We substitute Eq. 5.12 into Eq. 5.11.

$$\bar{\rho}_{OD} = \int_{-\infty}^{\infty} \mathrm{d}\bar{s} \left(\frac{1}{\sqrt{N_c}} \sum_{j_1=1}^{N_c} e^{f_{j_1}(\bar{\mathbf{r}}(\bar{s}), \bar{t}) + i\bar{\mathbf{k}}_{j_1} \cdot \bar{\mathbf{r}}(\bar{s})} \right)^{\star} \left(\frac{1}{\sqrt{N_c}} \sum_{j_2=1}^{N_c} e^{f_{j_2}(\bar{\mathbf{r}}(\bar{s}), \bar{t}) + i\bar{\mathbf{k}}_{j_2} \cdot \bar{\mathbf{r}}(\bar{s})} \right) \tag{5.14}$$

$$= \frac{1}{N_c} \sum_{j_1, j_2=1}^{N_c} \int_{-\infty}^{\infty} \mathrm{d}\bar{s} \, \exp\left[f_{j_1}^{\star}(\bar{\mathbf{r}}(\bar{s}), \bar{t}) + f_{j_2}(\bar{\mathbf{r}}(\bar{s}), \bar{t}) + i \left(\bar{\mathbf{k}}_{j_2} - \bar{\mathbf{k}}_{j_1} \right) \cdot \bar{\mathbf{r}}(\bar{s}) \right] \tag{5.15}$$

Expanding $\bar{\mathbf{r}}(\bar{s})$ with Eq 5.2 and expanding the exponential term with Eq. 5.13,

$$
= \frac{1}{N_c} \sum_{j_1,j_2=1}^{N_c} \int_{-\infty}^{\infty} \mathrm{d}\bar{s} \, \exp\Bigg\{ \sum_{\eta=x,y,z} \Bigg[-\frac{(\eta_0 + n_{0_\eta}\bar{s} - \eta_{j_2})^2}{2w_{j_2\eta}^2}
$$

$$
+ \, i\,\alpha_{j_2\eta}(\eta_0 + n_{0_\eta}\bar{s}) \, + \, i\,\beta_{j_2\eta}(\eta_0 + n_{0_\eta}\bar{s})^2
$$

$$
- \, \frac{(\eta_0 + n_{0_\eta}\bar{s} - \eta_{j_1})^2}{2w_{j_1\eta}^2}
$$

$$
- \, i\,\alpha_{j_1\eta}(\eta_0 + n_{0_\eta}\bar{s}) \, - \, i\,\beta_{j_1\eta}(\eta_0 + n_{0_\eta}\bar{s})^2
$$

$$
+ \, (k_{j_2\eta} - k_{j_1\eta})(\eta_0 + n_{0_\eta}\bar{s}) \Bigg] \Bigg\} \tag{5.16}
$$

Grouping terms by multiples of $\bar{s}$ and $i\bar{s}$

$$
= \frac{1}{N_c} \sum_{j_1,j_2=1}^{N_c} \int_{-\infty}^{\infty} \mathrm{d}\bar{s} \, \exp\Bigg\{ \sum_{\eta=x,y,z} \Bigg[\Bigg(-\frac{1}{2w_{j_2\eta}^2} - \frac{1}{2w_{j_1\eta}^2} + i\left(\beta_{j_2\eta} - \beta_{j_1\eta}\right) \Bigg) n_{0\eta}^2 \bar{s}^2
$$

$$
+ \Bigg(-\frac{(\eta_0 - \eta_{j_2})}{w_{j_2\eta}^2} - \frac{(\eta_0 - \eta_{j_1})}{w_{j_1\eta}^2}
$$

$$
+ i\left(\alpha_{j_2\eta} + 2\beta_{j_2\eta}\eta_0 + k_{j_2\eta} - \alpha_{j_1\eta} - 2\beta_{j_1\eta}\eta_0 - k_{j_1\eta}\right) \Bigg) n_{0\eta}\bar{s}
$$

$$
+ \Bigg(-\frac{(\eta_0 - \eta_{j_2})^2}{2w_{j_2\eta}^2} - \frac{(\eta_0 - \eta_{j_1})^2}{2w_{j_1\eta}^2}
$$

$$
+ i\left(\alpha_{j_2\eta}\eta_0 + \beta_{j_2\eta}\eta_0^2 + k_{j_2\eta}\eta_0 - \alpha_{j_1\eta}\eta_0 - \beta_{j_1\eta}\eta_0^2 - k_{j_1\eta}\eta_0\right) \Bigg) \Bigg] \Bigg\} \tag{5.17}
$$

To analytically integrate Eq. 5.17, we will define the following.

$$
a_{j_1 j_2} = \sum_{\eta=x,y,z} \left[\frac{1}{2w_{j_1\eta}^2} + \frac{1}{2w_{j_2\eta}^2} + i\left(\beta_{j_1\eta} - \beta_{j_2\eta}\right) \right] n_{0_\eta}^2 \tag{5.18}
$$

$$
b_{j_1 j_2} = \sum_{\eta=x,y,z} \left[\frac{(\eta_0 - \eta_{j_1})}{w_{j_1\eta}^2} + \frac{(\eta_0 - \eta_{j_2})}{w_{j_2\eta}^2} \right.
$$

$$
\left. + i\left((\alpha_{j_1\eta} - \alpha_{j_2\eta}) + 2(\beta_{j_1\eta} - \beta_{j_2\eta})\eta_0 + (k_{j_1\eta} - k_{j_2\eta}) \right) \right] n_{0\eta} \tag{5.19}
$$

$$
c_{j_1 j_2} = \sum_{\eta=x,y,z} \left[\frac{(\eta_0 - \eta_{j_1})^2}{2w_{j_1\eta}^2} + \frac{(\eta_0 - \eta_{j_2})^2}{2w_{j_2\eta}^2} \right.
$$

$$
\left. + i\left((\alpha_{j_1\eta} - \alpha_{j_2\eta})\eta_0 + (k_{j_1\eta} - k_{j_2\eta})\eta_0 + (\beta_{j_1\eta} - \beta_{j_2\eta})\eta_0^2 \right) \right] \tag{5.20}
$$

$$
a_{j_1 j_2} = a_{j_2 j_1}^\star \qquad b_{j_1 j_2} = b_{j_2 j_1}^\star \qquad c_{j_1 j_2} = c_{j_2 j_1}^\star \tag{5.21}
$$

$$\bar{\rho}_{OD} = \frac{1}{N_c} \sum_{j_1,j_2=1}^{N_c} \int_{-\infty}^{\infty} \mathrm{d}\bar{s} \, \exp\left[-\left(a_{j_1j_2}\bar{s}^2 + b_{j_1j_2}\bar{s} + c_{j_1j_2}\right) \right] \tag{5.22}$$

We can now complete the square.

$$a_{j_1j_2}\bar{s}^2 + b_{j_1j_2}\bar{s} + c_{j_1j_2} = a_{j_1j_2}\left(\bar{s} + \frac{b_{j_1j_2}}{2a_{j_1j_2}}\right)^2 - \left(\frac{b_{j_1j_2}^2 - 4a_{j_1j_2}c_{j_1j_2}}{4a_{j_1j_2}}\right) \tag{5.23}$$

Substituting Eq. 5.23 into Eq. 5.22 yields an integral we can solve with reference to Eq. A.8.

$$\bar{\rho}_{OD} = \frac{1}{N_c} \sum_{j_1,j_2=1}^{N_c} \int_{-\infty}^{\infty} \mathrm{d}\bar{s} \, \exp\left\{ -\left(a_{j_1j_2}\bar{s}^2 + b_{j_1j_2}\bar{s}^2 + c_{j_1j_2}\right) \right\} \tag{5.24}$$

$$= \frac{1}{N_c} \sum_{j_1,j_2=1}^{N_c} \int_{-\infty}^{\infty} \mathrm{d}\bar{s} \, \exp\left\{ -a_{j_1j_2}\left(\bar{s} + \frac{b_{j_1j_2}}{2a_{j_1j_2}}\right)^2 \right\} \exp\left\{ \frac{b_{j_1j_2}^2 - 4a_{j_1j_2}c_{j_1j_2}}{4a_{j_1j_2}} \right\}$$

$$\tag{5.25}$$

And we can solve this integral analytically.

$$\boxed{\bar{\rho}_{OD} = \frac{1}{N_c} \sum_{j_1,j_2=1}^{N_c} \pi^{\frac{1}{2}} a_{j_1j_2}^{-\frac{1}{2}} \exp\left\{ \frac{b_{j_1j_2}^2}{4\,a_{j_1j_2}} - c_{j_1j_2} \right\}} \tag{5.26}$$

Thus, the optical density along a ray projected from $\bar{r}_0$ along the $\hat{\mathbf{n}}_0$ direction is computed by Eq. 5.26. All of the variables are provided by solutions to the LVM EoM or from the properties of the cast ray.

5.2.5   Intersecting the Volume

The optical density, Eq. 5.26, depends upon the values of the vectors used to determine the rays cast through the condensate volume. These vectors include the vector from the origin to the center of the viewer's eye, $\bar{\mathbf{r}}(\bar{s})$, the unit vector from the eye to the gaze point, $\hat{\mathbf{n}}_0$, and the center of each cloud, $\bar{x}_j\hat{\mathbf{i}} + \bar{y}_j\hat{\mathbf{j}} + \bar{z}_j\hat{\mathbf{k}}, j = 1, 2, \ldots N_c$. As

described by Eqs. 5.40 and 5.41 We are able to define rays that are rooted in a plane surrounding the eye position or some distance D_{pp} along $\hat{\mathbf{u}}_0$ between the eye and the gaze point.

The condensate clouds reside within a volume of space which is undefined by these equations. The intersection of the volume by projections along the gaze vector $\hat{\mathbf{n}}_0$ is assumed based on the construction of eye point and gaze point. In other words, there is no term used to define an intersection with the bounding volume. Additionally, there is no term that in which such intersections influence the calculation of the optical density. In many graphical rendering systems it is useful to define a bounding volume, which could limit the total distance along a ray that is integrated. These limits would be input to the integral for the optical density as minimum and maximum values of the $\bar{s}$ variable. However, such limits are not required to evaluate Eq. 5.26.

Additionally, the condensate clouds, as constructed with the LVM wave function and Equations of Motion, are not defined within an explicit bounding volume. For certain, the integration of the wave function should be invalid at some distance from the condensate clouds, but we assume that this distance is much farther than the volume in which the clouds evolve over the total time of the simulation. Therefore, the positions of the eye and gaze point are assumed to be localized the volume for which the LVM wave function and Equations of Motion are valid. No other viewpoint is of value.

Under these assumptions, no bounding volume is required to be explicitly defined to integrate the optical density, which is a summation over sample points. Other calculations–such as the velocity field–may necessitate a bounding volume. Such calculations uniquely process each sample point within the condensate clouds; in other words, something more complicated than a summation over the sample points. In such cases, a bounding volume is appropriate to limit the total number of computations.
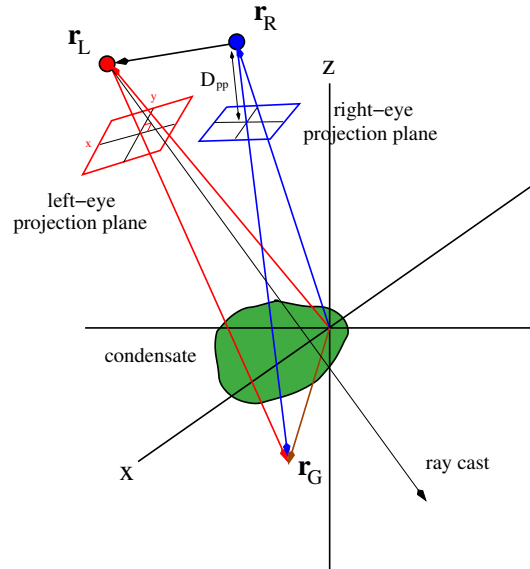
Figure 5.3: Projecting rays into a sample to build a stereographic image.

Alternatively, a pair of view frustum planes [32] may be utilized as in many other three dimensional rendering systems.

5.2.6 Stereographic Projections

We have described integration of the optical density along a vector from the eye position to a gaze point which passes through the condensate clouds. To compose an image, we require at least one vector per pixel. Further, a stereographic rendering requires two images.

Figure 5.3 extends the notions developed in Section 5.2.2 to capture a pair of images. The concepts are the same, but we now add a pair of gaze vectors: $\mathbf{r}_L$ for the left-eye viewpoint and $\mathbf{r}_R$ for the right-eye viewpoint. The vector $\mathbf{r}_{EE}$ is the eye-to-eye vector from the left-eye to the right-eye. This vector controls the placement of the

eyes relative to each other and the amount of stereographic separation experienced by a viewer.

Additionally, we have to alternate our render between three coordinate systems. First, we have the coordinates of the wave function, centered at the origin of the axes in Figure 5.3. In the equations below, vectors represented in these coordinates have a (wf) superscript applied.

$$\mathbf{r_L}^{(\mathrm{wf})} = x_L^{(\mathrm{wf})}\hat{\mathbf{i}} + y_L^{(\mathrm{wf})}\hat{\mathbf{j}} + z_L^{(\mathrm{wf})}\hat{\mathbf{k}} \tag{5.27}$$

$$\mathbf{r_R}^{(\mathrm{wf})} = x_R^{(\mathrm{wf})}\hat{\mathbf{i}} + y_R^{(\mathrm{wf})}\hat{\mathbf{j}} + z_R^{(\mathrm{wf})}\hat{\mathbf{k}} \tag{5.28}$$

$$\mathbf{r_G}^{(\mathrm{wf})} = x_G^{(\mathrm{wf})}\hat{\mathbf{i}} + y_G^{(\mathrm{wf})}\hat{\mathbf{j}} + z_G^{(\mathrm{wf})}\hat{\mathbf{k}} \tag{5.29}$$

$$\hat{\mathbf{u}}_L^{(\mathrm{wf})} = \frac{\mathbf{r_G}^{(\mathrm{wf})} - \mathbf{r_L}^{(\mathrm{wf})}}{|\mathbf{r_G}^{(\mathrm{wf})} - \mathbf{r_L}^{(\mathrm{wf})}|} \qquad \text{Left eye to gaze point.} \tag{5.30}$$

$$\hat{\mathbf{u}}_R^{(\mathrm{wf})} = \frac{\mathbf{r_G}^{(\mathrm{wf})} - \mathbf{r_R}^{(\mathrm{wf})}}{|\mathbf{r_G}^{(\mathrm{wf})} - \mathbf{r_R}^{(\mathrm{wf})}|} \qquad \text{Right eye to gaze point.} \tag{5.31}$$

$$\mathbf{r_{EE}}^{(\mathrm{wf})} = \mathbf{r_R}^{(\mathrm{wf})} - \mathbf{r_L}^{(\mathrm{wf})} \qquad \text{Left eye to Right eye.} \tag{5.32}$$

$$\hat{\mathbf{x}}^{(\mathrm{wf})} = \hat{\mathbf{i}} \qquad \hat{\mathbf{y}}^{(\mathrm{wf})} = \hat{\mathbf{j}} \qquad \hat{\mathbf{z}}^{(\mathrm{wf})} = \hat{\mathbf{k}} \tag{5.33}$$

$$\hat{\mathbf{z}}_L^{(\mathrm{wf})} = \hat{\mathbf{u}}_L^{(\mathrm{wf})} \tag{5.34}$$

$$\hat{\mathbf{y}}_L^{(\mathrm{wf})} = \frac{\mathbf{r_{EE}}^{(\mathrm{wf})} \times \hat{\mathbf{u}}_L^{(\mathrm{wf})}}{|\mathbf{r_{EE}}^{(\mathrm{wf})} \times \hat{\mathbf{u}}_L^{(\mathrm{wf})}|} \tag{5.35}$$

$$\hat{\mathbf{x}}_L^{(\mathrm{wf})} = \hat{\mathbf{z}}_L^{(\mathrm{wf})} \times \hat{\mathbf{y}}_L^{(\mathrm{wf})} \tag{5.36}$$

$$\hat{\mathbf{z}}_R^{(\mathrm{wf})} = \hat{\mathbf{u}}_R^{(\mathrm{wf})} \tag{5.37}$$

$$\hat{\mathbf{y}}_R^{(\mathrm{wf})} = \frac{\mathbf{r_{EE}}^{(\mathrm{wf})} \times \hat{\mathbf{u}}_R^{(\mathrm{wf})}}{|\mathbf{r_{EE}}^{(\mathrm{wf})} \times \hat{\mathbf{u}}_R^{(\mathrm{wf})}|} \tag{5.38}$$

$$\hat{\mathbf{x}}_L^{(\mathrm{wf})} = \hat{\mathbf{z}}_R^{(\mathrm{wf})} \times \hat{\mathbf{y}}_R^{(\mathrm{wf})} \tag{5.39}$$

The optical density at any point on the Left or Right projection planes is thus calculated by the ray For each image we define a grid of pixels centered around the

$\mathbf{r}_L$ and $\mathbf{r}_R$ gaze vectors. We label these vectors with L and R and the subscript *grid*. We can convert their positions into wave function coordinates with the following equations.

$$\mathbf{r_L}^{(\text{wf})}(i,j) = \mathbf{r_L}^{(\text{wf})} + \mathrm{D_{pp}}\hat{\mathbf{u}}_L^{(\text{wf})} + x_{L,\text{grid}}(i)\hat{\mathbf{x}}_L^{(\text{wf})} + y_{L,\text{grid}}(j)\hat{\mathbf{y}}_L^{(\text{wf})} \tag{5.40}$$

$$\mathbf{r_R}^{(\text{wf})}(i,j) = \mathbf{r_R}^{(\text{wf})} + \mathrm{D_{pp}}\hat{\mathbf{u}}_R^{(\text{wf})} + x_{L,\text{grid}}(i)\hat{\mathbf{x}}_R^{(\text{wf})} + y_{L,\text{grid}}(j)\hat{\mathbf{y}}_R^{(\text{wf})} \tag{5.41}$$

for all i and j along the grid.

We can now render the optical density of the condensate clouds as two images. For each pair of images we define our eye positions, gaze point, and number and spacing of pixels. The results of solving the LVM Equations of Motion are input into the rendering equations, resulting in a value for the optical density along each ray for each eye.

5.3 Final Composition

This optical density values are input into a 2D plotting program to render a frame, mapping values to colors that summarize the optical density. This process is repeated, creating images for both the right and left eye across all time steps. The images are stored as Portable Network Graphics (PNG) [29] files to reduce artifacts from color space compression that result from lossy image formats such as JPEG [27].

Next, all of the images are processed into a video which stitches the right and left eye images from each time step into a side-by-side frame. The video is rendered with high-quality settings to reduce visual artifacts from compression while maintaining a manageable file size.

Finally, the video can be viewed using video playback software. Some software can read a video of side-by-side Left and Right views and display it on the Oculus Rift.

In this manner, 3-D stereographic videos of time-evolving Bose-Einstein Condensates may be viewed.

5.4 Summarized Procedure

The steps described above can be repeated via the following generalized procedure. This procedure is repeated at least twice. First, the evolution from the Initial Split until the clouds overlap for the Final Split is rendered. The Final Split doubles the number of clouds, so a modified program is utilized to render the time evolution of the Final Split. The same procedure is repeated with the modified programs.

This procedure is near-real-time and can be expected to take several minutes to complete. Compared to the alternative scheme described in Section 2.5.2, it is of sufficiently small time frame to be of use. However, there is potential to optimize the procedure for real-time rendering. This would enable playback of the simulation on a virtual reality headset, like the Oculus Rift, and use head tracking to control the viewpoint. These extensions are not described in this thesis.

- Run the 3D LVM program to get a solution file and the input file to go with it.

- Configure and run the "oculus_lvm_movie" program. This creates a collection of left-eye and right-eye optical density data files: l000, l001, ..., r000, r001, ...

- Run Gnu Plot with the command file "png_movie.gnu". This yields a collection of left-eye and right-eye images: l000.png, l001.png, ..., r000.png, r001.png, ...

- Run the "trim_oculus_frames.sh" script. This crops all of the images to a uniform size and removes the white space surrounding the image.

- Run script "make_oculus_movie.sh" which uses the program "avconv" (a variant of "ffmpeg") to stitch the individual images into a trio of video files: (1) left-eye movie, (2) right-eye movie, and (3) side-by-side to view on the oculus.

5.5 Example Visualizations

Shown below are visualizations of the optical density from a simulation of the Atom Interferometry experiment. Two examples are show: one without a Test Mass as a control and a second with an exaggerated Test Mass. The tools developed to render this simulation are intended to explore the design parameters for future high-fidelity simulations using computationally expensive tools. The simulation and visualization tools cannot estimate the value of Big G.

5.5.1 Simulation Parameters

Variables that can be adjusted via this tool include the following.

- M_{TM} the mass of the Test Mass.

- $\mathbf{r}_{TM}$ the location of the Test Mass relative to the center of the initial condensate cloud.

- $\omega_{T,x}$, $\omega_{T,x}$, and $\omega_{T,x}$, the frequencies of the harmonic trap. A higher frequency corresponds to a trap that squeezes the condensate tighter. The trap is not required to be spherical.

- g, the coefficient representing the scattering length (distance of interaction between atoms in a cloud). This can be used adjust the interaction between atoms to model specific situations. For instance, setting $g = 0$ removes all affects of repulsion between the atoms. This is also modified to model different species of atoms in the condensate.

- N, the number of atoms in the initial condensate.

- N_c, the number of clouds created from the initial split.

- G, the Gravitational Constant, which can be modified to test the sensitivity of the simulation to different measurements of Big G. Again, this simulation and visualization tool box do not provide a detailed estimate of Big G.

5.5.2   Visualization Parameters

Each frame-pair visualizes the optical density of the evolving system from the left-eye and right-eye perspectives. In addition to the physical parameters for the simulation, the parameters determining the visualization results can be adjusted. For each eye position in the frame-pairs, the following parameters can be adjusted to influence the final images.

- Resolution in the $x-$ and $y-$directions. These determine the number of pixels represented in each direction in the final frames. These need not be symmetric as it can be advantageous to increase the resolution in one direction, but save computational using a lower resolution in the other direction.

- Spacing between the center of each pixel. This determines the field of view for the frame. Having a lower spacing provides a finer view of over a smaller area. A larger spacing provides less detail of the area, but more area can be captured..

- Number of frames to render or time step size between frames. These adjust the total number of frames necessary to be rendered.

- $\mathbf{r}_L$ and $\mathbf{r}_R$, positions of the rendering planes from the origin of the condensate clouds.

- D_{pp}, distance from the eyeball position to the rendering planes.

- $\mathbf{r}_{EE}$, distance between each eye, which can be adjusted to increase the stereo-scopic separation.

The total computation necessary to render each frame is directly proportional to the number of total pixels to be rendered. These parameters allow the user to trade visual fidelity and time to render. Course renders at relatively large distances give good overviews of the total expansion as the system evolves. Granular renders at close distances enhance the details of the Final Split.

5.5.3 Parameters of Examples

In the examples below, the Test Mass is large, $M_{TM} = 10^5\,\text{kg}$, and quite close, $|\mathbf{r}_{TM}|^2 = 10^{-2}\,\text{m} = 1\,\text{cm}$. These values were chosen to exaggerate the effects of Big G in the Final Split so they are visually apparent. This is sufficient to demonstrate the utility of the simulation and visualization tools. There are $N = 10^5$ atoms in the Initial Condensate. The interaction coefficient is given by Eq. 2.8, $g = \frac{4\pi\hbar^2 a}{M}$, where a is the scattering length. The scattering length for ^{87}Rb is $\approx 0.529 \times 10^{-8}$ meters. In scaled units this value is $\bar{g} \approx 0.0133$.

Figure 5.4 displays the dimensions of the Initial Split images in Figures 5.6 and 5.7. The events from the Initial Split through Overlap are simulated across 500 ms. This is divided as 50 ms for the Initial Split and Separation phases, 400 ms for the Evolution phase, and 50 ms for the Overlap phase. The LVM solver samples these events across 50000 time steps, each of which is $\delta t = 10^{-5}\,\text{s} = 10\,\mu\text{s}$. From the LVM samples, 100 samples are rendered to represent the optical density. The viewpoint of these renderings is $100\,L_o = 1\,mm$, along the z-axis.

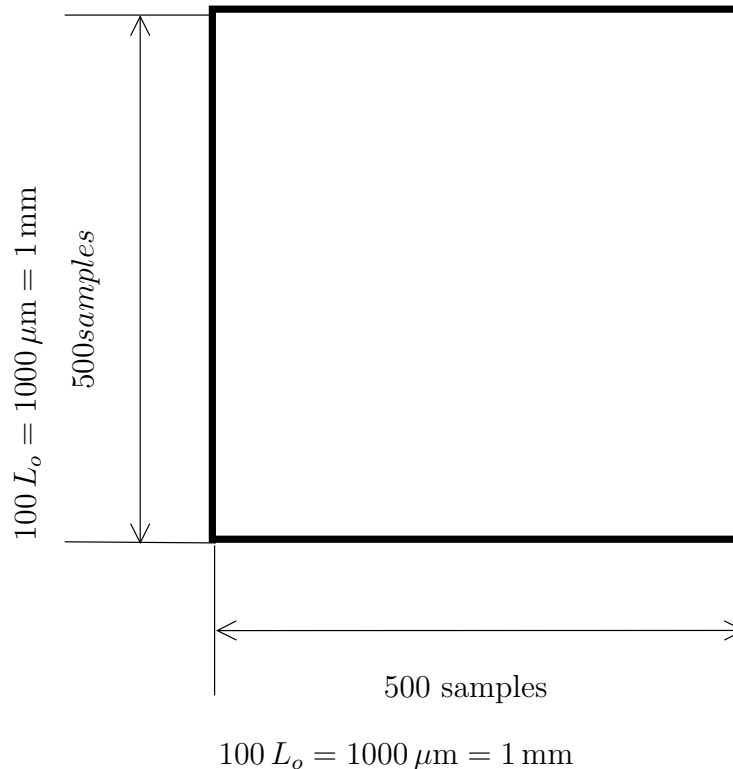Figure 5.4 displays the dimensions of the Final Split images in Figure 5.8. Note

Figure 5.4: Dimensions and sample resolutions of the images in Figures 5.6 and 5.7.

that the vertical resolution is much lower than the horizontal resolution. More resolution is required to clearly define the interference fringes, which run vertically. Additionally, these images are much closer to the condensate than the Initial Split images. The Final Split is sampled by the LVM solver over $10^{-3}\,s = 10\,\mathrm{ms}$, split into 50000 time steps, each of which is $\delta t = 5 \times 10^{-8}\,\mathrm{s} = 50\,\mathrm{ns}$. From the LVM samples, 100 samples are rendered to represent the optical density.

All images are colored to help accentuate the solutions to the wave function–the number of atoms–at each point. Dark red indicates high optical densities, with descending values ordered as the spectrum of white light: bright red, orange, yellow, green, and bright blue. Dark blue indicates zero.

Additional runs of the simulation over a variety of inputs will be necessary to develop an intuition regarding the physical constraints of the Atom Interferometer.
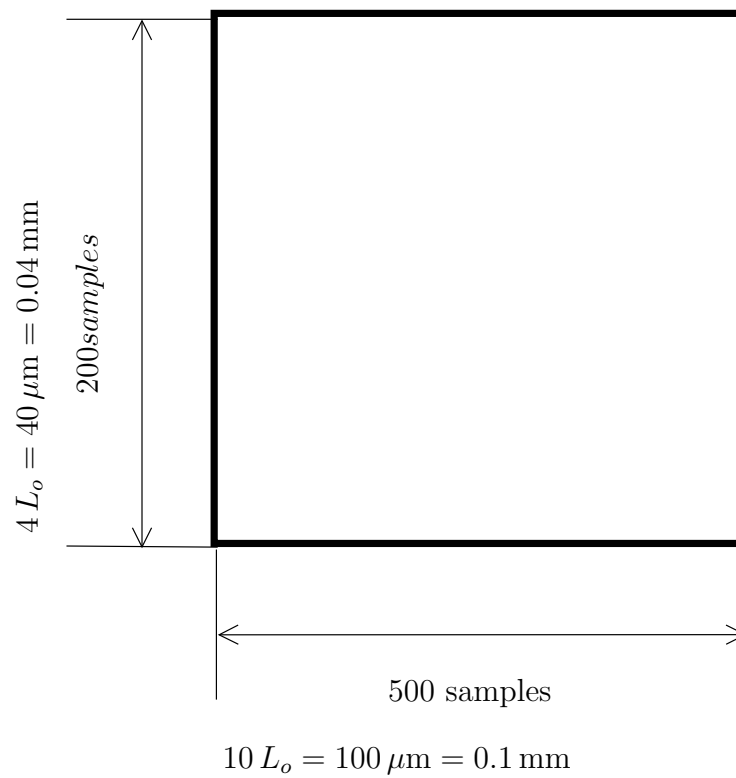
Figure 5.5: Dimensions and sample resolutions of the images in Figure 5.8.

This thesis does not present those results; it is left for future endeavors.

5.5.4 Initial Split Without Test Mass

Figure 5.6 displays a series of time steps in the Atom Interferometry simulation following the Initial Split event. No Test Mass is present. The optical density of the Atom Interferometer is visualized as it evolves between the Initial Split and Final Split events. The initial condensate, not shown, is compressed by the harmonic trap and is too small to be seen from this viewpoint and with this resolution. The same is true as the clouds overlap for the Final Split event.

Notice the cloud widths increase as they move from the origin in the presence of the same trap that confined the initial condensate to a much smaller volume. After the Initial Split the clouds are less dense; each cloud contains half as many atoms as the initial condensate. Consequently, the reduced density enables the condensate atoms to repel each other into a larger volume.

5.5.5 Initial Split With Test Mass

Figure 5.7 displays a series of time steps in the Atom Interferometry simulation in which a Test Mass present. The Test Mass, not shown, is to the right of the system along the x-axis. All other parameters are the same as described in sections 5.5.3 and 5.5.4.

Compared with the visualizations in Figure 5.6 several differences can be noted. First, the images 5.7.(f) through (j) clearly show the condensate clouds shifting to the right while the harmonic trap is turned off. Compare these to the equivalent images in Figure 5.6. It is clear that this is a result of the Test Mass. This effect is also noticeable by comparing 5.7.(e) with 5.7.(j).
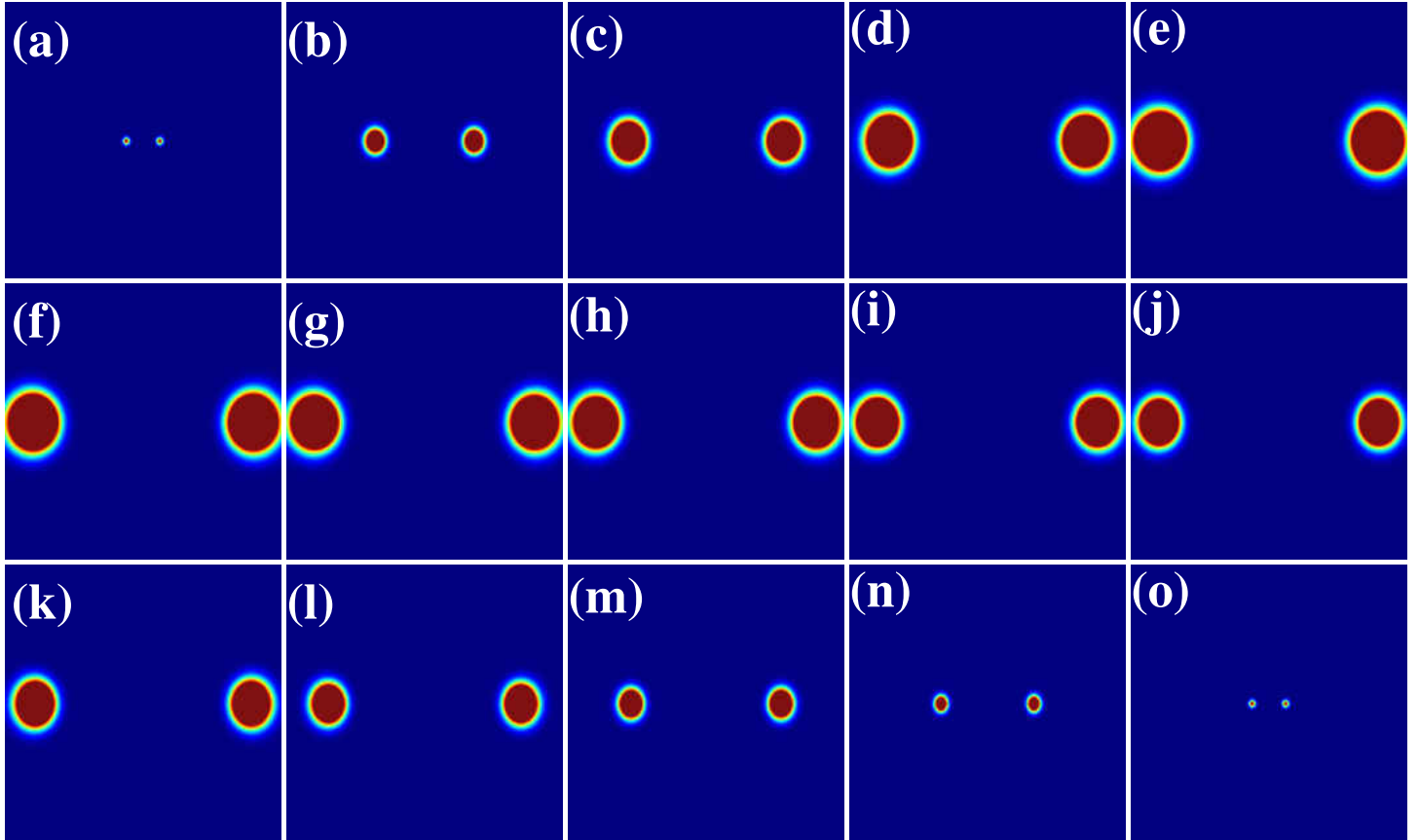
Figure 5.6: Initial Split of condensate without a Test Mass. Images (a) to (e): Clouds separating under the harmonic trap. Time steps 1, 3, 5, 7, and 9. Images (f) to (j): Clouds evolving with the harmonic trap turned off. Time steps 25, 41, 57, 73, and 90. Images (k) to (o): The harmonic trap is restored and the clouds return to the center to overlap for the Final split. Time steps 91, 93, 95, 97, and 99. Total elapsed time as shown is 198 ms.

Figure 5.7: Initial Split of condensate with a Test Mass of 10^5 kg. Images (a) to (e): Clouds separating under the harmonic trap. Time steps 1, 3, 5, 7, and 9. Images (f) to (j): Clouds evolving with the harmonic trap turned off. Notice the clouds moving to the right relative to their positions in (e) or in 5.6.(e). Time steps 25, 41, 57, 73, and 90. Images (k) to (o): The harmonic trap is restored and the clouds return to the center to overlap for the Final split. Time steps 91, 93, 95, 97, and 99. Total elapsed time as shown is 198 ms.
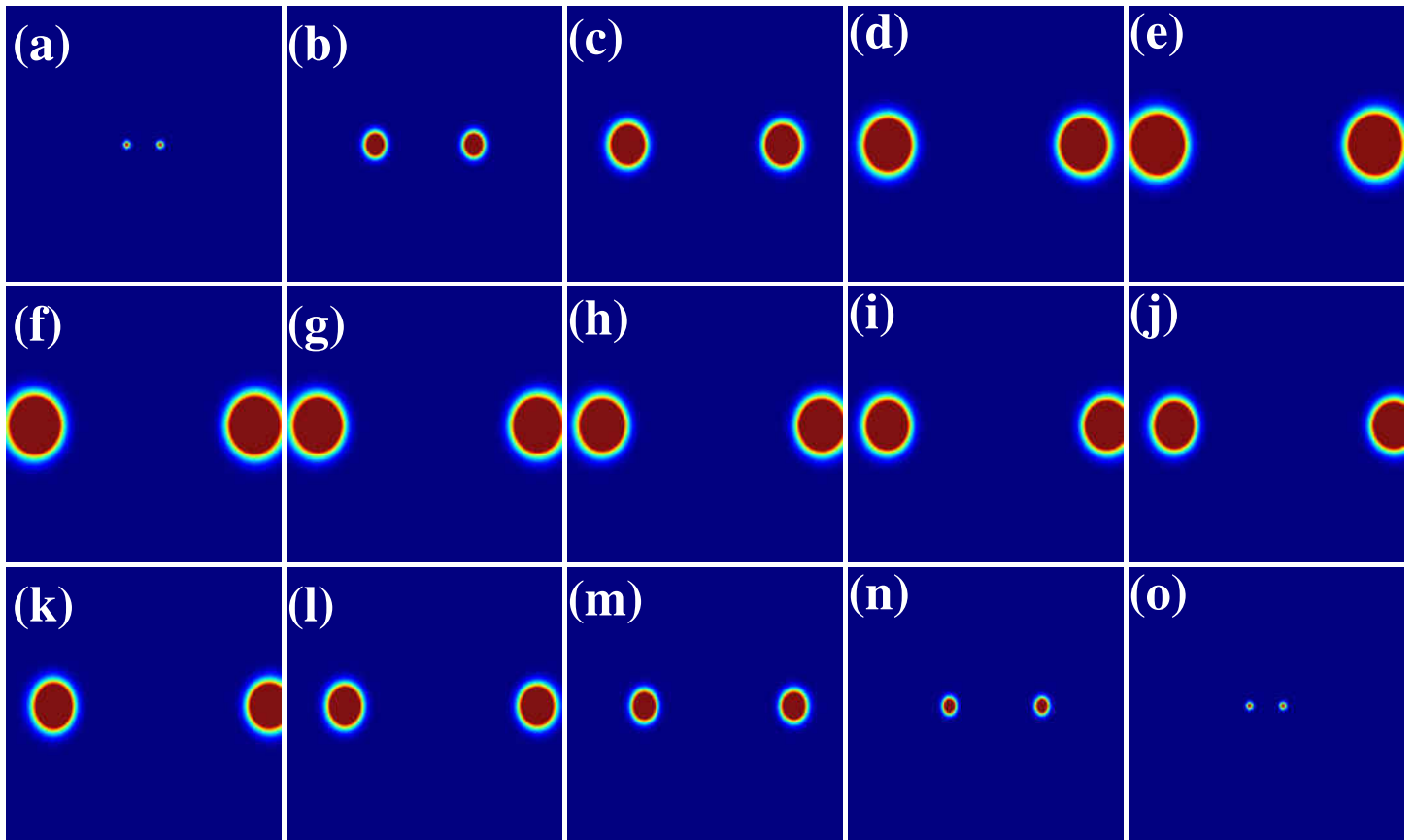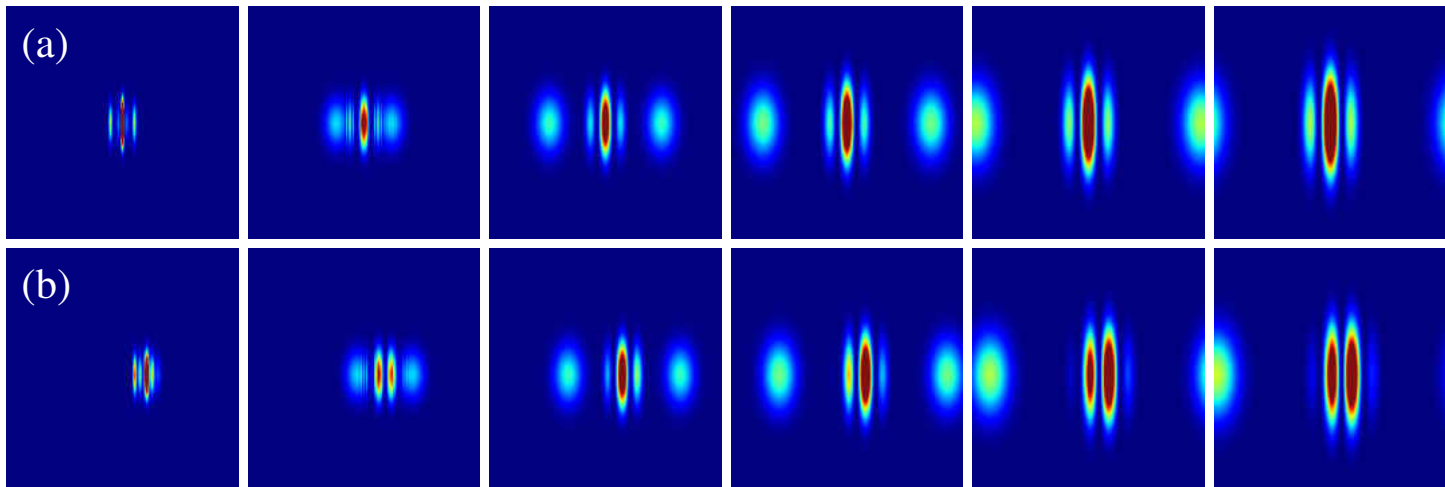
5.5.6 Final Split

Figure 5.8: Comparison of the Final Split without a Test Mass (a) and with a Test Mass (b).

Figure 5.8 compares several time steps in the evolution of the Final Split. Each image is captured from the same vantage point and centered at the origin of Initial Condensate.

Recall, the pair of clouds created in the Initial Split may have a relative velocity as they overlap in the Final Split. During the Final Split, the clouds are doubled into two pairs of clouds. Two of the clouds separate from the center in the $-x$ and $+x$ directions. These clouds posses double the relative velocity gained by the Initial Split clouds. The remaining clouds have nearly zero relative velocity and overlap near the origin of the Initial Condensate.

Series (a) demonstrates the Final Split without a Test Mass present. You can clearly see two clouds separating and moving away from the center. Additionally, as the center evolves, three interference fringes form. The two outer fringes represent the relative velocity induced by the repulsion between the clouds as they are split and overlap. This was actual not expected a priori, but the effect is confirmed by

removing the repulsion effects (setting $g = 0$), which eliminates the outer fringes.

Series (b) demonstrates the Final Split with a Test Mass present to the far right of the system. Compared to series (a), the clouds are shifted to the right as they overlap. Again, two of the Final Split clouds can be seen moving away from the center. Initially, the center displays three fringes, similar to series (a). However, four fringes are evident by the fourth image; the outer pair of fringes are very faint. The two fringes in the center are of approximately equal density.

5.5.7   Estimating Big G

Our input values are $M_{TM} = 10^5$ kg, $|\mathbf{r}_{TM}|^2 = 0.1$ m, and $T_D = 0.4$ s. From the images in Figure 5.8, we estimate the center of mass in series (b) has shifted relative to series (a), $\delta x \approx 1L_o = 10^{-5}$ m. Recall our approximation for Big G, Eq. 3.4.

$$G \approx \frac{2\,\delta x\,|\mathbf{r}_{TM}|^2}{M_{TM}T_D^2} \approx \frac{2\,(10^{-5}\,\mathrm{m})(0.1\,\mathrm{m})^2}{(10^5\,\mathrm{kg})(0.4\,\mathrm{s})^2} \tag{5.42}$$

$$\approx 1.25 \times 10^{-11}\,\mathrm{m^3kg^{-1}s^{-2}} \tag{5.43}$$

This approximation preserves the order-of-magnitude of the current recommended value of Big G [9]. As expected the simulation cannot provide a precise estimate for Big G. Additionally, this estimated value utilizes an approximation that is also unable to precisely determine G. However, these approximations do show the relationships between the experimental parameters and the relative effects of varying them.

CHAPTER 6

CONCLUSION

This thesis has presented a mathematical model to simulate an Atom Interferometry experiment for measuring the Gravitational Constant, Big G. The results of the simulation can be visualized and displayed on a virtual reality headset, like the Oculus Rift. The simulation approximates solutions to the Gross-Pitaevskii Equation using Gaussian distributions containing phase coefficients. The Equations of Motion for the simulated system are found using the Lagrangian Variational Method.

The simulation is not a precise experiment. It cannot measure the value of Big G, but it can approximate the sensitivity of the input conditions (Section 5.5.1) for the Atom Interferometry scheme. Specifically, as described in Section 3.1, an initial condensate is split into multiple clouds that move apart. The simulation can estimate the separation of the cloud centers. The simulation can also estimate the expansion of the cloud widths as the force applied by the harmonic trap is decreased.

The examples visualized in Sections 5.5.4 and 5.5.5 are possible by studying simulations with infeasible results. Specifically, an ifeasible result would preclude the experiment from being placed inside a future revision of the Cold Atom Laboratory [10] to fly aboard the International Space Station. For example, the widths of the clouds cannot overlap the experimental area. This was corrected by increasing the trap strength and providing a larger initial velocity during the Initial Split. This forced the cloud widths to remain smaller. Additionally, allowing the Evolution event to run for too long a time enabled the widths to expand unreasonably. Also not shown are examples in which the cloud centers moved far beyond the range available in a realistic experimental setting. Thus, varying the input parameters enables a study of design parameters to be included in a higher-fidelity experiment at a later time.

Interference fringes are simulated, representing differences in relative velocity in

the clouds as they overlap in the Final Split. In a precise experiment, the interference fringes and the shift in the center of mass of the overlapped clouds are used to measure Big G. However, in this simulation, they are useful to confirm that different input values produce shifts in the overlapped cloud centers and changes to the interference pattern. Specifically, as presented in Section 5.5.6, we can see the effects from both the repulsion between condensate clouds and a Test Mass represented in the number and amplitude of the interference fringes. We can also observe a shift in the cloud centers toward the Test Mass.

Finally, the tools as presented enable one to create videos of the time-evolution of the Atom Interferometer system. These cannot be presented in print form, but they are available to interested parties. Additionally, these videos can be displayed in stereographic 3D via a virtual reality headset.

6.1   Comparison to Grid Methods

The LVM method to simulate the Atom Interferometer provides a massive reduction in computer storage and time. Though this method is an approximation, the reduction in computing resources makes it feasible to simulate the Atom Interferometer in the first place.

We defined the simulation parameters in Section 5.5.3; the LVM solver produces 50000 time steps, each of which represents a solution–a wave function–of the GPE. Each cloud requires 12 parameters to be fully specified, each in three dimensions: position, velocity, width, and the change over time of the width. On commodity computer processors each parameter is represented by an 8 byte floating point number. During the Initial Split two clouds are created, which requires storage of 96 bytes per wave function. The total storage to quantify the 50000 wave functions of the Initial Split are stored in 5×10^5 timesteps $\times$ 96bytes $=$ 48MB.

As described in Section 2.5, a single wave function evaluated on a low-resolution grid requires on the order of 50 GB to store. Comparing the storage requirements of a grid method with the LVM solution, this is a savings in storage on the order of 10^{10}bytes$/10^2$bytes $= 10^8$ per wave function.

Additionally, the LVM solutions are the input parameters of Gaussian functions that can be sampled at any resolution of interest. Grid methods are limited to the size of the grid, which cannot be increased without expanding the storage requirements. In particular, the Final Step visualizations were rendered at a resolution of 5 samples per μm. The Initial Split images represent the condensate clouds expanding across a distance of $1000 \, \mu$m. Thus, to maintain the same fine resolution within the Final Split images across the entire simulation, a grid of $5000^3 = 75$ billion positions is required. This is three orders of magnitude the number of grid points required–1000 times the storage and time–to render the condensates discussed in Section 2.5.

Time is also a limited commodity. The LVM solver is able to produce 50000 wave functions within several seconds. Additionally, rendering the frames from these solutions can be completed within a few minutes. Comparatively, the Crank-Nicolson solutions from Section 2.4 require hours to produce single wave functions at limited resolutions.

6.2   Future Work

The examples presented in Section 5.5 are exaggerated with an infeasibly massive Test Mass. This was chosen to clearly demonstrate the simulation model and provide useful feedback. As such, these examples are limited in their applicability to determine the feasibility of the Atom Interferometer. The attempt to characterize the sensitivity of the input parameters remains as a future endeavor. The results of such work will influence the design of a high-fidelity simulation, leading to a feasibility study of the

Atom Interferometer.

Next, only the optical density is discussed as a quality of interest. Other qualities like the phase value and velocity field are of interest in building intuition for more detailed experiments. The optical density is a scalar value whose rendering equations (see Section 5.2.4) have an algebraic representation. A field value, like velocity, requires additional work to calculate and render. There is no universally agreed upon rendering methodology to display field values, so much work is required to define a visual representation that is useful.

It is hoped that these tools will continue to be useful and the Atom Interferometer can be characterized successfully.

REFERENCES

[1] H. Cavendish, 1798 Phil. Trans. R. Soc. London 88 469526.

[2] B. N. Taylor, W. H. Parker, and D. N. Langenberg, *Determination of e/h, Using Macroscopic Quantum Phase Coherence in Superconductors: Implications for Quantum Electrodynamics and Fundamental Physical Constants*, Review of Modern Physics, Volume 41, Issue 3, Pages 375-496, 1969.

[3] E. R. Cohen and B. N. Taylor, *The 1973 Least-Squares Adiustment of the Fundamental Constants*, Journal Physical Chemistry Reference Data, Volume 2, Issue 4, Pages 663-734, 1973.

[4] E. R. Cohen and B. N. Taylor, *The 1986 adjustment of the fundamental physical constants*, Review of Modern Physics, Volume 59, Issue 4, Pages 1121-1148, 1987.

[5] P. J. Mohr and B. N. Taylor, *CODATA recommended values of the fundamental physical constants: 1998*, Review of Modern Physics, Volume 72, Issue 2, Pages 351-495, 2000.

[6] P. J. Mohr and B. N. Taylor, *CODATA recommended values of the fundamental physical constants: 2002*, Review of Modern Physics, Volume 77, Issue 1, Pages 1-107, 2005.

[7] P. J. Mohr, B. N. Taylor, and D. B. Newell, *CODATA recommended values of the fundamental physical constants: 2006*, Review of Modern Physics, Volumne 80, Issue 2, Pages 633-730, 2008.

[8] P. J. Mohr, B. N. Taylor, and D. B. Newell, *CODATA recommended values of the fundamental physical constants: 2010*, Review of Modern Physics, Volume 84, Issue 4, Pages 1527-1605, 2012.

[9] Committee on Data for Science and Technology, *2014 CODATA recommended values*, International Council for Science, Committee on Data for Science and Technology, http://physics.nist.gov/cgi-bin/cuu/Value?bg.

[10] *Cold Atom Lab*, http://coldatomlab.jpl.nasa.gov/.

[11] J. Crank and P. Nicolson, *A practical method for numerical evaluation of solutions of partial differential equations of the heat conduction type*, Proceedings of the Cambridge Philosophical Society, Volume 43, Issue 1, Pages 5067, 1947.

[12] M. Edwards, B. Benton, J. Howard, C.W. Clark, *Momentum-space Engineering of Gaseous Bose-Einstein Condensates*, Physical Review A, Volume 82, Page 063613, 2010.

[13] J. B. Fixler; G. T. Foster; J. M. McGuirk; M. A. Kasevich (2007-01-05), *Atom Interferometer Measurement of the Newtonian Constant of Gravity*, Science 315 (5808): 7477.

[14] G. T. Gillies, *The Newtonian gravitational constant: recent measurements and related studies*, Reports on Progress in Phyics, Volume 60, Number 2, 151-225 (1997).

[15] *Laser Interferometry Gravitational-Wave Observatory*, https://www.ligo.caltech.edu/.

[16] B.P. Abbott et al. (LIGO Scientific Collaboration and Virgo Collaboration), *Observation of Gravitational Waves from a Binary Black Hole Merger*, Physical Review Letters, Volume 116, Issue 06, Pages 061102, 11 February 2016.

[17] A. Messiah, Quantum Mechanics, Dover Publications, NY, 1995.

[18] A. Michelson and E. Morley, *On the Relative Motion of the Earth and the Luminiferous Ether*, American Journal of Science, Volume 34 Issue 203, Pages 333345, 1887.

[19] P. Muruganandam and S. K. Adhikari, *Fortran Programs for the Time-Dependent Gross-Pitaevskii Equation in a Fully Anisotropic Trap*, Journal of Computer Physics Communications, Volume 180, Issue 10, October 2009, pgs 1888-1912.

[20] N. Murray, M. Krygier, M. Edwards, K.C. Wright, G.K. Campbell, and C.W. Clark, *Probing the circulation of ring-shaped Bose-Einstein condensates*, Phys. Rev. A **88**, 053615 (2013).

[21] Oculus Rift, https://www.oculus.com/en-us/

[22] V. M. Pérez-García, H. Michinel, J. I. Cirac, M. Lewenstein, P. Zoller, *Dynamics of Bose-Einstein condensates: Variational solutions of the Gross-Pitaevskii equations*, Physical Review A, Volume 56, Number 2, August 1997.

[23] J. Bardeen, L. N. Cooper, and J. R. Schrieffer, *Microscopic Theory of Superconductivity*, Physical Review **106**, 162 - 164 (1957)

[24] Bose, S.N., *Plancks Gesetz und Lichtquantenhypothese*, Zeitschrift für Physik **26** 178181 (1924).

[25] Einstein, A., *Quantentheorie des einatomigen idealen Gases.* Sitzungsberichte der Preussischen Akademie der Wissenschaften 1: 3. (1925).

[26] C. J. Pethick and H. Smith, *Bose-Einstein Condensation in Dilute Gases*, Cambridge, 2002.

[27] W. B. Pennebaker and J. L. Mitchell *JPEG: Still Image Data Compression Standard*, Springer, 1993

[28] L. Pitaevskii and S. Stringari, *Bose-Einstein Condensation*, Oxford Science Publications, 2003

[29] T. Boutell, et. al, *Portable Network Graphics (PNG) Specification (Second Edition)*, W3C, https://www.w3.org/TR/PNG/.

[30] T. Quinn, *Fundamental constants: Measuring big G*, Nature 408, 919-921 (2000)

[31] S. Schlamminger, *A Cool Way to Measure Big G*, Nature, Vol 510, 478-479, 26 June 214.

[32] K. Sung, P. Shirley, and S. Baer, *Essentials of Interactive Computer Graphics: Concepts and Implementation*, CRC Press, 2008

[33] G. M. Tino and M. A. Kasevich, *Atom Interferometry*, Proceedings of the International School of Physics "Enrio Fermi", Course 188, Italian Physical Society, 2014.

[34] T. Young, *A Course of Lectures on Natural Philosophy and the Mechanical Arts*, Volume 1, William Savage, ed., Lecture 39, Pages 463464, 1807.

Appendix A

SOME USEFUL GAUSSIAN INTEGRALS

This appendix derives some Gaussian integrals useful in the derivation presented in the main body of the text. Consider the following class of Gaussian integrals:

$$J_k(\eta_0, w_0) \equiv \int_{-\infty}^{\infty} \eta^k e^{-(\eta-\eta_0)^2/w_0^2} \, d\eta, \quad k = 0, 1, 2, \ldots \qquad (A.1)$$

we can evaluate this class of integrals by changing the variable of integration:

$$x \equiv \frac{\eta - \eta_0}{w_0}, \quad \eta = \eta_0 + w_0 x, \quad d\eta = w_0 dx. \qquad (A.2)$$

Expressed in terms of this new integration variable, the integral now has the form

$$J_k(\eta_0, w_0) = \int_{-\infty}^{\infty} (\eta_0 + w_0 x)^k \, e^{-x^2} \, w_0 dx. \qquad (A.3)$$

We now use the binomial theorem to express the factor $(\eta_0 + w_0 x)^k$ as a series of powers of x:

$$(\eta_0 + w_0 x)^k = \sum_{s=0}^{k} \binom{k}{s} \eta_0^{k-s} (w_0 x)^s. \qquad (A.4)$$

Inserting this into the integral in Eq. (A.3) gives

$$J_k(\eta_0, w_0) = w_0 \sum_{s=0}^{k} \binom{k}{s} \eta_0^{k-s} w_0^s \int_{-\infty}^{\infty} x^s e^{-x^2} \, dx. \qquad (A.5)$$

The integral now appearing in the sum above is well–known (after all, integration is the art of transforming the integral until you can look it up!). We have

$$\int_{-\infty}^{\infty} x^s e^{-x^2} \, dx = \left\{ \begin{array}{ll} 0 & s = \text{ odd integer} \\ \left(\frac{s!}{(s/2)!}\right) \frac{\pi^{1/2}}{2^s} & s = \text{ even integer} \end{array} \right\} \qquad (A.6)$$

Using this result we can write a final expression for the integrals:

$$J_k(\eta_0, w_0) = \left(w_0 \pi^{1/2}\right) \sum_{m=0}^{[k/2]} \binom{k}{2m} \eta_0^{k-2m} \left(\frac{w_0}{2}\right)^{2m} \frac{(2m)!}{m!}. \qquad (A.7)$$

Where the upper limit of the sum, $[k/2]$, is the greatest integer less than or equal to $k/2$.

In the derivation of the final Lagrangian in the main body of this document, integrals of this type are found repeatedly. However, only for $k = 0, 1, 2$. Thus we present the values of these integrals for convenient reference:

$$J_0 \left(\eta_0, w_0 \right) = \int_{-\infty}^{\infty} e^{-(\eta - \eta_0)^2 / w_0^2} \, d\eta = \left(w_0 \pi^{1/2} \right) \tag{A.8}$$

$$J_1 \left(\eta_0, w_0 \right) = \int_{-\infty}^{\infty} \eta \, e^{-(\eta - \eta_0)^2 / w_0^2} \, d\eta = \left(w_0 \pi^{1/2} \right) \eta_0 \tag{A.9}$$

$$J_2 \left(\eta_0, w_0 \right) = \int_{-\infty}^{\infty} \eta^2 e^{-(\eta - \eta_0)^2 / w_0^2} \, d\eta = \left(w_0 \pi^{1/2} \right) \left(\eta_0^2 + \frac{1}{2} w_0^2 \right) \tag{A.10}$$

Appendix B

DERIVATIVES OF $\bar{L}_4$

In this appendix we will give the derivatives of $\bar{L}_4$, the Lagrangian term corresponding to the interactions between particles. This term has the form:

$$
\bar{L}_4(\bar{\eta}, \bar{\mathbf{w}}) = \frac{\left(\frac{1}{2}\bar{g}N\right)}{(2\pi)^{3/2} N_c^2} \left[\sum_{j_1=1}^{N_c} \left(\frac{1}{\bar{w}_{j_1 x}\bar{w}_{j_1 y}\bar{w}_{j_1 z}} \right) + 2^{5/2} \sum_{\substack{j_1,j_2=1 \\ j_1 \neq j_2}}^{N_c} \prod_{\eta'=x,y,z} \left(\frac{\exp\left\{ -\frac{\left(\bar{\eta}'_{j_1} - \bar{\eta}'_{j_2}\right)^2}{\bar{w}_{j_1\eta'}^2 + \bar{w}_{j_2\eta'}^2} \right\}}{\left(\bar{w}_{j_1\eta'}^2 + \bar{w}_{j_2\eta'}^2 \right)^{1/2}} \right) \right] .
$$

$$(B.1)$$

This quantity depends on the center coordinates and widths of the Gaussian clouds in the trial wave functions. The two categories of derivatives of $\bar{L}_4$ that appear in the LVM equations of motion are with respect to these two variables. We state each of these derivatives of $\bar{L}_4$, obtained by direct differentiation, in turn below.

The derivative with respect to center coordinate η_j is given by

$$
\frac{\partial \bar{L}_4}{\partial \bar{\eta}_j} = -\frac{4\bar{g}N}{(\pi)^{3/2} N_c^2} \sum_{\substack{j_1=1 \\ j_1 \neq j}}^{N_c} \frac{(\bar{\eta}_j - \bar{\eta}_{j_1})}{\bar{w}_{j\eta}^2 + \bar{w}_{j_1\eta}^2} \left(\prod_{\eta'=x,y,z} \frac{\exp\left\{ -\frac{\left(\bar{\eta}'_j - \bar{\eta}'_{j_1}\right)^2}{\bar{w}_{j\eta'}^2 + \bar{w}_{j_1\eta'}^2} \right\}}{\left(\bar{w}_{j\eta'}^2 + \bar{w}_{j_1\eta'}^2 \right)^{1/2}} \right) .
$$

$$(B.2)$$

The derivative with respect to the width $\bar{w}_{j\eta}$ has the form

$$
\frac{\partial \bar{L}_4}{\partial \bar{w}_{j\eta}} = \frac{\frac{1}{2}\bar{g}N}{(2\pi)^{3/2} N_c^2} \left[-\frac{1}{\bar{w}_{jx}\bar{w}_{jy}\bar{w}_{jz}\bar{w}_{j\eta}} \right.
$$

$$
+ \; 2^{7/2} \sum_{\substack{j_1=1 \\ j_1 \neq j}}^{N_c} \left(\frac{\bar{w}_{j\eta}\left[2\left(\bar{\eta}_j - \bar{\eta}_{j_1}\right)^2 - \left(\bar{w}_{j\eta}^2 + \bar{w}_{j_1\eta}^2\right) \right]}{\left(\bar{w}_{j\eta}^2 + \bar{w}_{j_1\eta}^2\right)^2} \right) \prod_{\eta'=x,y,z} \frac{\exp\left\{ -\frac{\left(\bar{\eta}'_j - \bar{\eta}'_{j_1}\right)^2}{\bar{w}_{j\eta'}^2 + \bar{w}_{j_1\eta'}^2} \right\}}{\left(\bar{w}_{j\eta'}^2 + \bar{w}_{j_1\eta'}^2 \right)^{1/2}} \left. \right] .
$$

$$(B.3)$$